REPORT DOCUMENTATION PAGE

1. Report No.	2.	3. Recipient's Accession No.

4. Title and Subtitle
FINE SEDIMENT ERODIBILITY IN LAKE OKEECHOBEE, FLORIDA

5. Report Date
November 1989

6.

7. Author(s)
Kyu-Nam Hwang
Ashish J. Mehta

8. Performing Organization Report No.
UFL/COEL-89/019

9. Performing Organization Name and Address
Coastal and Oceanographic Engineering Department
University of Florida
336 Weil Hall
Gainesville, FL 32611

10. Project/Task/Work Unit No.
Lake Okeechobee Phosphorus Dynamics Study, Task 4.4

11. Contract or Grant No.

12. Sponsoring Organization Name and Address
South Florida Water Management District
P.O. Box V, 3301 Gun Club Road
West Palm Beach, FL 33402

13. Type of Report
Final

14.

15. Supplementary Notes

16. Abstract

Resuspension of sediment at the bottom of Lake Okeechobee composed of fine-grained material has been examined. A sediment transport model was used to simulate likely trends in the evolution of the vertical suspended sediment concentration profile resulting from wave action, and the corresponding eroded bed depth was calculated through mass balance. Requisite information on characteristic parameters and relationships related to fine sediment erodibility were derived from field sampling of bottom sediment in the lake, and through laboratory experiments using this sediment and lake water.

Simulated sediment concentration profiles under "storm" waves exhibit an evident qualitative agreement with observed trends in profile evolution at muddy coasts. Characteristic features are the formation of a strong gradient in suspension concentration termed the lutocline, and a fluid mud layer near the bed. The concentration over approximately 80 % of the water column down from the surface is typically quite low throughout, and most of the sediment is elevated to a relatively small height above the bed. Upward entrainment of the lutocline is constrained by the submerged weight of the high concentration layer below the lutocline, and by the lack of a strong mechnism for upward diffusion. As expected, simulation of the "post-storm" calm, assuming no wave action, results in a depression of the elevated lutocline and bed reformation.

17. Originator's Key Words	18. Availability Statement
Erosion Fine sediment Lake mud Lake Okeechobee	

19. U. S. Security Classif. of the Report	20. U. S. Security Classif. of This Page	21. No. of Pages	22. Price
Unclassified	Unclassified	159	

It is emphasized that measurement of sediment concentration at or near the water surface alone, neglecting near-bed high concentration suspension dynamics, can lead to an order of magnitude underestimation of the erodible bed depth. Gleason and Stone (1975) measured a surface concentration of 102 $mg\ L^{-1}$ at a site with a water depth of 4.6 m during a storm in Lake Okeechobee and suggested bed material erosion of 2.3 mm assuming uniform water column concentration. Considering the characteristic features of the vertical concentration profile, however, the simulated results suggest that the erodible bed thickness in the lake is likely to be on the order of 2 cm corresponding to surface concentration of 102 $mg\ L^{-1}$.

Through an operational definition of the fluidized mud layer thickness, bulk densities defining the upper and lower levels of the fluid mud layer have been determined to be 1.0023 $g\ cm^{-3}$ and 1.065 $g\ cm^{-3}$, respectively. Applying these values to the bottom density profiles as identified from bottom cores, the thickness of the fluid mud layer is found to range from 5 cm to 12 cm, which is consistent with values reported by Gleason and Stone (1975).

The thickness of the fluid mud layer arising from wave action and associated rise of the lutocline have also been examined through model simulations with and without the initial presence of fluid mud over the bed. The thickness of the resulting fluid mud layer in both cases was of the same order (10 cm in the former case and 8 cm in the latter), while the average concentration of this layer in the former case was somewhat higher than in the latter case ($\sim 40\ g\ L^{-1}$ in the former case versus $\sim 20\ g\ L^{-1}$ in the latter). During resuspension the fluid mud layer rises rapidly, with the rise of the lutocline to a certain height being dependent upon the intensity of wave action.

On the other hand, bed erosion continues to occur as long as the applied wave bottom stress amplitude exceeds the bed shear strength, thus supplying eroded sediment mass to the fluid mud layer and resulting in an increment in the concentration of this layer.

An effort has been made to establish the correspondence between the erodibile mud thickness due to resuspension during storm wave action, and the fluidized mud zone thickness as identified from bottom cores. The actual thickness of this "active" mud surficial layer at a site will of course depend on the intensity and frequency of wave action, water depth and the thickness and character of the bottom mud. The thickness of this active mud layer (fluidized mud thickness plus erodible bed thickness) in Lake Okeechobee appears to be on the order of 10 cm below the mud-water interface during calm conditions.

An evident conclusion is that accurate measurement of instantaneous vertical concentration profiles is vitally important in studies on bottom sediment-induced turbidity, and in establishing the erodible thickness of the bed by wave action. Such profiling, when carried out effectively, can also yield valuable information on the microstructure of fine sediment suspension. Furthermore, it is essential to track the evolution of the near-bed suspended sediment load, since this non-Newtonian "slurry" is usually responsible for sedimentation problems in many episodic environments, and is likely to be highly significant in governing phosphorus release during resuspension events in the lake.

UFL/COEL-89/019

FINE SEDIMENT ERODIBILITY IN LAKE OKEECHOBEE, FLORIDA

by

Kyu-Nam Hwang
Ashish J. Mehta

Sponsor:

South Florida Water Management District
P.O. Box V, 3301 Gun Club Road
West Palm Beach, FL 33402

November, 1989

ACKNOWLEDGMENT

This investigation was conducted as a part of the Lake Okeechobee Phosphorus Dynamics Study funded by the South Florida Water Management District, West Palm Beach, Florida (SFWMD). The authors wish to acknowledge Brad Jones and Dave Soballe of SFWMD for their assistance and Dr. Ramesh Reddy for coordinating the University of Florida team effort. Acknowledgement is also due to Dr. Robert Kirby and Prof. Paul Visser for their principal participation in the field effort, and to Dr. Mark Ross, who provided a copy of his numerical model which is used in a modified form in this study. Thanks are extended to the staff of the Coastal Engineering Laboratory, particularly Vernon Sparkman, for help with the laboratory experiments. Graduate assistant Xueming Shen carried out laboratory core analysis.

TABLE OF CONTENTS

LIST OF FIGURES

LIST OF TABLES

LIST OF SYMBOLS

A_b = Horizontal water motion (amplitude) at the bottom

a = Settling velocity coefficient

a_m = Coefficient defining critical shear stress for mass erosion

a_s = Coefficient defining critical shear stress for surface erosion

b = Settling velocity coefficient; Minor radius of a water particle orbit

b_m = Coefficient defining critical shear stress for mass erosion

b_s = Coefficient defining critical shear stress for surface erosion

C = Sediment suspension concentration (mass/unit volume)

$\overline{C}$ = Time mean concentration

C_1 = Sediment concentration below which free settling occurs

C_2 = Sediment concentration corresponding to maximum settling velocity

C_3 = Sediment concentration corresponding to maximum settling flux

C_b = Concentration of the eroded or deposited bed

C_o = Initial suspension concentration

C_D = Drag coefficient

C_f = Average concentration of fluid mud layer

C_{fo} = Average concentration of fluid mud layer at initial time

C_T = Temperature correction factor

C' = Instantaneous concentration component about mean

c_s = Coefficient defining critical shear stress for surface erosion

D = Molecular diffusivity

d = diameter of spherical sediment particle

d_{25} = Sediment grain size diameter of 25 % greater than (by weight) fraction

d_{50} = Sediment grain size diameter of 50 % greater than (by weight) fraction

d_{75} = Sediment grain size diameter of 57 % greater than (by weight) fraction

E = Turbulent momentum diffusivity

F = Sediment flux

F_t = Turbulent diffusion flux of sediment

F_b = Vertical bed flux of sediment

F_d = Vertical diffusion flux of sediment

F_e = Vertical erosional flux of sediment

F_p = Vertical depositional flux of sediment

F_s = Vertical settling flux of sediment

F_{so} = Maximum vertical settling flux of sediment

F_t = Turbulent diffusion flux

f_w = Wave friction factor

G_1 = Specific gravity of fluid

G_s = Specific gravity of sediment particle

g = Acceleration due to gravity

H = Heavyside function ; Wave height

h = Water depth

K = Turbulent mass diffusivity

K_n = Vertical mass diffusivity for neutral flow

K_z = Vertical mass diffusivity for stratified flow

k = Wave number

$\vec{k}$ = Vertical unit vector

k_1 = Settling velocity coefficient

k_2 = Settling velocity coefficient

k_s = Equivalent bed roughness

L = Wave length

l = Prandtl's mixing length

m = Eroded sediment mass per unit bed area; settling velocity coefficient

m_1 = Coefficient defining erosion rate coefficient for mass erosion

N = Total number of classes

n = Settling velocity coefficient; Manning's coefficient

P = Percentage of sediment finer by weight

p = Probability of deposition

p_1 = Coefficient defining bulk density variation with bed depth

p_2 = Coefficient defining bulk density variation with bed depth

p_3 = Coefficient defining bulk density variation with bed depth

p_4 = Coefficient defining bulk density variation with bed depth

R_a = Hydrometer reading

R_c = Corrected hydrometer reading

R_e = Reynolds number

R_f = Flux Richardson number

R_i = Gradient Richardson number

S_t = Turbulent Schmidt number

s_1 = Coefficient defining surface erosion rate

s_2 = Coefficient defining surface erosion rate

T = Wave period

t = Time variable

$\vec{U}$ = Velocity vector with cartesian components

$\vec{U}'$ = Instantaneous component vector about mean

u = Velocity component in x-direction

$\overline{u}$ = Time mean velocity in x-direction

u_b = Maximum near-bed orbital velocity in x- direction

u_* = Friction velocity in x-direction

v = Velocity component in y-direction

$\overline{v}$ = Time mean velocity in y-direction

W = Mass of sediment

W_s = Sediment settling velocity

W_{sm} = Maximum settling velocity of sediment

W_{sn} = Minimum settling velocity of sediment

W_{so} = Maximum settling velocity of sediment

$\overline{w}$ = Time mean velocity in z-direction

x = Longitudinal cartesian coordinate direction; log average of sediment concentration

y = Lateral cartesian coordinate direction

z = Elevation variable

z_b = Mobile/stationary fluid mud interface; eroded or deposited bed depth

z_f = Thickness of fluid mud layer

z_{fo} = Thickness of fluid mud layer at initial time

α = Settling velocity coefficient; stabilized diffusivity constant

α_w = Wave diffusivity constant

β = Settling velocity coefficient; stabilized diffusivity constant; wave diffusivity constant

β_1 = Wave diffusivity constant

β_2 = Wave diffusivity constant

ρ = Fluid density

ρ_3 = Bulk density at upper fluid mud interface

ρ_B = Bulk density

ρ_l = Bulk density at lower fluid mud interface

ρ_s = Sediment granular density

ρ_w = Water density

μ = Dynamic viscosity of fluid

ν = Kinematic viscosity of fluid

ε = Erosion rate

ε_i = Erosion resistance defining parameters

ε_M = Erosion rate coefficient

$\varepsilon_{M.s}$ = Erosion rate coefficient for surface erosion

$\varepsilon_{M.m}$ = Erosion rate coefficient for mass erosion

σ = Wave frequency

τ_b = Applied bed shear stress

τ_{ce} = Critical bed shear stress for erosion

$\tau_{ce.s}$ = Critical bed shear stress for surface erosion

$\tau_{ce.m}$ = Critical bed shear stress for mass erosion

τ_{cd} = Critical shear stress for deposition

τ_{cm} = Maximum critical shear stress for deposition

τ_{cn} = Minimum critical shear stress for deposition

τ_s = Bed shear strength

τ_v = Vane shear strength

SUMMARY

Resuspension of sediment at the bottom of Lake Okeechobee composed of fine-grained material has been examined. A sediment transport model was used to simulate likely trends in the evolution of the vertical suspended sediment concentration profile resulting from wave action, and the corresponding eroded bed depth was calculated through mass balance. Requisite information on characteristic parameters and relationships related to fine sediment erodibility were derived from field sampling of bottom sediment in the lake, and through laboratory experiments using this sediment and lake water.

Simulated sediment concentration profiles under "storm" waves exhibit an evident qualitative agreement with observed trends in profile evolution at muddy coasts. Characteristic features are the formation of a strong gradient in suspension concentration termed the lutocline, and a fluid mud layer near the bed. The concentration over approximately 80 % of the water column down from the surface is typically quite low throughout, and most of the sediment is elevated to a relatively small height above the bed. Upward entrainment of the lutocline is constrained by the submerged weight of the high concentration layer below the lutocline, and by the lack of a strong mechnism for upward diffusion. As expected, simulation of the "post-storm" calm, assuming no wave action, results in a depression of the elevated lutocline and bed reformation.

It is emphasized that measurement of sediment concentration at or near the water surface alone, neglecting near-bed high concentration suspension dynamics, can lead to an order of magnitude underestimation of the erodible bed depth. Gleason and Stone (1975) measured a surface concentration of 102 $mg\ L^{-1}$ at a site with a water depth of 4.6 m during a storm in Lake Okeechobee and suggested bed material erosion of 2.3 mm assuming

uniform water column concentration. Considering the characteristic features of the vertical concentration profile, however, the simulated results suggest that the erodible bed thickness in the lake is likely to be on the order of 2 cm corresponding to surface concentration of 102 $mg\ L^{-1}$.

Through an operational definition of the fluidized mud layer thickness, bulk densities defining the upper and lower levels of the fluid mud layer have been determined to be 1.0023 $g\ cm^{-3}$ and 1.065 $g\ cm^{-3}$, respectively. Applying these values to the bottom density profiles as identified from bottom cores, the thickness of the fluid mud layer is found to range from 5 cm to 12 cm, which is consistent with values reported by Gleason and Stone (1975).

The thickness of the fluid mud layer arising from wave action and associated rise of the lutocline have also been examined through model simulations with and without the initial presence of fluid mud over the bed. The thickness of the resulting fluid mud layer in both cases was of the same order (10 cm in the former case and 8 cm in the latter), while the average concentration of this layer in the former case was somewhat higher than in the latter case ($\sim 40\ g\ L^{-1}$ in the former case versus $\sim 20\ g\ L^{-1}$ in the latter). During resuspension the fluid mud layer rises rapidly, with the rise of the lutocline to a certain height being dependent upon the intensity of wave action. On the other hand, bed erosion continues to occur as long as the applied wave bottom stress amplitude exceeds the bed shear strength, thus supplying eroded sediment mass to the fluid mud layer and resulting in an increment in the concentration of this layer.

An effort has been made to establish the correspondence between the erodibile mud thickness due to resuspension during storm wave action, and the fluidized mud zone thickness as identified from bottom cores. The actual thickness of this "active" mud surficial layer at a site will of course depend on the intensity and frequency of wave action, water depth and the thickness and character of the bottom mud. The thickness of this active mud layer (fluidized mud thickness plus erodible bed thickness) in Lake Okeechobee appears to be on the order of 10 cm below the mud-water interface during calm conditions.

An evident conclusion is that accurate measurement of instantaneous vertical concentration profiles is vitally important in studies on bottom sediment-induced turbidity, and in establishing the erodible thickness of the bed by wave action. Such profiling, when carried out effectively, can also yield valuable information on the microstructure of fine sediment suspension. Furthermore, it is essential to track the evolution of the near-bed suspended sediment load, since this non-Newtonian "slurry" is usually responsible for sedimentation problems in many episodic environments, and is likely to be highly significant in governing phosphorus release during resuspension events in the lake.

CHAPTER 1
INTRODUCTION

1.1 Significance of Problem

The critical need to predict the turbidity in water due to fine-grained sediment suspension under wave action over mud deposits for sedimentation and erosion studies, as well as sorbed contaminant transport, is well known. Since fall velocities of fine sediment particles are very small, they can be easily transported by hydrodynamic flows such as waves and currents. The presence of these particles in the water column affects accoustic transmission, heat absorption and depth of the eutrophic zone (Luettich et al., 1989). Because these sediments also have a strong affinity for sorbing nutrients and toxic chemicals, sediments which have been deposited on the bottom may function as a source of contaminants to the water column if they are disturbed by eroding forces resulting, for instance, from wave action. An outstanding example of a water body for these problems is Lake Okeechobee, the largest shallow lake in Florida. This lake shows typical signs of artificial eutrophication mainly due to increased phosphorus loading associated with the surrounding region.

The transport processes of fine sediments are particularly important in a wave dominated environment (e. g., in shallow lakes and estuaries), since they may repeatedly settle to the bottom and be resuspended throughout the water column by periodic forces such as astronomical tides or by episodic forces such as storm events. The accurate prediction of fine sediment transport behavior, which is typically performed through numerical solutions of the sediment mass transport equation, is strongly contingent upon an understanding of the structure of the vertical profile of sediment concentration and interaction with the flow field. However, modeling of fine sediment transport is limited by the knowledge of physical mechanisms relating the response of mud beds to wave action. Waves tend to loosen the

mud deposit and generate steep suspension concentration gradients, making the sediment load near the bottom typically orders higher than that near the surface. Neglecting this characteristic of sediment concentration profiles under wave action can therefore lead to significant errors in calculating the associated flux of sediment mass and consequently in estimating the erodibility of mud deposit.

It is therefore highly instructive to examine the vertical structure of concentration and its interaction with the wave flow field in order to make a comparison with field observed trends on the erodible depth of deposit. Through analysis of laboratory and field measurements within a descriptive frame work for the vertical concentration profile and erodible bed depth, an attempt is made in this study to approach the problem in a manner such as to hopefully yield useful information on the depth of erosion.

1.2 Objective and Scope

The objectives of this study were as follows:

1. To simulate prototype trends in the evolution of fine sediment concentration profiles due to fine-grained bed material load by progressive, nonbreaking wave action.

2. To estimate the corresponding depth of bottom erosion as determined by the response of the muddy sediment deposit to eroding forces caused by waves.

3. To examine a possible connection between the erodible mud thickness thus obtained and the fluidized mud zone thickness determined from bottom coring, with specific reference to Lake Okeechobee.

The scope of this study was therefore defined as follows:

1. Erosion and deposition of fine sediment beds under waves was considered in a physically realistic but simplified manner in order to simulate prototype trends in concentration profile evolution.

2. Field data collection and laboratory experiments were conducted with Lake Okeechobee bottom sediment, in order to determine relevant parameters including erosion

and deposition relationships to serve as input data to simulate the concentration profile evolution and to estimate the depth of bottom erosion in a physically realistic manner.

3. In developing the simple vertical concentration structure model, only vertical tranport fluxes were considered. Diffusive flux was determined on the basis of classical mixing length theory, introducing the effects of stratification of bulk density to diffusion. The strong variability of the settling velocity with sediment concentration was accounted for in calculating the deposition flux.

1.3 Outline of Upcoming Chapters

Chapter 2 describes the idealized vertical structure of suspended sediment concentration profile and its evolution trend under waves. This chapter also suggests a reasonable method to calculate the erodible thickness of mud deposit as related to vertical variation of suspension concentration. In Chapter 3, the theroretical approach to the vertical transport process is briefly presented in order to develop the numerical model for determining the vertical structure of suspension concentration. The settling-diffusion equation for vertical transport is given as the governing equation, including bed fluxes, diffusion and settling. Chapter 4 presents the objectives, procedures and results from field data collection and laboratory experiments with the following themes: 1) Characterization of lake sediment through the particle size, organic material and mineralogical composition analyses. 2) Measurements of bulk density and vane shear strength to evaluate bed properties. 3) Settling velocity determination under quiescent condition. 4) Determination of erosion rate for given bed densities and bed shear stresses, using an annular flume. Chapter 5 describes the application of the vertical transport model to Lake Okeechobee, using the experimental data obtained in Chapter 4. This chapter also includes the modeling procedure used, based on the theory described in Chapter 3, as well as simulated results for the evolution of concentration profile and erodible bed thickness under waves and under no wave condition. Conclusions, recommendations for future research and miscellaneous closing comments are

given in Chapter 6. Appendix A presents vertical descriptions and profiles of bulk density and shear strength of core samples collected from various sites in Lake Okeechobee. Appendices B and C contain concentration profiles obtained during the settling column tests and annular flume erosion tests, respectively.

CHAPTER 2
VERTICAL STRUCTURE OF SUSPENSION UNDER WAVES

2.1 Typical Features of Concentration Profile

For the fine-grained suspended sediments, a key feature of vertical concentration profiles is the occurrence of steep vertical gradients with concentration that can be orders higher near the bottom than at the water surface (Maa and Mehta, 1987). Figure 2.1 shows the instantaneous vertical concentration distribution in terms of the turbulence-mean concentration $C(z,t)$ profile, as well as the corresponding horizontal orbital velocity $u(z,t)$ profile of non-breaking progressive waves. Here z is the vertical coordinate and t is time. In order to focus on the various sediment transport mechanisms influencing the vertical concentration distribution, the idealized concentration profile is presented with only two significant steep concentration gradients.

As depicted in Figure 2.1, the uppermost layer is the mobile suspension layer, which has a relatively low concentration. The mobile suspension layer is differentiated from the fluid mud layer by a steep concentration gradient commonly termed the lutocline (Parker and Kirby, 1982). The lutocline is a pycnocline representing a sharp density gradient due to sediment. Formation of lutoclines is due to the entrainment of the mud/water interface resulting from the effects of shear-induced upward diffusion which is strongly stabilized by the negative buoyancy of the high concentration suspension combined with hindered gravitational settling. Below the lutocline, there is a fluid mud layer which has a relatively high concentration suspension. The lower gradient defines the cohesive bed wherein there is sufficient interparticle contact to result in a finite measurable effective stress (Parker, 1986). Within the cohesive bed, the deforming bed is separately identified from the stationary bed, since wave orbital motion penetrates into the cohesive bed, which in turn may then undergo

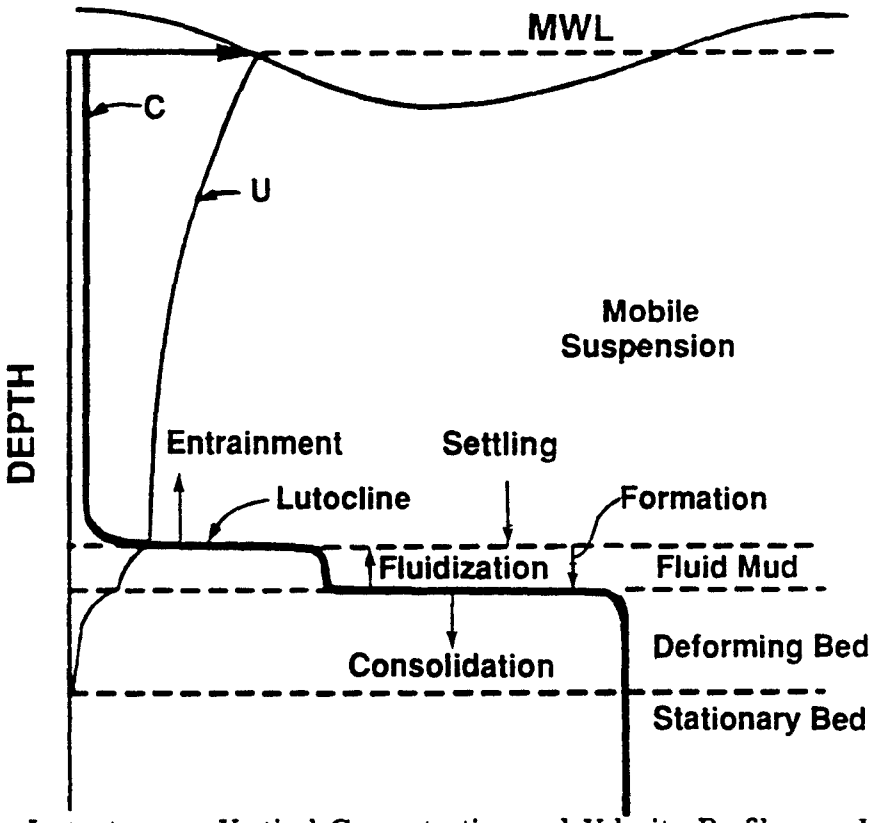

Figure 2.1: Instantaneous Vertical Concentration and Velocity Profiles, an Idealized Description

elastic deformation and subsequent fluidization (Maa, 1986). The deforming bed layer thus develops between fluid mud above and a stationary bed below.

In a general sense, three processes which govern the concentration profile are erosion, deposition and bed consolidation. For cohesive sediments, however, it is not always easy to define terms such as erosion and deposition unambiguously, since the sediment and fluid mixture does not always exhibit a drastic discontinuity between bed and suspension. For example, both gravitational settling of sediment onto the lutocline and formation of the bed by dewatering of fluid mud may be thought of as deposition type processes, while fluidization of the cohesive bed as well as entrainment of fluid mud due to hydrodynamic forcing can be considered to be erosion type phenomena. Knowledge of the sediment transport components, identified in Figure 2.1, is briefly summarized in Chapter 3.

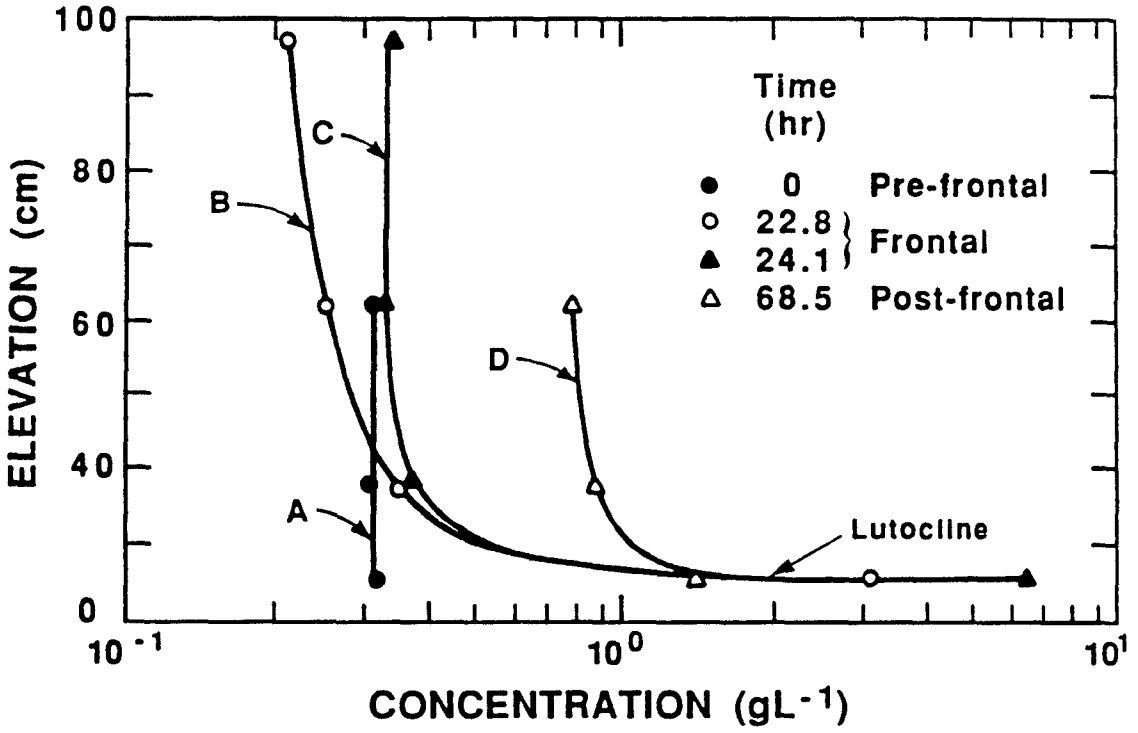

Figure 2.2: Vertical Suspended Sediment Profiles Obtained before, during and after the Passage of a Winter Cold Front at a Wave- Dominated Coastal Site in Louisiana. (adapted from Kemp and Wells, 1987)

2.2 Evolution of Concentration Profile

A representative illustration of suspension concentration profile evolution by wave action over coastal mud flats is presented by the data of Kemp and Wells (1987), as shown in Figure 2.2. Out of the four instantaneous (turbulence-mean), vertical concentration profiles for suspended sediment, profile A represents pre-frontal condition, profiles B and C during the passage of a winter cold front and profile D post-frontal. The data were obtained over a three day period at a site on the eastern margin of the Louisiana chernier plain where the tidal range is less than 0.5 m. Wave height during front passage was on the order of 13 cm and period 7 sec. Of particular interest is the development of a near-bed, high concentration suspension layer by the frontal wind-generated waves (profiles B and C), which was previously absent (profile A). The post-frontal profile D further suggests that this layer may have persisted following the front, conceivably due to the typically low rate at which such a layer

dewaters. The suspension concentration in the upper water column was higher following the front than during the front, possibly due to sediment advection from a neighboring area of higher turbidity.

Concentration profiles qualitatively similar to those shown in **Figure 2.2** have been reproduced in laboratory flume tests involving wave action over soft muddy deposits (Ross, 1988). Notable features were the development of a rapidly saturated fluid mud layer next to the bottom, the occurrence of a persistent lutocline, and relatively low concentrations in the upper column. Furthermore, the upper column profile was observed to be approaching equilibrium at a very low rate. These laboratory observations are supportive of concentration profiles measured in the field by Kemp and Wells (1987).

The elevation of the stabilized lutocline is largely determined by a balance between the rate of turbulent kinetic energy input and the buoyancy flux determined by the sediment settling rate. Diffusion due to the wave field is characteristically slow above the lutocline in the water column, so that the concentration there increases to modest levels only. It follows that surface concentrations are not necessarily representative of what occurs at the bottom.

2.3 Erodible Thickness of Mud Bed

The formation of a high concentration fluidized layer of sediment at the bottom is characteristic of wave-influenced environments. The presence of such a layer with a marked lutocline is not restricted to estuaries and coastal waters, but can also exit in fresh water lakes as reported by Wolanski et al. (1989). In lakes such layers are episodically generated, but due to relatively low rates of dewatering, they may be more common and persistent than previously thought.

Gleason and Stone (1975) reported a concentration value of 102 $mg\ L^{-1}$ at the water surface during a storm event in the southern part of Lake Okeechobee, Florida. By assuming the entire water column of 4.6 m depth had a vertically uniform concentration of 102 $mg\ L^{-1}$, they reported an erodible bed thickness of 2.3 mm (see Figure 2.3*a*) which seems unrealistically small.

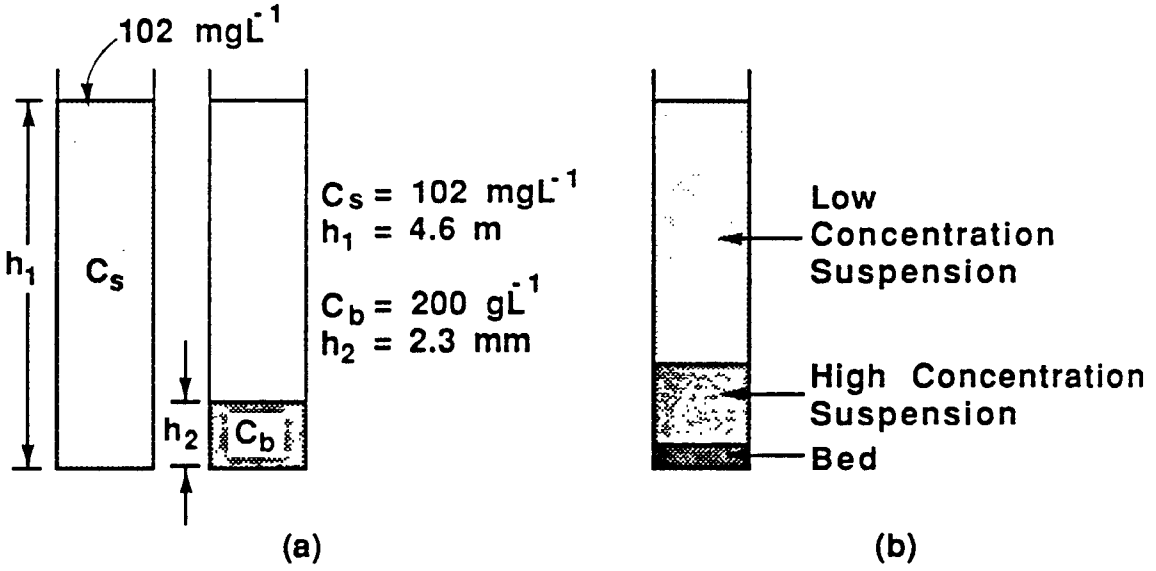

Figure 2.3: a) Relationship Between Uniform Suspension Concentration, C_s, in Water Column of Depth h_1, and The Corresponding Thickness, h_2, of Bed of Concentration C_b; b) High concentration suspension layer between low concentration suspension and bed

On the other hand, on the basis of an examination of bottom cores from the same lake Gleason and Stone (1975) concluded that a "fluid zone" comprised of a sediment deposit of a thickness on the order of $7 - 20$ *cm* probably occurs near the bed in this lake. Since fluidized mud is easily entrained by waves (Maa and Mehta, 1987), it is instructive to determine the depth of erosion by considering the sediment erosion/deposition caused by wave-induced bottom stress to ascertain the significance of the fluid zone in relation to turbidity generation and mud erosion potential. These issues are elaborated upon in the upcoming chapters.

CHAPTER 3
APPROACH TO VERTICAL TRANSPORT PROBLEM

3.1 Governing Equation

The temporal and spatial variations of suspended sediment concentration in the water column subjected to wave action are essentially governed by the mass conservation equation. By considering a differential control volume and equating the time rate of sediment accumulation inside the volume to the net flux of sediment through its boundaries in the cartesian coordinates (x, logitudinal: y, lateral: and z, vertical positive downwards from the water surface), the mass conservation equation for suspended sediment concentration can be written as

$$\frac{\partial C}{\partial t} = -\nabla \cdot \vec{F} \tag{3.1}$$

where $C(x, y, z, t)$ is the instantaneous sediment concentration (mass of sediment/volume of suspension) and $\vec{F}$ is the sediment flux vector. No decay term is of course needed in this equation since suspended sediment mass can be assumed to be conservative. The flux, $\vec{F}$, arises from fluid motion, molecular diffusion and sediment settling:

$$\vec{F} = \vec{U}C - D\nabla C + W_s C\vec{k} \tag{3.2}$$

where $\vec{u}$ is the fluid velocity vector, D the molecular diffusivity (assumed isotropic), W_s the settling velocity of the sediment and $\vec{k}$ the vertical unit vector.

It is usual to express Equation 3.1 in terms of time averaged values. In turbulent flow both fluid velocity and sediment concentration are random variables and these may be separated into (ensemble) mean and fluctuating components:

$$\vec{U} = \overline{\vec{U}} + \vec{U}' \tag{3.3}$$

$$C = \overline{C} + C' \tag{3.4}$$

Inserting these terms into Equation 3.2 and averaging over time results in

$$\overline{\vec{F}} = \overline{\vec{U}C} + \overline{\vec{U}'C'} - D\nabla\overline{C} + W_s\overline{C}\vec{k} \tag{3.5}$$

The second term on the right of this equation represents flux by turbulent movement. By analogy with the molecular diffusion, the turbulent diffusion flux ($\vec{F}_t$) is commonly assumed to be proportional to the gradient of mean concentration:

$$\overline{\vec{F}_t} = \overline{\vec{U}'C'} = -\vec{K} \cdot \nabla\overline{C} \tag{3.6}$$

where $\vec{K}$ is a diffusivity vector with cartesian coordinate components (K_x, K_y, K_z). By adding the flux due to the turbulent diffusivity, the time averaged Equation 3.1 becomes

$$\frac{\partial\overline{C}}{\partial t} = -\nabla(\overline{\vec{U}C} - D\nabla\overline{C} - \vec{K} \cdot \nabla\overline{C} + W_s\overline{C}\vec{k}) \tag{3.7}$$

Since turbulent diffusivity is much greater than molecular diffusivity, the terms corresponding to the latter are usually neglected in the above equation (McCutcheon, 1983). By rearranging Equation 3.1, the following reduced equation is obtained

$$\frac{\partial\overline{C}}{\partial t} + \overline{\vec{U}} \cdot \nabla\overline{C} + \frac{\partial(W_s\overline{C})}{\partial z} = \vec{K} \cdot \nabla^2\overline{C} \tag{3.8}$$

which can also be expanded as

$$\frac{\partial\overline{C}}{\partial t} + \overline{u}\frac{\partial\overline{C}}{\partial x} + \overline{v}\frac{\partial\overline{C}}{\partial y} + \frac{\partial[(W_s + \overline{w})\overline{C}]}{\partial z} = K_x\frac{\partial^2\overline{C}}{\partial x^2} + K_y\frac{\partial^2\overline{C}}{\partial y^2} + K_z\frac{\partial^2\overline{C}}{\partial z^2} \tag{3.9}$$

Since the present analysis is concerned with the vertical structure of sediment concentration, only the vertical transport terms need to be evaluted. In fact, Ross (1988) shows through non- dimensional scaling that in a typical coastal settling the horizontal and vertical advection terms and horizontal diffusion terms can be neglected in a simplified analysis. This allows Equation 3.10 to be reduced to

$$\frac{\partial C}{\partial t} = -\frac{\partial}{\partial z}(F_d + F_s) = \frac{\partial}{\partial z}(K_z\frac{\partial C}{\partial z} - W_sC) \tag{3.10}$$

where the overbars (denoting time average values) have been omitted. Equation 3.10 implies that the two most important terms affecting temporal changes in concentration are the vertical gradient in gravitational settling flux, F_s, and upward diffusive flux, F_d. Since advective effects have been neglected in this equation, the treatment inherently becomes somewhat restrictive as a result. However, it is advantageous to highlight the role of vertical mass fluxes in simulating wave-induced turbidity.

Boundary conditions at the water surface and sediment bed must be defined for the solution of Equation 3.10.

Surface boundary condition

At the water surface, $z = 0$, the net zero flux condition is essential so that

$$F(0,t) = K_z \frac{\partial C}{\partial z} \mid_{z_0} - W_s C \mid_{z_0} = 0 \tag{3.11}$$

This means there is no net transport across the free surface and, therefore, diffusion flux always counterbalances the settling flux.

Bed boundary condition

At the sediment bed, $z = z_b$, it is essential to define a bed flux term, F_b (mass of sediment per unit bed area per unit time) as concerns erosion (F_e) and deposition (F_p) fluxes. Consequently, the bed boundary conditions are specified as

$$F_b(z_b,t) = F_e - F_p \tag{3.12}$$

$$F_e = F_d \mid_{z_b} \; ; \; F_p = F_s \mid_{z_b} \tag{3.13}$$

The magnitudes of F_e and F_p are typically based on bed shear stresses relative to threshold erosion and deposition shear stress values, respectively. It is evident then that the characteristics of the concentration profile are quite sensitive to the time histories of erosion and deposition, since these represent the source or sink to the total mass in suspension.

3.2 Bed Fluxes

The bed fluxes are the overall source and sink components of sediment mass in the evolution of the vertical suspension profile, corresponding to the deposition flux, F_p, and the erosion flux, F_e. In the natural environment, it is often difficult to separately identify the phases of the deposition and those of the erosion as a consequence of the time-dependent nature of the flow field. For the purpose of mathematical modeling, however, deposition and erosion of fine cohesive sediment must be provided as separate, bed shear stress dependent, relationships.

3.2.1 Erosion

The erosional behavior of a mud bed depends on four principal factors: physico-chemical properties of the mud, chemical properties of the eroding fluid, flow characteristics, and bed structure (Parchure and Mehta, 1985). Bed erosion occurs when the resultant hydrodynamic lift and drag forces on the sediment at or below the bed interface exceed the resultant frictional, gravitational and physico-chemical bonding forces of the sediment grain or particle.

Erosion of cohesive sediment beds can be classified in two modes, surface erosion and mass erosion (Mehta, 1986). In the former mode, erosion occurs by separation of individual sediment particles from the bed surface as the hydrodynamic erosive forces exceed the frictional, gravitational and cohesive bed bonding forces. In the latter mode, the bed fails at some level beneath the bed surface where the bulk shear strength is unable to withstand the induced stress. Sometimes, in this case, erosion occurs by dislodging the large pieces of the soil.

Surface erosion is the typical mode in low concentration environments with mild to moderate flow conditions. At higher concentrations, which usually take place under more severe flow conditions, mass erosion often becomes dominant. This type of erosion is preceded by bed fluidization, under erosive flow conditions, in which a large degree of soil structural breakdown occurs. Such behavior is particularly evident under oscillating flows

due to waves (Alishahi and Krone, 1964), and erosion occurs to a depth where the bed shearstrength and the bed shear stress are equal.

Through the bed scour process, which results in decreasing bed elevation, erosion continues until the applied shear stress acts on the bed layer with equal or higher bed shear strength. Typically in prototype environments, the bed shear strength generally increases with depth in the upper few centimeters and it becomes comparatively uniform over depth below that level.

The time rate of increase of suspended sediment mass per unit bed area, m, may be described in a functional form as

$$F_e = \frac{\partial m}{\partial t} = f(\tau_b - \tau_s, \varepsilon_1, \varepsilon_2, \ldots, \varepsilon_N) \tag{3.14}$$

where τ_b is the bed shear stress, τ_s the bed shear strength and ε_i are other erosional resistance defining parameters. Equation 3.14 implies that the erosion flux is mainly determined by the excess shear stress, $\tau_b - \tau_s$.

Expression for the erosion flux for surface erosion under wave action (Maa, 1986) is given as

$$F_e = \varepsilon_M(\frac{\tau_b - \tau_{ce}}{\tau_{ce}}) \tag{3.15}$$

where ε_M is the erosion rate when $\tau_b = 2\tau_{ce}$ and $\tau_{ce} = \tau_s$ is the critical shear strength for surface erosion. Since shear strength of a uniform bed does not vary with depth, the erosion flux (F_e) remains constant, represented by ε_M, under a constant τ_b. Equation 3.15, although obtained from surface erosion studies, may be used for simulating mass erosion in an approximate way. For mass erosion, the rate coefficient, ε_M, is typically much larger than that for surface erosion under comparable conditions and must be evaluated either experimentally or by calibration against available data for specific eroding conditions.

3.2.2 Deposition

The rate of deposition, F_p, is obtained from (Mehta, 1988b)

$$F_p = \frac{dm}{dt} = -pW_sC \tag{3.16}$$

where p is defined as the probability of deposition, W_s is the settling velocity and C is the near-bed suspended sediment concentration. The probability of deposition, p, is described by

$$p = H(1 - \frac{\tau_b}{\tau_{cd}}) \tag{3.17}$$

where τ_b is the bed shear stress, τ_{cd} is a critical shear stress for deposition and $H(\frac{\tau_b}{\tau_{cd}})$ is a heavyside function represented as $H = 1$ when $\tau_b < \tau_{cd}$ and $H = 0$ when $\tau_b \geq \tau_{cd}$.

The concept of deposition probability, originally attributed to Krone (1962), implies that deposition occurs through the sorting of sediment aggregates which occurs because of the high rates of flow shearing near the bed boundary. When the aggregates are strong enough to withstand the near-bed shear stress, they stick to the bed and, if not, they are disrupted and resuspended.

For non-uniform sediment the settling velocity is usually represented by its distribution, $\phi(W_s)$, and its dependence on suspension concentration is considered on a class by class basis. Integrating Equation 3.16 under these conditions, Mehta and Lott (1987) suggested the following solution for the instantaneous concentration $(C(t))$

$$\frac{C}{C_o} = \sum_{i=1}^{N} \phi(W_{s_i}) \exp - H[1 - \frac{\tau_b}{\tau_{cn}}(\frac{W_{sn}}{W_{s_i}})^{\alpha}] \frac{W_{s_i}}{h} t \tag{3.18}$$

where

$$\alpha = \frac{\ln(\frac{\tau_{cm}}{\tau_{cn}})}{\ln(\frac{W_{sm}}{W_{sn}})} \tag{3.19}$$

and C_o is the initial suspension concentration, N is the total number of classes, $\phi(W_{s_i})$ is the frequency distribution of settling velocity with maximum value W_{sm} and minimum value W_{sn}, h is the water depth, and τ_{cm} and τ_{cn} are the maximum and minimum values, respectively, of the critical shear stress for deposition, τ_{ci}.

For $\tau_b \geq \tau_{cm}$ no initially suspended sediment will deposit, while for $\tau_b \leq \tau_{cn}$ the entire mass of suspended material will finally deposit. A consequence of settling by class is that for $\tau_{cn} < \tau_b < \tau_{cm}$ a fraction of the initially suspended sediment for which $\tau_{ci} < \tau_b$ will not deposit at steady state. A further consequence is that the size of the particles remaining in suspension will differ from the size in the deposit at steady state.

If the properties of the settling sediment are uniform, then $N = 1$ and $\tau_{cn} = \tau_{cm} = \tau_{cd}$. Consequently Equation 3.18 reduces to

$$\frac{C}{C_o} = \exp\left[-H(1 - \frac{\tau_b}{\tau_{cd}})\frac{W_s}{h}\right]t \tag{3.20}$$

A typical value for τ_{cd} is considered to be 0.1 $N\ m^{-2}$ (Mehta, 1988b). The settling velocity, W_s, is the critically important pamameter in specifying F_p, and is discussed further in the following section.

3.3 Settling Velocity

The settling velocity of cohesive sediment strongly varies with concentration in suspension. Moreover, the settling velocity is a function of the suspension and not exclusively of the sediment (Mehta, 1988a).

Aggregation occurs as a consequence of interparticle collision and cohesion of particles. Cohesion depends primarily on the mineralogical composition and the cation exchange capacity of the sediments (van Olphen, 1963). Collision frequency is dependent on Brownion motion, fluid shearing, and differential settling. Among these facters contributing to aggregation, fluid shearing seems to be the most important. Differential settling, however, becomes the most dominant factor under quiescent settling conditions such as at the time of slack water in estuaries (Mehta, 1988a). Brownion motion in natural environments is the least significant mechanism of the three (Krone, 1962).

Aggregated sediments or flocs have peculiar characteristics which differ from those of primary individual particles. Their relative particle density is reduced by the interstitial trapped water, and this causes a reduction in settling velocity. However, their shape and size become more spherical and larger with correspondingly reduced drag. Since the reduction in drag and increased size are much more significant than the decrease in density, the settling velocities of the flocs are substantially higher than those of individual particles.

Figure 3.1 is a descriptive plot of the relationship which may typically be found between the settling velocity, W_s, and the suspended sediment concentration, C. Also shown is the variation of the corresponding settling flux, $F_s = W_s C$. The settling velocity regime can be

conveniently divided into three sub-ranges depending upon the concentration. These are identified as free settling, flocculation settling and hindered settling. A short description of the physical characteristics of each regime is given below.

3.3.1 Free Settling

Free settling occurs in the range of C less than C_1 as identified in Figure 3.1. In this range the particles or aggregates settle independently without mutual interference and the settling velocity no longer depends on concentration. For cohesive sediments, the upper concentration limit, C_1, is considered to be in the range of 0.1 to 0.3 gL^{-1} (Mehta, 1988a).

The terminal velocity of individual sediment particles is determined by a force balance between drag and net negative buoyancy. For a spherical particle of diameter d, the settling velocity over the entire range of Renolds number, R_e, is expressed as

$$W^2 = \frac{4}{3}\frac{gd}{C_D}\frac{(\rho_s - \rho_w)}{\rho_w} \tag{3.21}$$

where C_D is the drag coefficient, g is the gravity acceleration, and ρ_s and ρ_w are sediment and fluid densities, respectively.

In the Stokes range ($R_e < 0.1$) the drag coefficient is given by

$$C_D = \frac{24}{R_e} \tag{3.22}$$

and the settling velocity is given by Stokes law (Vanoni, 1975)

$$W = \frac{gd^2}{18\nu}\frac{(\rho_s - \rho_w)}{\rho_w} \tag{3.23}$$

where ν is the kinematic viscosity of the fluid. For large R_e, C_D is still a function of R_e but cannot be expressed analytically.

The influence of the particle shapes on the settling velocity is typically expressed by an effective particle diameter. As this diameter is used, Equation 3.23 can be considered to be valid for the fine sediment in dispersed or flocculated conditions (Ross, 1988).

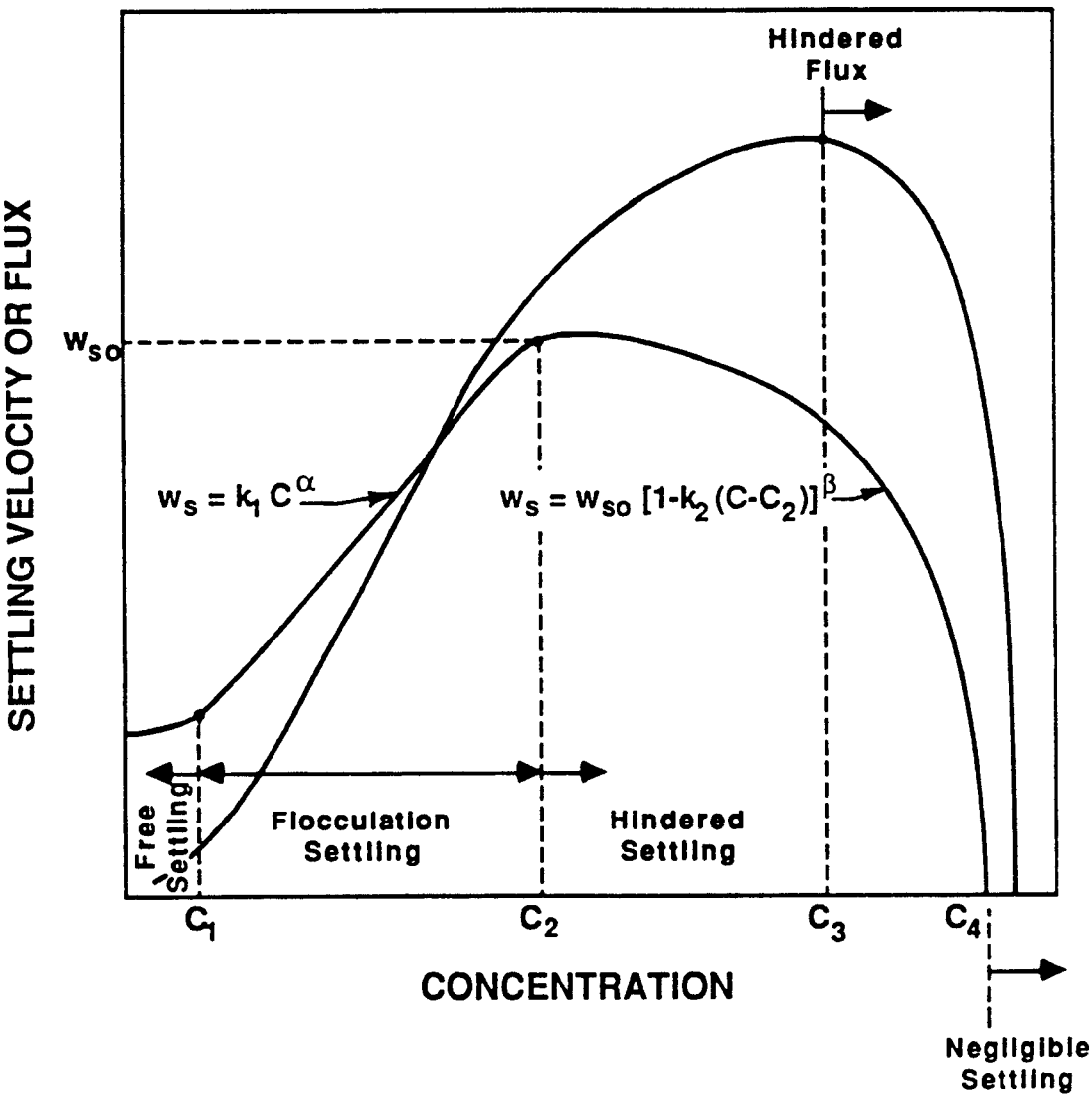

Figure 3.1: A Schematic Description of Settling Velocity Variation With Suspension Concentration of Fine-Grained Sediment

3.3.2 Flocculation Settling

Between concentrations C_1 and C_2, identified as the flocculation settling range, increasing concentration leads to increasing interparticle collision and consequently enhanced aggregation. This in turn means that the settling velocity increases with concentration due to the formation of stronger, denser and possibly larger aggregates.

In the flocculation settling range, the typical relationship of the settling velocity to the concentration is

$$W_s = k_1 C^{\alpha} \tag{3.24}$$

Theoretically, α is 4/3 as indicated in Figure 3.1, although the actual value typically varies between about 0.8 and 2 (Krone, 1962; Mehta, 1988a). The proportionality coefficient, k_1, can vary by an order of magnitude depending upon sediment composition and flow environment.

3.3.3 Hindered Settling

At concentrations in excess of C_2, the occurrence of an aggregate network hinders the upward transport of interstitial water. Consequently, W_s decreases with increasing C (Kynch, 1952) as indicated in Figure 3.1. This is commonly termed hindered settling.

The general expression for the settling velocity in the hindered settling region is

$$W_s = W_{so}[1 - k_2(C - C_2)]^{\beta} \tag{3.25}$$

where W_{so} is the maximum settling velocity that corresponds to C_2, k_2 is the inverse of the concentration in excess of C_2 at which $W_s = 0$ and theoretically β is 5. At concentrations greater than C_4 there is negligible settling.

3.3.4 Settling Flux

The behavior of the settling flux, F_s, is also shown in Fig. 3.1. Although the settling velocity decreases at concentrations in excess of C_2, F_s increases with C up to C_3 where it attains a peak value of F_{so}. This is due to the minuscule decrease of settling velocity

between C_2 and C_3 in comparison with the increase of concentration. At values of C higher than C_3 the flux also decreases relatively rapidly with increasing C.

3.4 Diffusive Flux

3.4.1 Wave Diffusion

There have been many attempts to estimate the mass diffusivity (or eddy diffusivity), K, as related to the momentum diffusivity (or eddy viscosity), E. Analogous with the dynamic viscosity μ, in Stokes' law for laminar flow, momentum diffusivity for the Reynolds stress in turbulent flows is defined by

$$\tau_{ij} = -\rho\overline{u_i' u_j'} = -\rho E_{ij}\frac{\partial \overline{u_i}}{\partial x_j} \tag{3.26}$$

where τ_{ij} are the components of the turbulent shearing tensor, $\rho\overline{u_i' u_j'}$ are the components of the Reynolds stress tensor, ρ is fluid density, and E_{ij} represent the components of the momentum diffusivity tensor. If turbulence is isotropic, $E_{ii} = E_{jj} = 0$ and $E_{ij} = E_{ji} = E$. It should be noted that E is approximately proportional to the first power of the mean velocity $\overline{u}$, since viscous forces in turbulent flow are approximately proportional to the square of the mean velocity rather than to its first power as in laminar flow (Schlichting, 1979). Consequently, E is not a property of the fluid like viscosity (μ) for laminar flow, but is a property of the flow and depends on the mean velocity. The ratio between mass (K) and momentum (E) diffusivities is commonly expressed by the turbulent Schmidt number

$$S_t = \frac{E}{K} \tag{3.27}$$

For many fine sediment related practical applications it may be assumed that $S_t = 1$ (Teeter, 1986). Consequently, this means the turbulent momentum diffusivity can be taken to be equal to the mass diffusivity.

The most commonly applied expression of vertical variation in mass diffusivity for turbulent unidirectional flow was developed by Rouse (Vanoni, 1975). Under wave action, however, the expression for the mass or momentum diffusivity has not been fully clarified yet. Since the oscillation of waves plays an important role in the diffusion process, the solution for

the diffusivity problem becomes more complicated. Kennedy and Locher (1972), Hwang and Wang (1982), and Maa (1986) have reviewed currently popular expressions for diffusivity under waves. There seems to be little consistency in the forms. Although most investigators have treated diffusivity as constant, laboratory experiments suggest that diffusivity varies with depth in the water column (Bhattacharya, 1971).

A plausible expression for the diffusivity under waves is given by Homma et al. (1962). By direct analogy to the mixing length theory, they gave the following expression:

$$K = \beta b^2 |\frac{\partial u}{\partial z}| \tag{3.28}$$

where β is a empirical constant, b is the minor radius of a water particle orbit, u is the horizontal component of orbital velocity, and z is the vertically downward negative at the water surface. As pointed out by Kennedy and Locher (1972), however, several shortcomings have been found in this expression. Again, Homma et al. (1965) presented a modified equation, introducing a mixing length, l, and following the hypothesis of von Karman in the form

$$l = \beta_1 \frac{\frac{\partial u}{\partial z}}{\frac{\partial^2 u}{\partial z^2}} \tag{3.29}$$

Since in the linear wave theory u is given as

$$u = \frac{H}{2}\sigma \frac{\cosh k(h+z)}{\sinh kh} \tag{3.30}$$

diffusivity is calculated as

$$K = \beta_2 \frac{H\sigma}{k \sinh kh} \frac{\sinh^3 k(h+z)}{\cosh^2 kh(h+z)} \tag{3.31}$$

where β_2 is a constant and equal to $\beta_1^2/2$, H the wave height, σ the wave frequency, and k the wave number.

Another plausible expression is given by Hwang and Wang (1982). They indicate, in the determination of diffusivity under wave field, Prandtl's mixing theory may not be applicable due to the large scale of the wave motion. Emphasizing the dominant role of the vertical components of wave induced particle velocity in the diffusion process, they assume that

diffusivity is proportional to the vertical velocity component of wave motion as well as the vertical excursion of the water particle, thus expressing the diffusivity as

$$K = \alpha_w \, w(z) \, 2b(z) \tag{3.32}$$

where α_w is a constant and $w(z)$ is the vertical orbital velocity. Again using linear wave theory, w and b are given as

$$w = \frac{H\sigma}{2} \frac{\sinh k(h+z)}{\sinh kh} \tag{3.33}$$

$$b = \frac{H}{2} \frac{\sinh k(h+z)}{\sinh kh} \tag{3.34}$$

and substituting Equations 3.33 and 3.34 into Equation 3.32, the following expression for K is obtained

$$K = \alpha_w \sigma H^2 \frac{\sinh^2 k(h+z)}{2 \sinh^2 kh} \tag{3.35}$$

This equation is considered as a promising expression, based on energy dissipation consideration, for diffusivity under wave action (Ross, 1988). Thimakorn (1984) also gave a diffusion coefficient similar to that given by Hwang and Wang (1982) to predict vertical concentation profiles for the suspension of natural clay in a wave flume.

It should be noted that Equation 3.35 is not applicable inside the wave boundary layer. Effects of the boundary layer next to the bed greatly increase the vertical mixing under waves due to the relatively large velocity gradients and shear (Neilson, 1979). However, diffusion in this layer is often neglected since it is very small (Maa, 1986). Outside the boundary layer, the velocity amplitude gradients increase with distance above the bottom to a maximum at the surface. This is the basis of Equation 3.35 given above.

3.4.2 Stabilized Diffusion

Suspended fine sediments increse the bulk density of suspension and lead to the vertical variation of suspension density. Bulk density, ρ_B, is related to suspension concentration, as

$$\rho_B = \rho_w + C(1 - \frac{\rho_w}{\rho_s}) \tag{3.36}$$

where ρ_w and ρ_s are the water and sediment granular densities, respectively. When the bulk density increases upwards the stratification is stable and it becomes unstable when the density variation is reversed.

Stratification due to bulk density variation alters the vertical fluid momentum and mass mixing characteristics. Furthermore, the diffusivities of momentum and mass are not affected in the same manner, the former usually having larger values (French, 1985; Oduyemi, 1986). In the case of flow with stable density stratification, vertical diffusion of mass and momentum are impeded because the stabilizing gravitational force of sediment suspension acts against the destabilizing shear induced force. If the density gradient is large enough, upward diffusion can be largely suppressed and will result in the formation of a stable interface (lutocline) with pratically no mixing between two layers.

For turbulence under conditions of local equilibrium, the most obvious measure of stability is given by the flux Richardson number (Abraham, 1988) R_f, which represents the mixing efficiency (the efficiency of the conversion from turbulent kinetic energy to potential energy):

$$R_f = -\frac{g\overline{w'\rho'_B}}{\rho_B \overline{u'w'}(\frac{\partial u}{\partial z})} = \frac{R_i}{S_t} \tag{3.37}$$

where R_i is the gradient Richardson number defined as

$$R_i = \frac{g}{\rho_B} \frac{\frac{\partial \rho_B}{\partial z}}{(\frac{\partial u}{\partial z})^2} \tag{3.38}$$

where g denotes gravity acceleration, and z represents the vertically downward positive axis. Positive values of R_f indicate stable stratification, negative values denote unstable stratification, and $R_f = 0$ corresponds to a neutral (non-stratified) condition. The dimensionless quantity R_f clearly determines the relative role of buoyancy in the generation of turbulent energy. In the case of $R_f < 0$, turbulent energy is increased and for $R_f > 0$, buoyancy becomes negative, indicating that kinetic energy is lost. If a positive R_f becomes large enough, it leads to complete suppresion of all turbulence. For simplicity of treatment in this study, the turbulent Schmidt number, S_t, will be assumed to be equal to one, so that $R_f = R_i$.

Classical phenomenologically based forms for mass diffusivity in stratified flow are typically of the Munk and Anderson (1948) form as

$$K_z = \frac{K_n}{(1+\beta R_i)^\alpha} \tag{3.39}$$

where K_z and K_n are the vertical mass diffusivities for stratified and neutral flows, respectively, and α and β are generally non-negative empirical constants. Note that for positive α and β, increasing density gradient ($\frac{\partial \rho_B}{\partial z}$) leads to increasing R_i and consequently decreases K_z relative to K_n. It means that stratification acts to reduce diffusion by damping.

Incorporating gravitational stabilization in wave diffusivity induces a high degree of non-linearity between the diffusive flux, F_d, and the vertical concentration gradient, $\frac{\partial C}{\partial z}$. The diffusive flux is expressed as

$$F_d = -K_z \frac{\partial C}{\partial z} \tag{3.40}$$

which indicates direct dependence of F_d on $\frac{\partial C}{\partial z}$. In the presence of density stratification, by substituting Equation 3.38 into 3.39, the diffusive flux becomes

$$F_d = -\frac{K_n}{(1+\beta R_i)^\alpha} \frac{\partial C}{\partial z} \tag{3.41}$$

From Equations 3.36 and 3.38, it is obvious that R_i in the above equation is a direct function of concentration gradient, $\frac{\partial C}{\partial z}$ by virtue of the bulk density gradient term, $\frac{\partial \rho_B}{\partial z}$. As a result, Equation 3.41 indicates that if β is not zero the diffusive flux is inversely proportional to $\frac{\partial C}{\partial z}$ due to R_i term as well as directly dependent on $\frac{\partial C}{\partial z}$. Due to this fact the diffusive flux is nonlinear in concentration gradient.

Figure 3.2 shows a plot of negative F_d versus $\frac{\partial C}{\partial z}$ for the coefficient sets given by Ross(1988). As observed in the figure, the flux initially increases with low values of $\frac{\partial C}{\partial z}$, reaches a maximum and then slowly decreases. For very high values of $\frac{\partial C}{\partial z}$, the gradient of the diffusive flux, $\partial F_d / \partial (\frac{\partial C}{\partial z})$ becomes zero and, with stabilized perturbations and local minima in mixing, a lutocline is developed in the vertical concentration profile. Consequently, the formation of lutocline is strongly related to the nonlinear dependence of F_d on $\frac{\partial C}{\partial z}$. Since the sediment settling acts against the vertical mixing, the growth and stability of

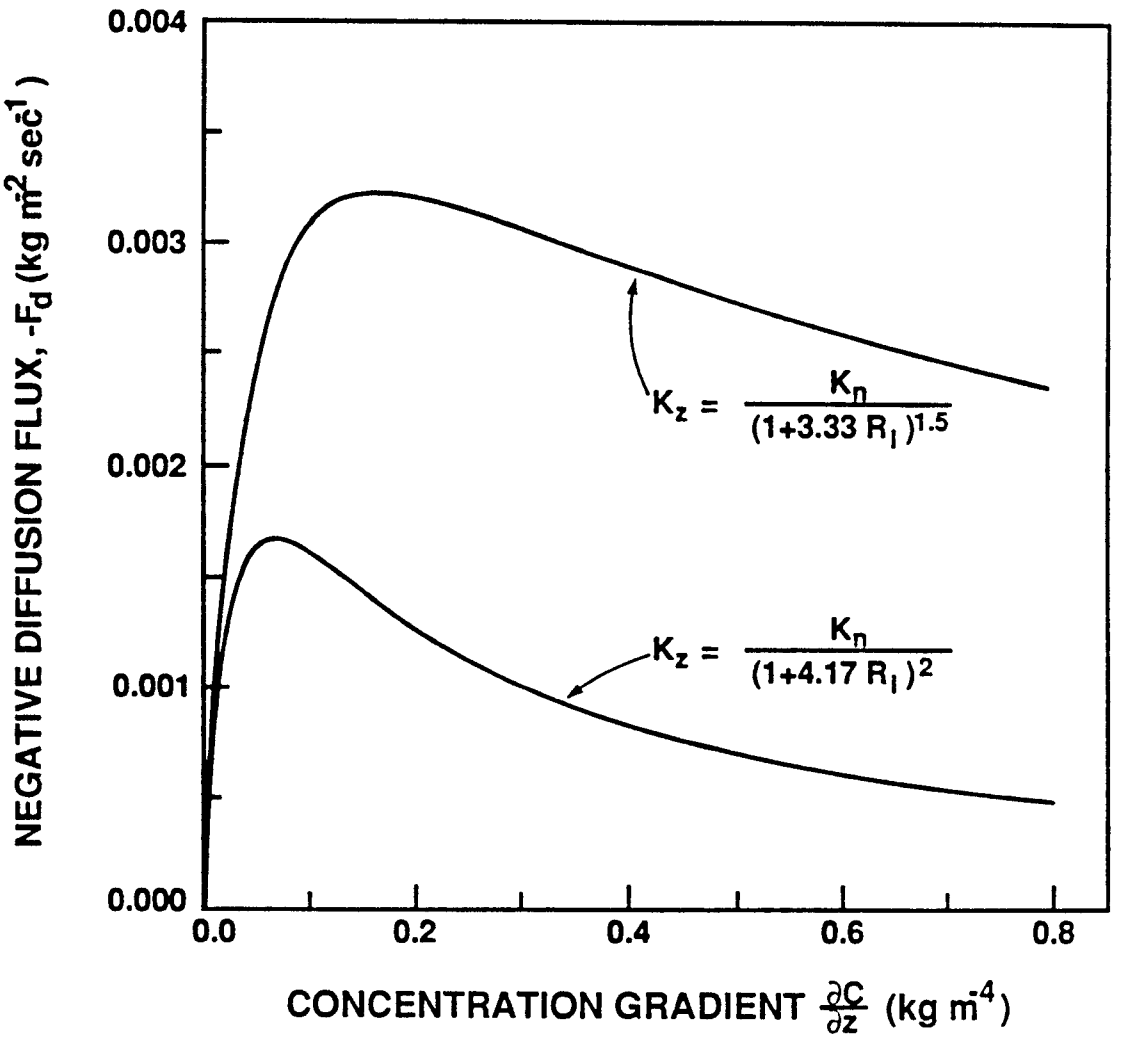

Figure 3.2: Nonlinear Relationship Between Diffusive Flux, F_d, and Concentration Gradient, $\frac{\partial C}{\partial z}$

the lutocline is further enhanced. This implies that lutoclines can be much more persistent in high sediment environments than other types of pycnoclines.

CHAPTER 4
EXPERIMENTS

4.1 Introduction

Field data collection and laboratory experiments were performed to determine the characteristic parameters and relationships related to the bottom fine sediment erodibility under the wave effects in Lake Okeechobee. These experiments consisted of characterization of the sediment, bed property tests, settling tests and erosion tests. Settling tests were carried out to determine the relationship between settling velocity and suspension concentration, while erosion tests were conducted to obtain relationships between the erosion rate, bed shear stress and bed density.

4.2 Characterization of Sediment

The identification of important factors characterizing the physico- chemical properties of the sediment is basically related to the prediction of cohesive sediment tranport. Mehta et al. (1986) specified essential properties of cohesive sediment in terms of grain size, mineralogical composition, percentage of organics, and the cation exchange capacity. In this section, these properties of sediment particles, except the cation exchange capacity, are discussed following a brief description of methodology for each test.

To specify the characteristics of fine sediment in Lake Okeechobee, samples were taken from the bed in March 1988 at five locations, sites 1, 2, 3, 4 and 5, identified in Figure 4.1. These samples were also used in the settling and erosion tests. Mud samples from site 1, 3 and 6 were additionally collected in October 1988 to supplement the spatial representation, and to evaluate possible effects of seasonal variations of settling properties. Water depths at each site were 3.96 m at site 1, 4.57 m at both sites 2 and 3, 4.88 m at site 4, 4.27 m at

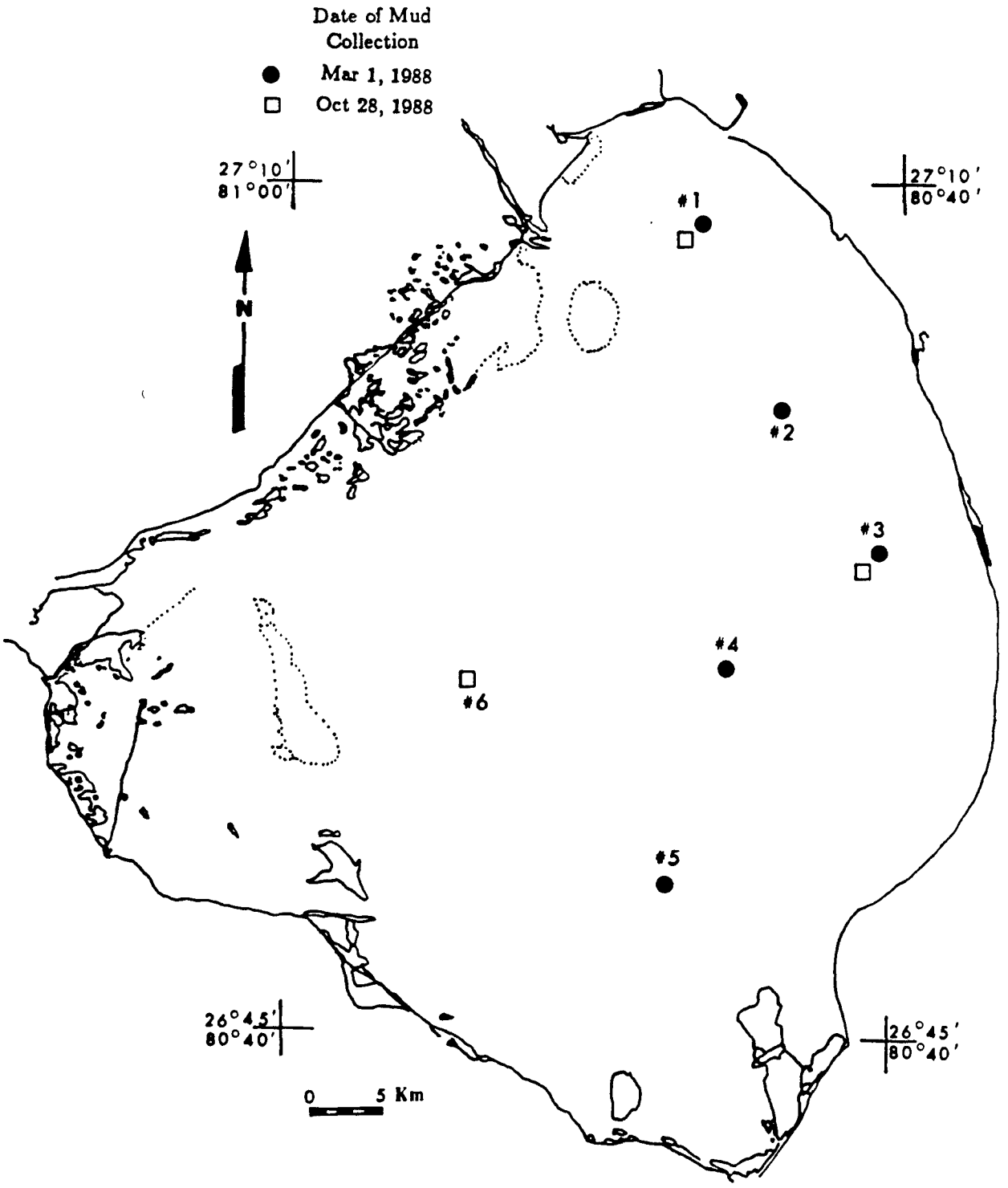

Figure 4.1: Sediment Sampling Sites in Lake Okeechobee

site 5, and 3.35 m at site 6. The mud samples were collected by using a grab sampler and brought to the Coastal Engineering Laboratory of the University of Florida.

The mud samples were first separated into coarse and fine-grained fractions by wet sieving through No. 200 Tyler sieve with an opening of 74 μm. This procedure was necessary due to the presence of extraneous large matter in the sediment. It was found that fine-grained material accounted for between 75 % to 90 % of the material. This means that the material was almost entirely in the fine size range.

4.2.1 Particle Size Distribution

The fine-grained fractions from all five locations were subjected to standard hydrometer test to obtain the grain size distribution (ASTM, 1987). The hydrometer test is a widely used method for estimating the soil particle size distribution ranging from the opening size of No. 200 sieve to around 0.001 mm. A modification was made so that the sediment was not dried initially, because Krone (1962) showed that redispersion of the flocculated sediment, once dried, remained incomplete. Therefore, the sediment used for the test was dried after finishing the hydrometer test in order to determine the total dry sediment weight required for the calculation of particle size distribution.

The procedure used for the hydrometer test is as follows:

1. A sufficient amount of wet mud was taken in a graduated cylinder (1000 ml) so that the dry weight of the sediment was about 50 g and was mixed with 125 ml of 4 % Calgon solution in order to disperse the sample easily.

2. The sediment mixture was allowed to stand about 16 hours, and then the sample was dispersed by a mixer for 3 minutes.

3. The entire mixture was transferred to the sedimentation cylinder. Distilled water was added to fill the cylinder to the 1000 ml mark. A control cylinder was prepared and filled with distilled water and 125 ml of the 4 % Calgon solution.

4. In order to mix the contents well, the cylinder of sediment suspension was carefully shaken. Hydrometer readings, R_a, were taken after 2, 5, 15, 30, 60, 250, 1440, 2880 and 4320 minutes.

Corrected hydrometer readings, R_c, were computed as

$$R_c = R_a - Zero\ correction + C_T \tag{4.1}$$

where C_T is the temperature correction factor, and "zero correction" represents both meniscus correction and dispersion agent correction.

Since ASTM 151H soil hydrometer made by Ertco was used in the tests, the percentage of the sediment finer (by weight) was calculated from

$$P = [\frac{(100000/W)\ G_s}{G_s - G_1}](R_c - G_1) \tag{4.2}$$

where G_s is the specific gravity of the sediment particles, G_1 is the specific gravity of the fluid in which soil particles are suspended, and W is the (oven-dry) mass of sediment used in the hydrometer test. The diameter of particle (corresponding to percent finer than a certain grain size in cumulative size distribution) was calculated according to Stokes' law.

Specific gravity of sediment particle (G_s) in Equation 4.2 was obtained using a standard method (ASTM, 1987) by filling the sediment-water mixture into a 500 *ml* volumetric flask and de- airing the mixture under high vacuum. Sediments from all sites were subjected to this measurement giving an average value of G_s equal to 2.14. Note that since G_s is equal to ρ_s/ρ_w, sediment granular density becomes 2.14 $g\ cm^{-3}$ with a given (assumed) value of $\rho_w = 1\ g\ cm^{-3}$.

Figure 4.2 shows the grain size distribution of the dispersed sediment from sites 1 through 5. The sediments from site 1 exhibited the smallest percent (28 %) of the clay size sediment, while sediment from site 5 exhibited the largest percent (44 %) of clayey material among the five sites. The material from sites 2, 3, and 4 showed the clay size sediment to be 29 %, 40 % and 39 %, respectively. The remainder were in the silt size range.

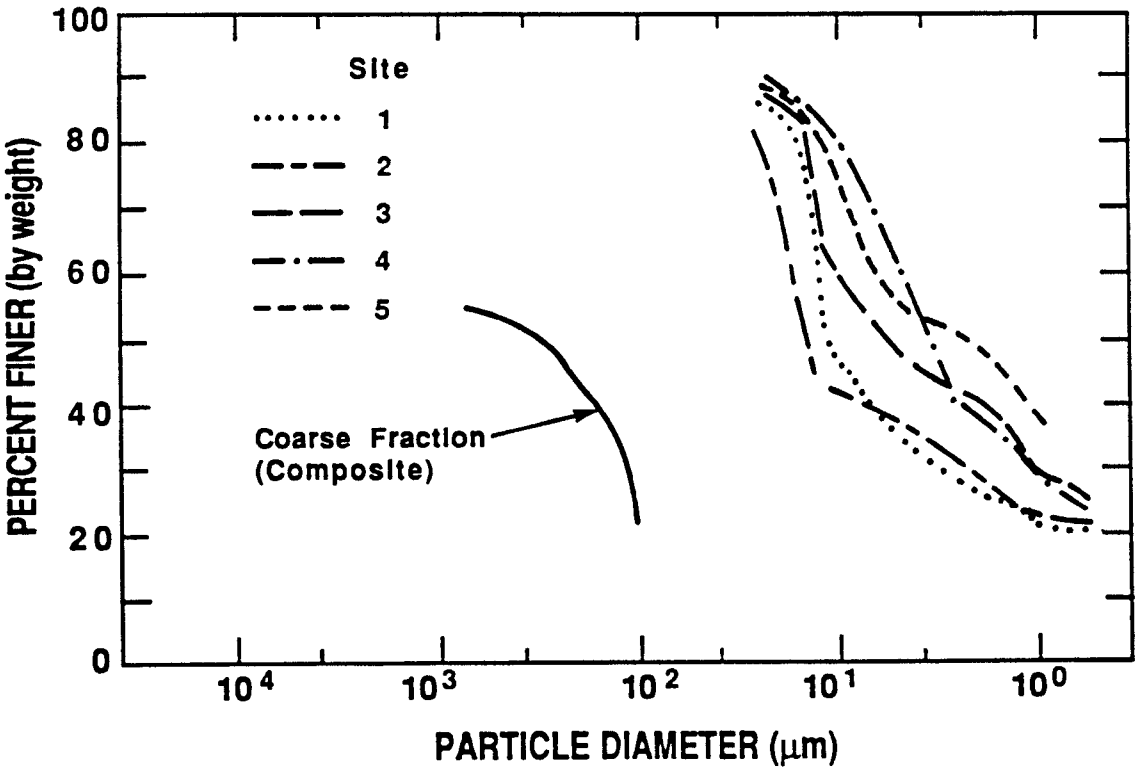

Figure 4.2: Fine-grained and Coarse (Composite) Particle Size Distributions from Sites 1, 2, 3, 4 and 5

Table 4.1 gives fine-grained particle size characteristics based on size distributions presented in Figure 4.2 for the fine-grained fractions at the five sites. This table shows that the dispersed median diameter, d_{50}, ranged from 3.4 to 14.4 μm, which is in the medium silt size. The fine-grained portion of the sediment from all sites seem to be comparatively similar. However, it is also apparent that the median diameters of fine-grained fractions from sites 3, 4, and 5 in the middle of the lake were somewhat smaller than the diameters from sites 1 and 2, which are located near the Kissimmee River. Furthermore, the sorting coefficient, $S_o = (d_{75}/d_{25})^{1/2}$, of the material from all sites appears to be relatively large, which is indicative of graded (broad) size distributions.

The coarse fractions from all sites were initially combined because they were relatively small in quantity. A large amount of shelly detritus was present in the composite sample. A standard sieve analysis was conducted on the composite sample to determine the size distribution of the coarse particles (ASTM, 1987). Sieves #20, #40, #60, #100, #140,

Table 4.1: Sediment Characteristics

Site No.	Fine Particle Characteristics				Ignition Loss (%)
	d_{25} (μm)	d_{50} (μm)	d_{75} (μm)	S_o (μm)	
1	15	10	2	2.7	40
2	24	15	1	4.1	36
3	13	7	0.6	4.5	43
4	8	0.4	0.7	3.4	38
5	10	3	0.6	4.2	41

and #160 were selected for the analysis. Figure 4.2 also shows coarse-grained particle size distribution. The median diameter of the coarse material is 400 μm (0.4 mm).

4.2.2 Organic Material

Characterization test for the amount of organic matter in the sediment, as defined by loss on ignition, was conducted at the Soil Science Laboratory of the University of Florida, using the standard combustion method (ASTM, 1987). Initially, 50 g of fine-grained wet sample was dried in an oven for a day at 50°C to remove the moisture, and cooled in a desiccator. Five grams of the dried sample were heated again for 12 hours in a combustion furnace at 550°C. This procedure ashed the organic matter in the sample. The ashed sample was carefully removed from the furnace and placed in the desiccator to cool. Then, the ashed sample was weighed again and the difference between the two weights was used to calculate the percentage of organic matter in the sediment. Table 4.1 gives the resulting percentage of organic content (loss on ignition) by weight of the sediment at sites 1 through 5.

The percentage of organic content is fairly uniform, ranging from 36 % to 41 %, and a considerable amount of organic matter is present in the sediment. The high organic fraction in the sediment is indicative of the rather low value of ρ_s (2.14 $g\ cm^{-3}$). Since the density of a organic matter has lower value than ρ_s for clayey soil, ρ_s tends to be low when the organics fraction in the sediment is high. Otsubo et al. (1987) also observed this trend in the relationship between the organics fraction in the sediment and ρ_s through the field

studies on the physical properties of sediment (water content, G_s, and loss on ignition) in Lake Kasumigaura in Japan. In their study they also recognized no particular seasonal or long-term change in three physical parameters for all sampling sites and suggested that the seasonal change of the organic content, including the other physical parameters, need not be considered in the sediment resuspension model. Although a comprehensive sediment sample program is still required to investigate seasonal variation of the organic content in Lake Okeechobee, this variation may in fact be negligible, following the observation by Otsubo et al. (1987).

4.2.3 Mineralogical Composition

In order to determine the predominant clay and non-clay constituents, X-ray diffraction analysis of the fine-grained fraction from site 5 was conducted in the Soil Science Laboratory. The results indicated the presence of clay minerals including kaolinite, sepiolite and montmorillonite. Kaolinite was the predominant constituent among them.

The presence of sepiolite in the sediment must be noted. This agrees with a previous report on the occurrence of sepiolite in the mineral portion of sapric horizons in a histosol south of Lake Okeechobee (Zelazny and Calhoun, 1977). Sepiolite is chemically precipitated and crystallized in alkaline sediments with significant quantities of Si and Mg (Zelazny and Calhoun, 1977). The greatest deposits of sepiolite occur throughout the world in association with non-clastic sediments such as carbonatic rocks, opal, chert, and phosphates.

The presence of quartz, a non-clay mineral, was detected in the sediment. Traces of other clay and non-clay minerals appear to be present as well, but their identification requires further confirmatory tests.

4.3 Bed Properties

Bed properties were examined through the measurements of the bed density and the vane shear strength of mud core samples. The bed density is important in assessing bed erodibility, and bed density and the vane shear strength together are important in estimating the fluidized mud thickness.

4.3.1 Field and Laboratory Work

A small vibracorer designed at the Coastal Engineering Laboratory of the University of Florida was used to collect the bottom sediments at various sites in Lake Okeechobee (Kirby et al., 1989). A total of 31 sites, which are identified in Figure 4.3, were selected. The selected sites were not strictly limited to the muddy zone but covered most relatively deep sedimentary zones in the lake, although most of them were within the muddy area.

The vibracorer basically had a concrete vibrator powered through a flexible drive from a gasoline motor on board the survey vessel. The concrete vibrator was clamped onto the top of a drill barrel. The drill barrel was 1.83 m in length and had an i. d. of 9.4 cm. It was fitted with a transparent CAB liner to contain the sample. A steel cutting shoe, plastic, petal-type core catcher and a non-return valve were fitted to permit core penetration and retention. A threaded collar on the top of the corer allowed a guide tube to be fitted. This was attached after the vessel had anchored and the corer had been hung over the side in the water. The guide tube permitted the vertical position of the corer to be maintained during drilling operations as well as allowed visual monitoring of bed penetration.

When the vibracorer was recovered, the transparent liner was capped at its base and removed from the core barrel. In circumstances where very loosely consolidated fluid mud type deposits were observed in the upper surface of the mud deposits, a Paar (DMA 35) densimeter was used on board the vessel to measure the density structure of the upper, lowly consolidated mud layers. This measurement was essential because the vertical structure of the loosely consolidated mud layers could have been easily altered during transport to the laboratory. The Paar densimeter is a small, battery operated device for accurate measurement of the density of slurries, using the principal of resonance of the vibrating sample. The frequency of resonance is directly influenced by the slurry, which is converted to density in the instrument and displayed digitally. The core liner was then capped at the top and numbered before being stored in an upright position for transport to the laboratory.

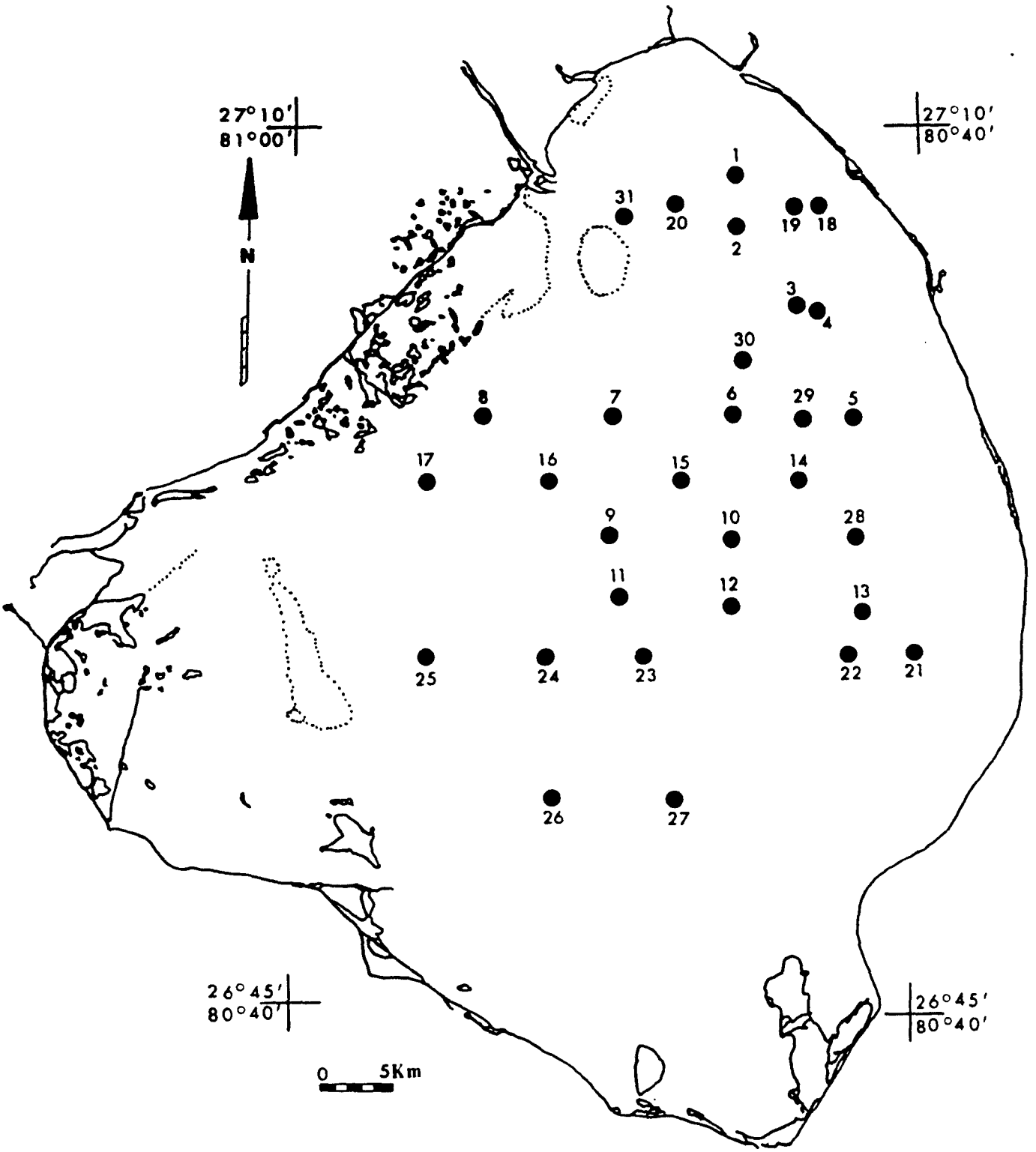

Figure 4.3: Bottom Core Sampling Sites in Lake Okeechobee (In the text a prefix OK and a suffix VC are added to denote these sites)

In the laboratory the cores were laid in a clamp and only the liner was cut down opposite sides with an electric saw. The core was then bisected by drawing a cheese wire down the cuts and through the sample. The bisected core was then opened so that both halves could be inspected. Shortly after cutting and before the sample could dry out to any extent, bulk density and shear strength measurements were carried out.

The bulk densities were measured gravimetrically and the shear strength measurements were conducted with a small calibrated vane, made by Wykeham Farrance Eng. (serial No. 971). Measurement was made at 5 *cm* increments of depth and the vane was inserted sideways into the axial (thickest) part of the halved core.

4.3.2 Bulk Density and Shear Strength Profiles

The measured bed bulk density and shear strength profiles for each site, including the descriptions of the observed vertical structure of the core mud samples, are contained in Appendix A. The profiles indicate that many of the cores had a loosely consolidated upper zone of fluid mud (in which in situ measurements of density were made). No shear strength readings are available in this low strength upper zone, first because shear strength measurements were only made in the laboratory and secondly because the strengths were below the resolution of the instrument.

In the firmer muds, it was observed that the density and vane shear strength measurements showed a close relation, despite obvious data scatter. Figure 4.4 shows density and shear strength profiles in a core sample from site OK2 VC. From the figure it is noted that the density and shear strength values generally show an increase with depth mainly due to self-weight consolidation effects.

Other samples also showed an overall increase in density and strength with depth, while the detailed profile showed a series of sharp density and strength reversals. As shown in Figure 4.5, the vane shear strength and density peaks and troughs are generally coincident (i. e., OK10 VC). In this core, however, while the shear strength increased with depth, the density of the weak mud layers was lower at 50 *cm* than at 2 *cm* below the surface. This

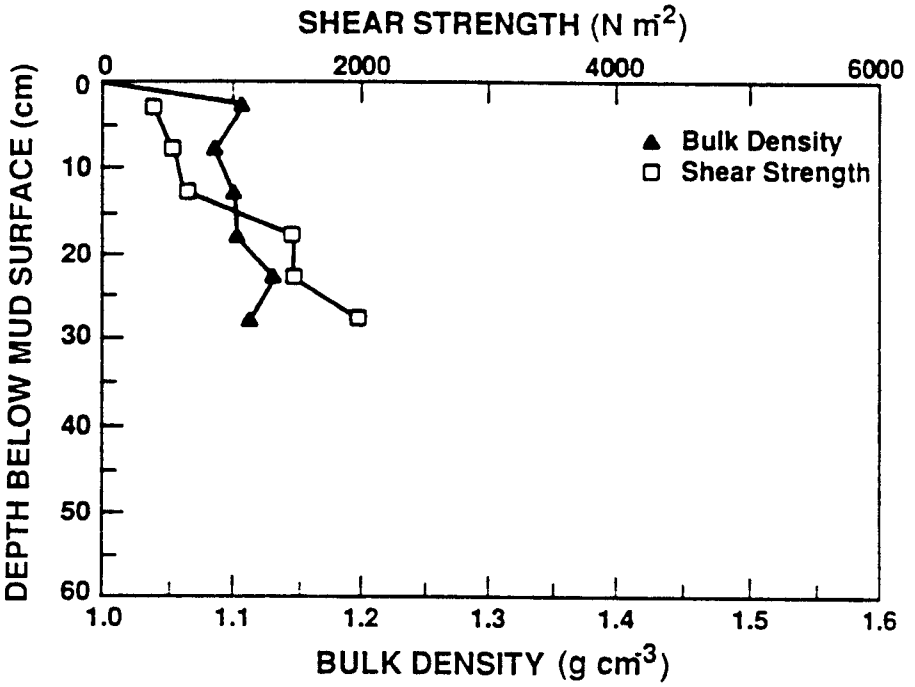

Figure 4.4: Bulk Density and Vane Shear Strength Variations for Site OK2VC

indicates that density is not an unambiguous analog for strength, which also depends upon mud composition.

Mud densities are in the range that might be expected, ranging typically from 1.01 $g\ cm^{-3}$ up to 1.2 $g\ cm^{-3}$ with a maximum value of 1.3 $g\ cm^{-3}$ in two cases examined. Sand densities are higher, reaching 1.8 $g\ cm^{-3}$.Shear strengths reach almost 6 $kN\ m^{-2}$ at times, which is consistent with vane shear strengths given by the Task Committee on Erosion of Cohesive Materials (1968). Through a study to find a relationship between vane shear strength and critical shear stress, the Task Committee showed that vane shear strengths measured for several different clay minerals ranged approximately from 1 $kN\ m^{-2}$ to 9 $kN\ m^{-2}$.

A plot of vane shear strength, τ_v, versus density, ρ_B, has been produced (Fig. 4.6), showing expected scatter of data points. The mean line was drawn by eye, without recourse to the least square fit method. A best fit curve for the data intercepts the density axis

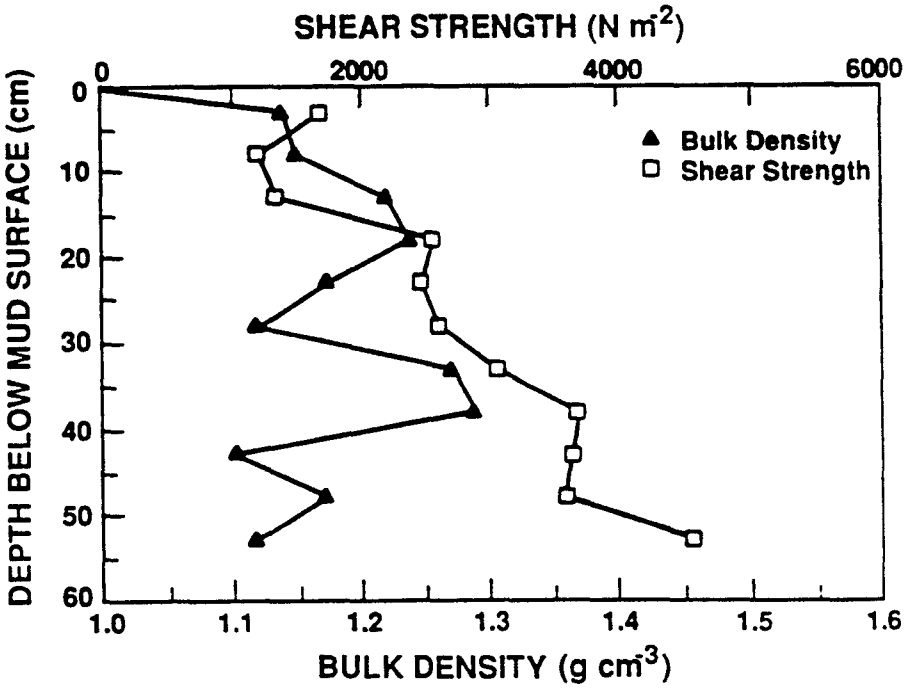

Figure 4.5: Bulk Density and Vane Shear Strength Variations for Site OK10VC

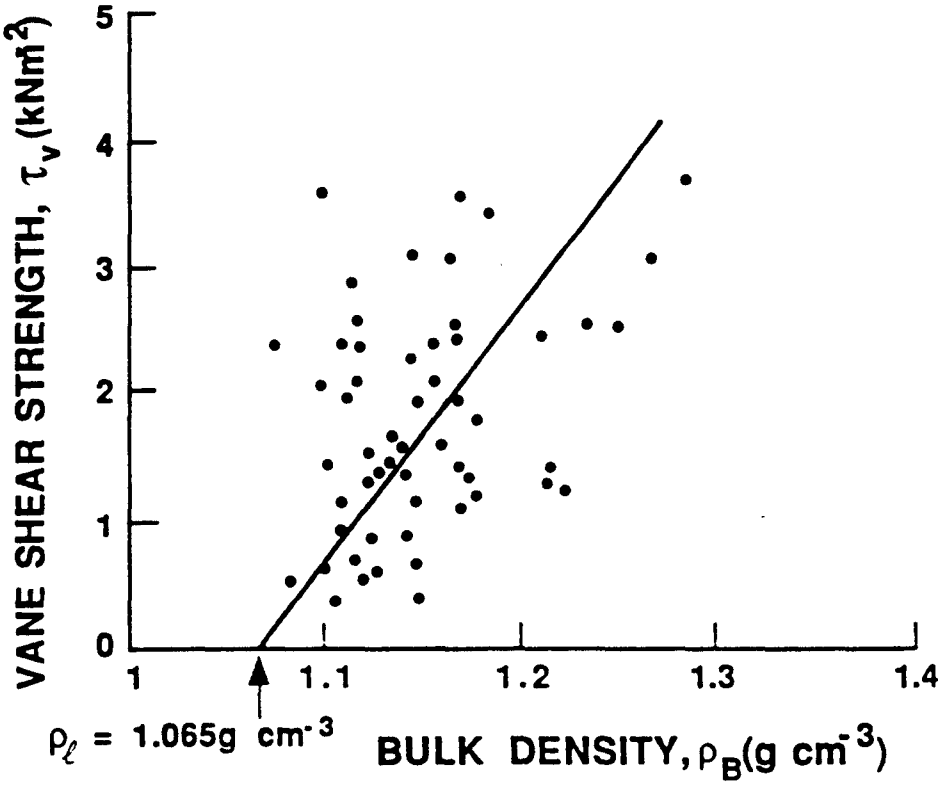

Figure 4.6: Vane Shear Strength Variation with Bulk Density based on all Bottom Core Samples

at 1.065 $g\ cm^{-3}$. At density values below 1.065 $g\ cm^{-3}$, the shear strength becomes zero, implying that the mud behaves as a fluid.

This evidence seems to suggest that the fluid mud layers could regularly be resuspended during windy weather, while the underlying mud is relatively unaffected by erosion. The intricate and small scale lamination of the deeper mud layers supports this observation.

4.4 Settling Tests

Several methods have been used to measure the settling velocity of fine sediment in suspension. Previous studies and particular conditions for each can be found in Heltzel and Teeter (1987). Two indirect approaches which are commonly used are the bottom accumulation method and the point concentration (pipette) method. The pipette method measures the temporal change in local concentration so that $\partial C/\partial t$ can be known at a particular point, while the accumulation method records the temporal change in the actual mass flux, W_sC, at the bottom.

Another approach was selected to yield the settling velocity versus concentration relationship based on measuring the temporal history of the concentration profile. This method, which can be used to measure the settling velocity in settling columns, is called the concentration profile or multi-depth method (McLaughlin, 1958 ; Fitch, 1957).

The actual procedure developed by Ross (1988) was chosen. This method uses multi-depth concentration sampling and numerical integration of the sediment settling equation (mass conservation). In order to make the experimental condition similar to the field condition, water brought from Lake Okeechobee was used instead of local tap water. Mud samples for the tests were collected from six different sites within Lake Okeechobee in two different seasons. Sampling sites and times of sampling are described in section 4.4.3 and identified in Figure 4.1.

4.4.1 Procedure

Settling tests were carried out by using a specially designed 2 m tall settling column at the Coastal Engineering Laboratory. The column was originally designed by Lott (1987).

It consisted of a plexiglass pipe 10 *cm* in diameter. Tap hoses, 5 *cm* in diameter and 10 *cm* in length, were attached to the sides at nine elevations. The column configuration is shown in Figure 4.7. The following procedure was used for each test:

1. A small amount of the fine-grained sediment slurry of high concentration was placed in a 20 liter carbuoy. The carbuoy was filled with the lake water to the marked height which represented the required volumn (15.7 liters) to fill the column. The carbuoy was then well shaken and agitated for a few minutes to premix the suspension thoroughly.

2. After a vacuum bubbler tube was inserted into the column, the premixed suspension was poured into the column. In order to ensure uniform distribution of the suspended sediment, the suspension was vigorously mixed for two additional minutes in the column using the bubbler tube.

3. The bubbler tube was then quickly removed and the first set of about 20 *ml* samples were taken from the top hose to the bottom hose as fast as possible. Samples were collected in 50 *ml* glass bottles which were tightly capped, labeled, and set aside. Samples were then taken after 5, 15, 30, 60, 120, and 180 minutes. The height and temperature of the suspension were noted at each time of sampling. The sampling tubes were flushed before each withdrawal to ensure the removal of residues.

4. Gravimetric analysis was used to determine the profiles of concentration with depth at each sampling time. A fixed volume of sample was taken using the pipette, then filtered by a vacuum pump, and finally dried in an oven for a day at $50°C$. The dried sample was then removed from the oven and cooled before weighing it on a Mettler balance scale which could measure the weight up to 0.1 *mg*.

5. Dividing the weight of the dried sediment by the fixed selected volume gave the concentration of the sample at the time and depth the sample was taken. The concentration data at each time and depth were then entered into an input data file to be used for a settling velocity calculation routine which was developed by Ross (1988).

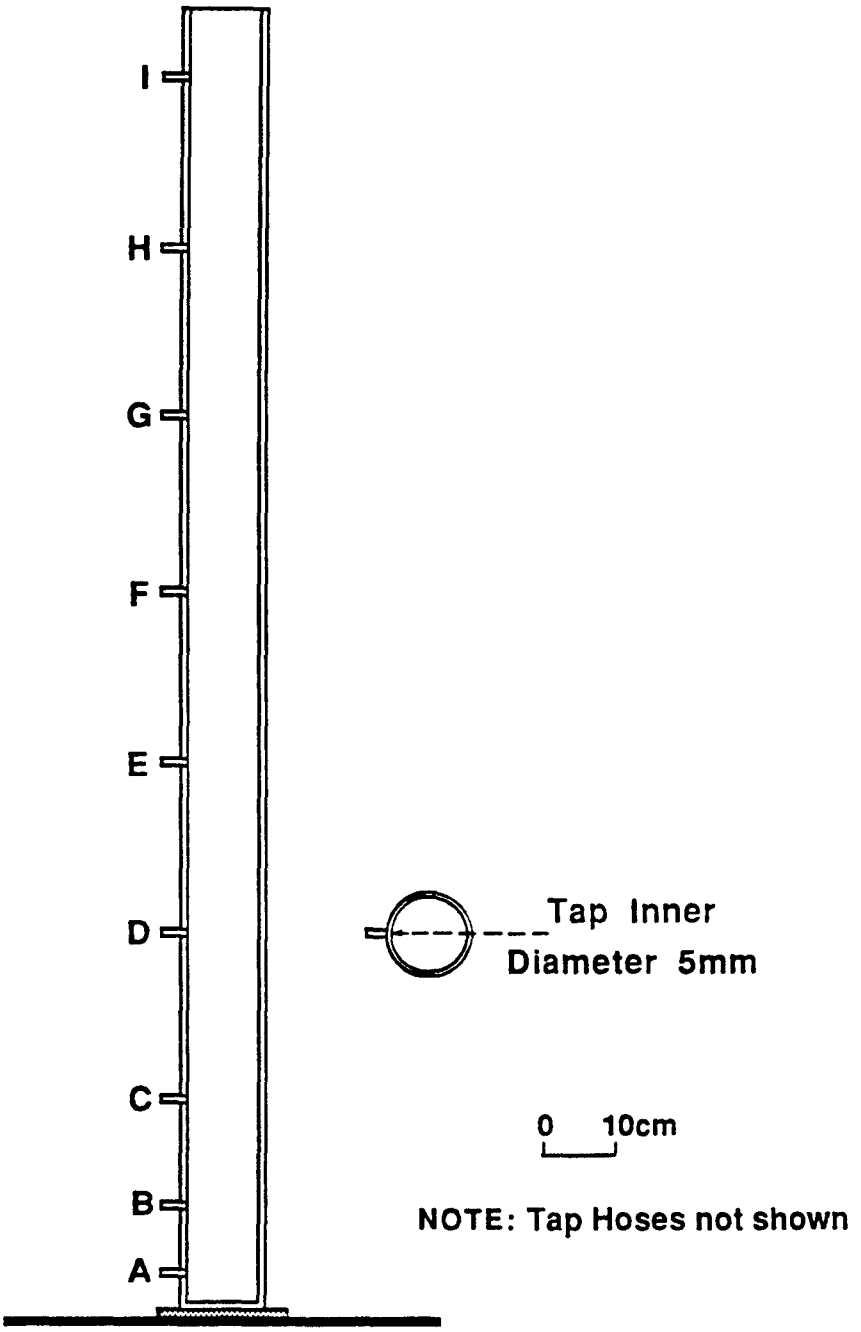

Figure 4.7: Scale Drawing of the Settling Column

4.4.2 Settling Velocity Calculation

In the quiescent conditions, the one dimensional mass conservation equation governs the vertical settling of mass, and is expressed as

$$\frac{\partial C}{\partial t} = -\frac{\partial F_s}{\partial z} = -\frac{\partial (W_s C)}{\partial z} \tag{4.3}$$

This equation relates the time rate variation of suspended sediment concentration, $C(z,t)$, to the vertical gradient in settling flux, $F_s = W_s C$. Since the settling velocity, $W_s(C)$, varies with z, W_s cannot be taken directly out of the spatial derivative.

Ross (1988) developed a computer program to calculate the sediment settling velocity at each elevation and time. The program is based on the finite difference method. The difference equation chosen for the program was as follows:

$$W_{s_i}^{j+1} = -\frac{1}{x_i^j}\frac{\Delta z_i}{\Delta t^j}[x_i^{j+1} - x_i^j] + \frac{1}{2}(W_{s_{i-1}}^j x_{i-1}^j + W_{s_{i-1}}^{j+1} x_{i-1}^{j+1}) \tag{4.4}$$

where x_i^j is the log average of the sediment concentration and Δz_i is the vertical distance between (i) th and $(i+1)$ th sample elevation. The term, Δt^j, is the time increment and j is the time index. This is shown graphically in Figure 4.8. The log average concentration is defined as

$$x_i^j = C^{\frac{1}{2}(\ln C_{i+1}^j + \ln C_i^j)} \tag{4.5}$$

It should be noted that the log average, instead of the arithmetic average, was used to calculate the mid-point concentration. This is due to the trend of concentration profile, which typically shows logarithmic shape. Ross (1988) gives the details, including the boundary conditions for solution of Equation 4.4.

4.4.3 Test Conditions

A total of fourteen settling column tests were conducted on the muds from six different sites within the muddy zone of Lake Okeechobee. Conditions for each test are given in Table 4.2. Locations of mud samples used for tests are identified in Fig. 4.1.

As shown in Table 4.2, the mud samples used for the first seven tests are those collected from five different sites in Mar. 1988, as described in section 4.2. Through these tests, the

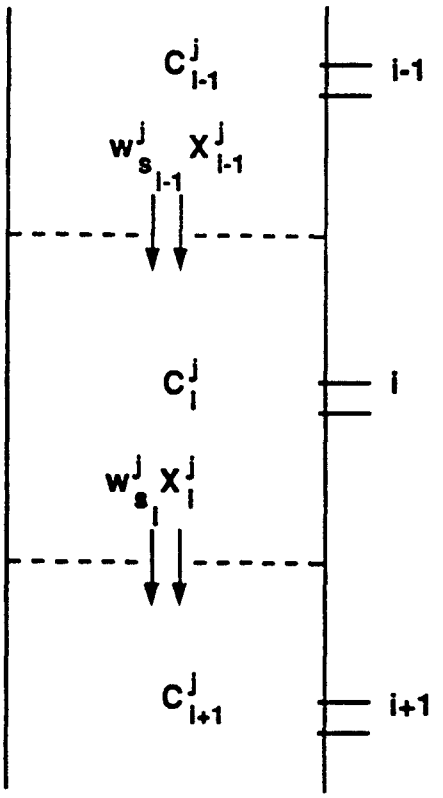

Figure 4.8: Grid Indexing used in the Settling Velocity Calculation Program

Table 4.2: Settling Test Conditions

Test No.	Location of Mud Sample	Date of Mud Collection	Temp. of Suspension ($T°C$)	Variation of Suspension Height (cm)	C_o ($g\ L^{-1}$)
1	site 1	Mar 1, 1988	27.4 - ****	162.8 - 135 5	1.8
2	site 2	Mar 1, 1988	29.0 - 32.0	163.3 - 139.8	2.8
3	site 2	Mar 1, 1988	26.3 - ****	161.7 - 135.2	14.1
4	site 3	Mar 1, 1988	****	157.5 - 130.0	5.0
5	site 4	Mar 1, 1988	27.0 - ****	163.5 - 140.8	2.8
6	site 4	Mar 1, 1988	25.5 - ****	164.0 - 137.5	23.7
7	site 5	Mar 1, 1988	28.7 - 30.8	161.3 - 133.5	2.7
8	site 6	Oct 28, 1988	19.0 - 20.9	164.3 - 139.8	3.2
9	site 6	Oct 28, 1988	19.6 - 22.3	167.1 - 145.4	6.5
10	site 6	Oct 28, 1988	19.4 - 20.6	159.3 - 137.4	13.6
11	site 6	Oct 28, 1988	21.6 - 22.1	163.5 - 141.3	19.9
12	site 1	Oct 28, 1988	22.0 - 23.1	164.2 - 142.6	1.9
13	site 1	Oct 28, 1988	20.6 - 19.7	171.2 - 150.7	4.6
14	site 1	Oct 28, 1988	21.0 - 24.5	174.1 - 152.3	11.9

Note: * * ** indicates no value obtained.

spatial variation of settling properties could be estimated. For tests 12 through 14, the mud sample was collected from the same location as that of test 1, but in a different season in order to evaluate possible seasonal effect on the settling properties. To supplement the spatial representation of settling properties, mud sample from site 6 was additionally collected in Oct. 1988. This sample was investigated through tests 8 to 11.

From Table 4.2, it is observed that the temperature change of sediment suspension in the laboratory column was relatively small during each test, indicating the maximum variation to be 3.5^oC. For the tests as a whole, however, temperature varied from 19^oC to 32^oC.

The height of sediment suspension is also given in Table 4.2. The first value given for each test represents the sediment suspension height at initial time of each test, and the other values represent heights which resulted after the final collection of samples at the last sampling time. It is noticeable that the sediment suspension heights decreased by approximately 25 *cm* in all tests.

Initial sediment concentration, C_o, used in the tests is also given in the last column of Table 4.2, and varied from 1.8 $g\ L^{-1}$ to 23.7 $g\ L^{-1}$. Since the settling velocity in general varies measurably with the suspension concentration, various initial concentrations were selected to obtain the settling velocities in an extensive range of the suspension concentration. The initial concentration represents the concentration at zero time immediately after mixing when the concentration was nearly uniform over depth.

4.4.4 Results and Discussion

Concentration profiles. Concentration profiles measured in selected tests are shown in Figures 4.9 through 4.12. Other profiles are contained in Appendix B. Three distinct settling regimes are apparently observed from the profiles, which Ross (1988) described as low ($C < 2$ $g\ L^{-1}$), moderate, and high ($C > 20\ g\ L^{-1}$) concentration settling regimes, respectively.

Figure 4.9 shows concentration profiles from the test 1, which was conducted using mud from site 1 in Mar. 1988 as described in Table 4.2. This profile illustrates well the

settling of low concentration due to low initial concentration (1.8 $g\ L^{-1}$). Suspension concentration decreased everywhere in the column except immediately at the bed. For example, the suspension concentration gradually decreased with time from 1.8 $g\ L^{-1}$ up to approximately 0.1 $g\ L^{-1}$ at 130 *cm* above the bottom of the column. Ross (1988) attributed this decrease to aggregate sorting during the flocculation process.

It is noted that the variation from low to high concentration occurred with no significant development of a moderate concentration region.

In Figure 4.10, concentration profiles from test 2 at an initial concentration of 14.1 $g\ L^{-1}$ are shown. These profiles can be considered to be representitive of the moderate concentration settling regime. Two marked interfaces are noticed in these profiles. Both interfaces converge with time. Ross also observed these interfaces and described the upper interface in this profile as separating the concentration "thinning" layer (above) from the constant settling layer (below); and the lower layer interface indicates the beginning of hindered settling and decreasing vertical flux rates. Here, "thinning" means the decrease of the suspension concentration with time at any elevation of the column.

Finally, high concentration settling, which is generally called hindered settling, is illustrated well in Fig. 4.11. As observed in these profiles, the initial concentration was 23.7 $g\ L^{-1}$. A characteristic feature for this regime is the corresponding decrease in sediment flux with increase in concentration. In this case, concentration increases everywhere with time and the settling occurs in mass.

In Fig. 4.12, concentration profiles from test 11 are shown. The initial suspension concentration in this test was 19.9 $g\ L^{-1}$. It should be noticed that a lutocline representing a step gradient in the concentration profile developed shortly after the initiation of the test. For example, at 120 minutes the lutocline was 100 *cm* above the bottom of the column, and at 180 minutes, it was at 60 *cm*. Below the lutocline, the sediment was in the form of a high concentration, but not a significantly thick structured bed, since 180 minutes is typically insufficient to develop the thick structured phase by dewatering.

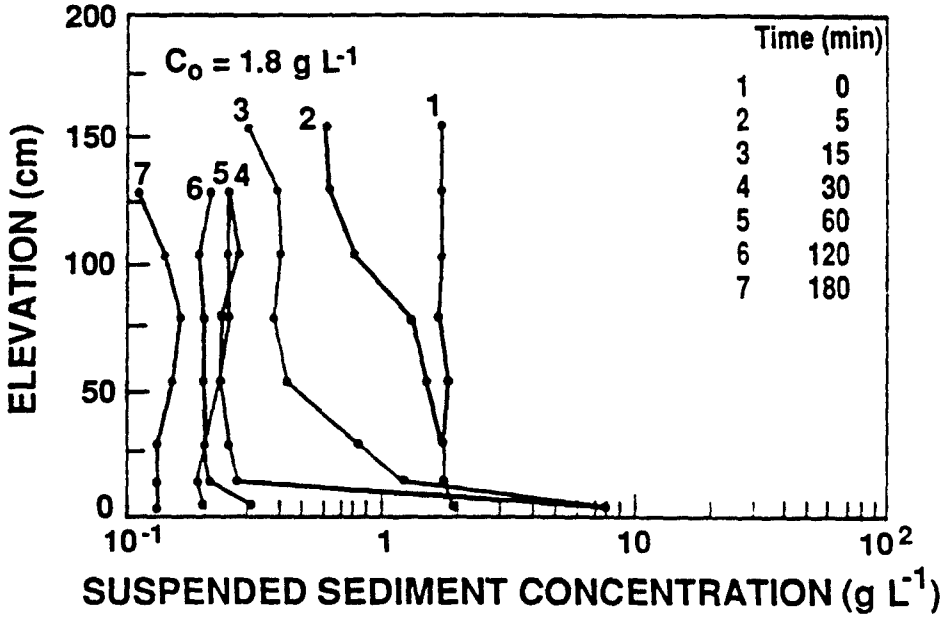

Figure 4.9: Concentration Profiles from Settling Test 1; Initial Concentration of 1.8 $g\ L^{-1}$

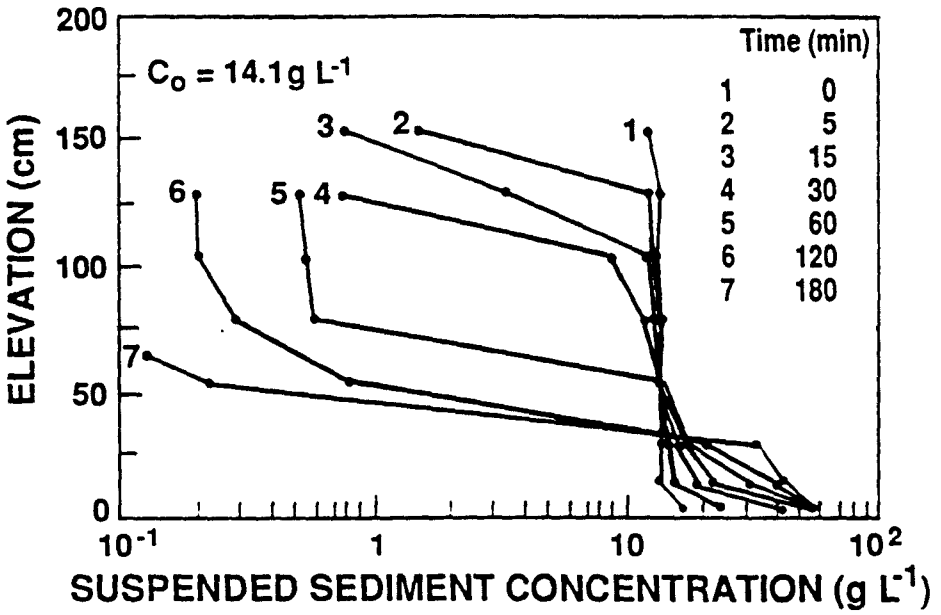

Figure 4.10: Concentration Profiles from Settling Test 3; Initial Concentration of 14.1 $g\ L^{-1}$

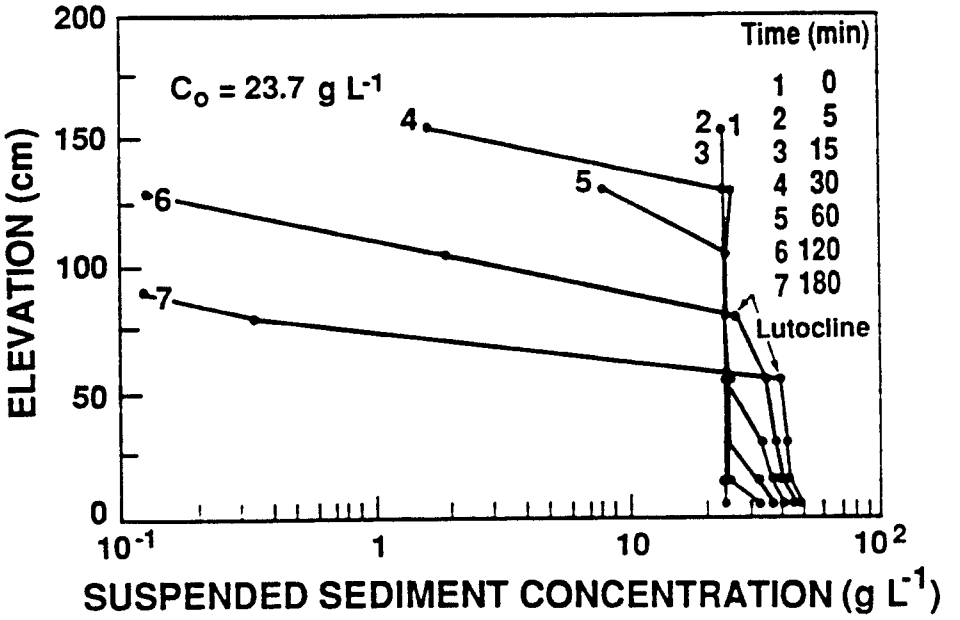

Figure 4.11: Concentration Profiles from Settling Test 6; Initial Concentration of 23.7 $g\ L^{-1}$

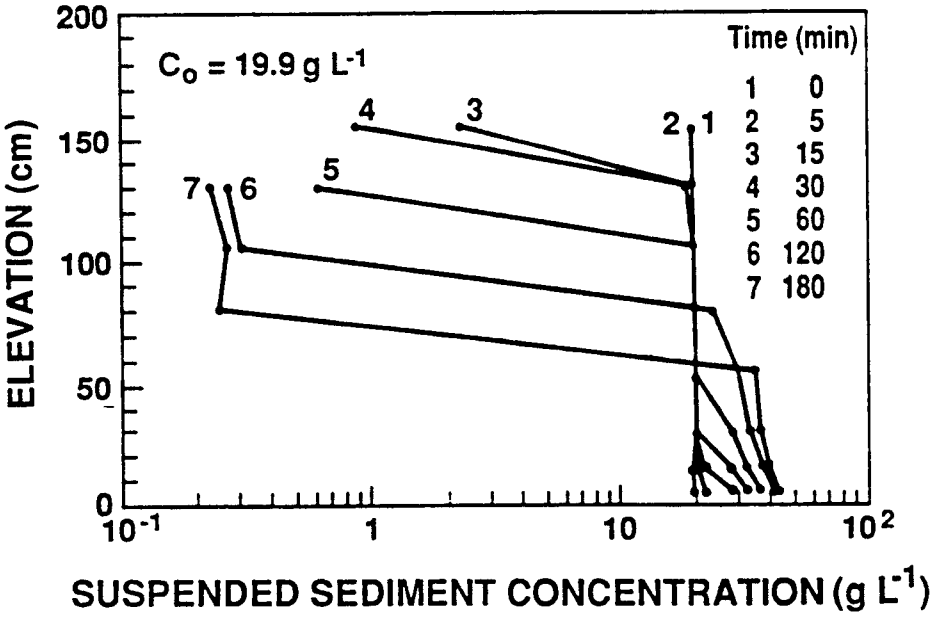

Figure 4.12: Concentration Profiles from Settling Test 11; Initial Concentration of 19.9 $g\ L^{-1}$

Settling velocity profiles. The concentration profiles from the fourteen settling tests were used to calculate the settling velocities of sediment from the six different sites. In order to determine the settling velocity at different concentrations, these profiles were entered into the numerical program for settling velocity calculation. The resulting settling velocity profiles for different sites are shown in Figures 4.13 through 4.15.

Figure 4.13 shows the settling velocity and the corresponding settling flux plots for site 1. As shown in the figure, the data were quite scattered but clearly indicated an increasing velocity region and a decreasing velocity region. The reasons for the scatter around the fitted line have been explained by Ross (1988). He attributed the scatter to a slight time variation in the settling velocity due to collision and flocculation, and limitations in the bubbler mixing procedure used for obtaining an initially uniform suspension.

The data shown in Fig. 4.13 seem to indicate a parabolic shape, which is somewhat different in comparison with the typical settling velocity profile given in Fig. 3.1, especially in flocculation settling region. Typically, the settling velocity profile in the flocculation settling region is represented by a straight line. However, in Fig. 4.13 the parabolic shape is observed to extend from the hindered settling region into flocculation settling region following similar observation by Wolanski at al. (1989). Noticing this parabolic shape, the following relationship

$$W_s = \frac{aC^n}{(C^2 + b^2)^m} \tag{4.6}$$

which is modified from Wolanski et al. (1989), has been developed to represent both flocculation settling and hindered settling.

It should be noted that depending on the concentration, Equations 3.24 and 3.25 can be simplified as follows:

$$W_s = ab^{-2m}C^n \quad \text{if } C^2 \ll b^2 \tag{4.7}$$

$$W_s = aC^{n-2m} \quad \text{if } C^2 \gg b^2 \tag{4.8}$$

By applying the least square fit method to the obtained settling velocity data, the four

unknown coefficients of a, b, n and m can be determined from these simplified forms. Referring to Fig. 4.13, Equation 4.7 represents a straight line in the flocculation settling region and Equation 4.8 in the hindered settling region. The gradient of the straight line in the flocculation settling region directly gives the value of n in Equation 4.7. The value of a in Equation 4.8 is the value of W_s when the straight line in the hindered settling region intersects the vertical line at $C = 1\ g\ L^{-1}$. In Fig. 4.13, the resulting values of a, b, n and m were 33.38, 4.39, 1.02 and 1.48, respectively.

Furthermore, a simple differenciation of Equation 4.6 with respect to C gives the peak value of the settling velocity, W_{so}. The maximum value, W_{so}, and the corresponding C_2 are defined by

$$W_{so} = ab^{n-2m}\frac{(\frac{2m}{n}-1)^{m-\frac{n}{2}}}{(\frac{2m}{n}-1)^{\frac{1}{2}}} \tag{4.9}$$

$$C_2 = \frac{b}{(\frac{2m}{n}-1)^{\frac{1}{2}}} \tag{4.10}$$

Note that the settling flux, F_s, is obtained by multiplying the settling velocity with the concentration. Replacing n by $n+1$ in Equation 4.6, therefore, the corresponding equation for F_s is obtained as

$$F_s = W_s C = \frac{aC^{n+1}}{(C^2+b^2)^m} \tag{4.11}$$

In the same way as before, the peak value, F_{so}, of the flux and the corresponding C_3 can be defined by

$$F_{so} = ab^{n+1-2m}\frac{(\frac{2m}{n+1})^{m-\frac{n+1}{2}}}{(\frac{2m}{n+1})^m} \tag{4.12}$$

$$C_3 = \frac{b}{(\frac{2m}{n+1}-1)^{\frac{1}{2}}} \tag{4.13}$$

In Table 4.3, the characteristic coefficients (n, m, a and b) of Equation 4.6 are given for different sites, including the characteristic parameters (W_{so}, C_2, F_{so} and C_3) for the settling velocity and flux relationships.

Figure 4.14 shows the settling velocities of sediment from sites 2, 4 and 5, and the settling velocity profile obtained from Equation 4.6. There is a noticeable similarity in the

Table 4.3: Values of Characteristic Coefficients and Parameters For W_s and F_s

Site No.	n	m	a	b	W_{so} $(mm\ sec^{-1})$	C_2 $(g\ L^{-1})$	F_{so} $(Kg\ m^{-2}\ sec^{-1})$	C_3 $(g\ L^{-1})$
1	1.83	1.89	33.38	2.54	1.47	2.46	4.67	4.38
2, 4 and 5	1.02	1.48	33.38	4.39	0.73	3.18	3.30	6.43
3 and 6	1.96	1.96	33.38	4.19	0.52	4.19	2.83	7.36

flocculation settling regions for sites 2, 4, and 5, as well as in their corresponding hindered settling regions. In Fig. 4.15 the sediments from sites 3 and 6 also show similarity in the settling velocity, even though these two sediments were collected in different seasons as indicated in Table 4.2.

In Figure 4.16, the settling velocity profile for site 1 is given as a representive one in order to examine any seasonal variation. From the data it is observed that the settling velocities of sediment from site 1 were not affected by any measurable seasonal difference (Spring versus Fall). It may be surmized that the influence of season on the settling velocity of sediment in the muddy zone of Lake Okeechobee may not be significant.

In order to compare the spatial variability of the settling velocity, profiles for each of the six sites have been combined in Figure 4.17. Data from all sites show W_s variation in the range of two orders of magnitude, from about 0.01 to 1 $mm\ sec^{-1}$. At the end of the low concentration regime, W_s varies approximately from 0.02 to 0.3 $mm\ sec^{-1}$. This may be considered to represent the free settling velocity.

It is observed that the sediments from all sites seem to exhibit similar behavior in the hindered settling region, which is beyond the peak value of W_s (on the order of 1 $mm\ sec^{-1}$ at about 3 $g\ L^{-1}$). This phenomenon may be attributed to the dominant effect of the aggregate network on dewatering rather than sediment composition on the settling behavior. However, the effect of sediment composition is clearly seen in the flocculation settling range. Site 1 shows the highest W_s and sites 3 and 6 the lowest. Sites 2, 4 and 5 are intermediate but approach site 1 towards the free settling regime.

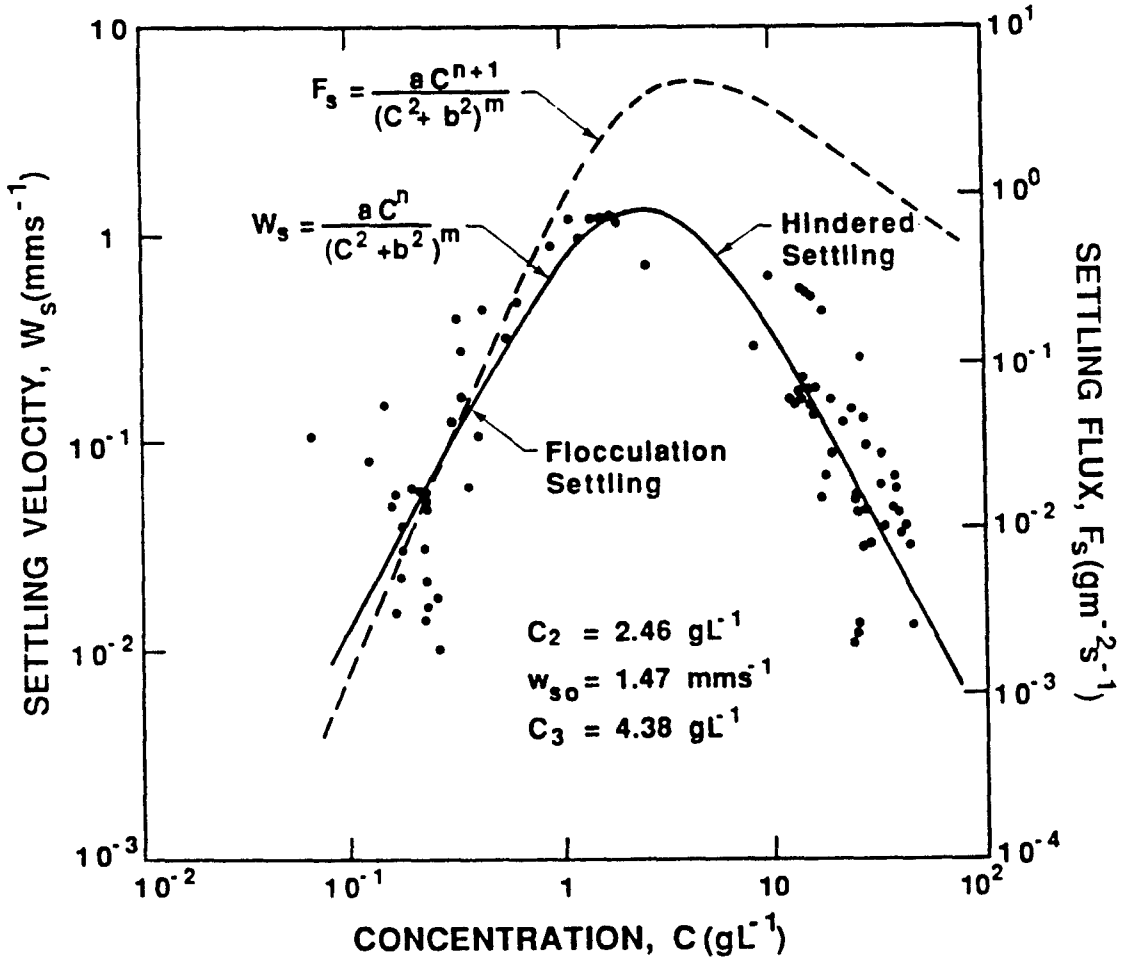

Figure 4.13: Settling Velocity and Settling Flux Variations with Concentration for Site 1

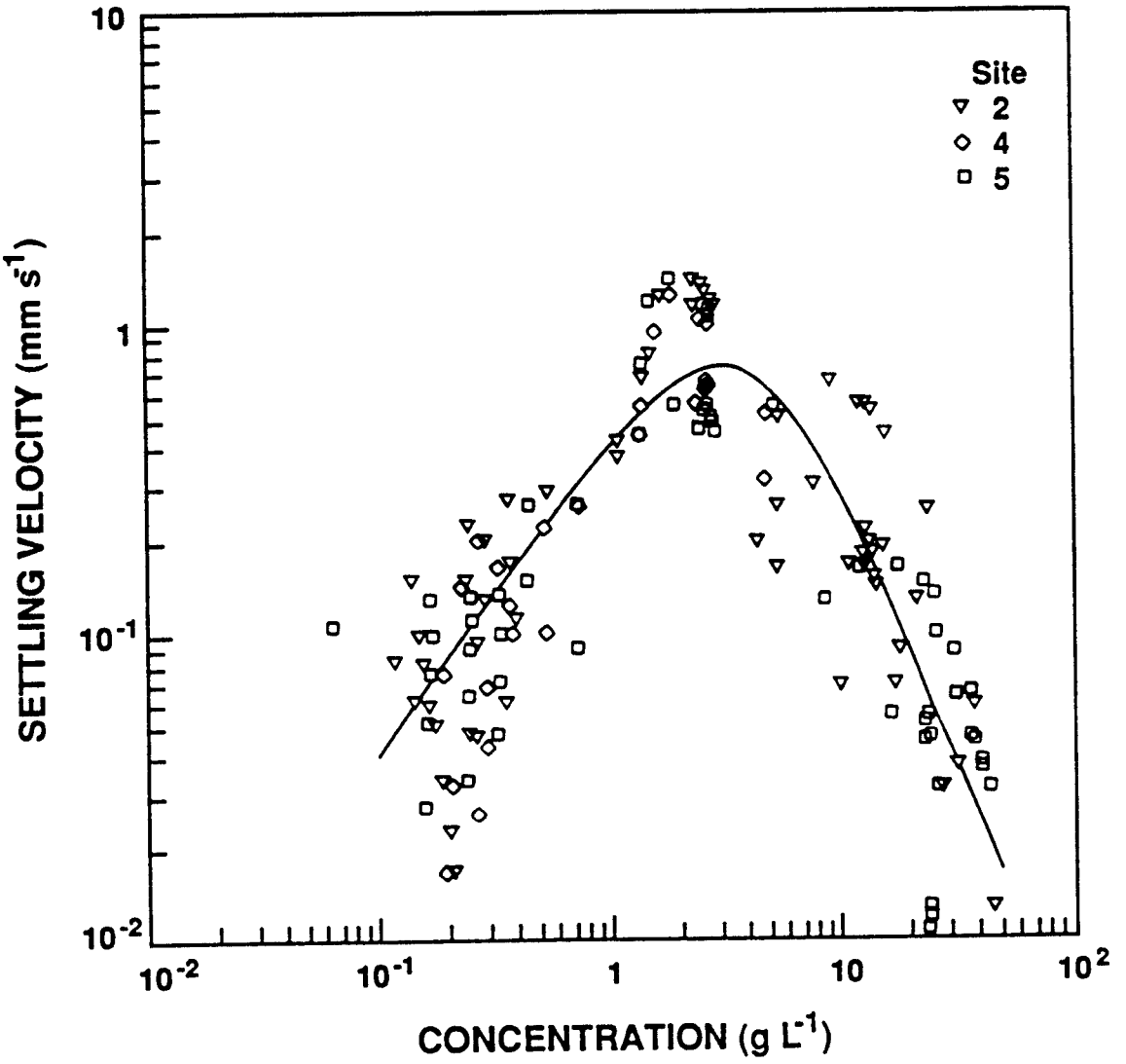

Figure 4.14: Settling Velocity Variation with Concentration for Sites 2, 4 and 5

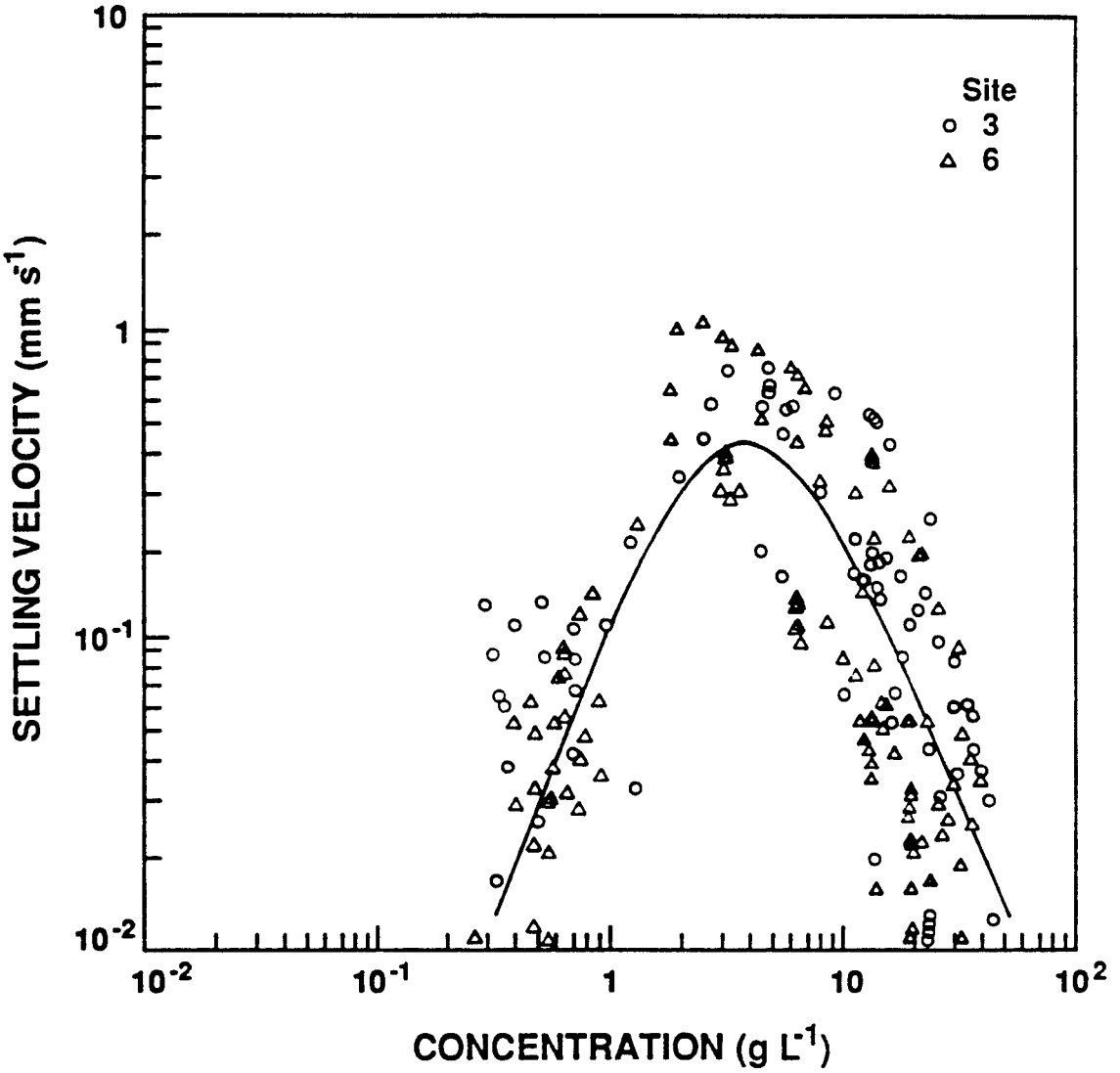

Figure 4.15: Settling Velocity Variation with Concentration for Sites 3 and 6

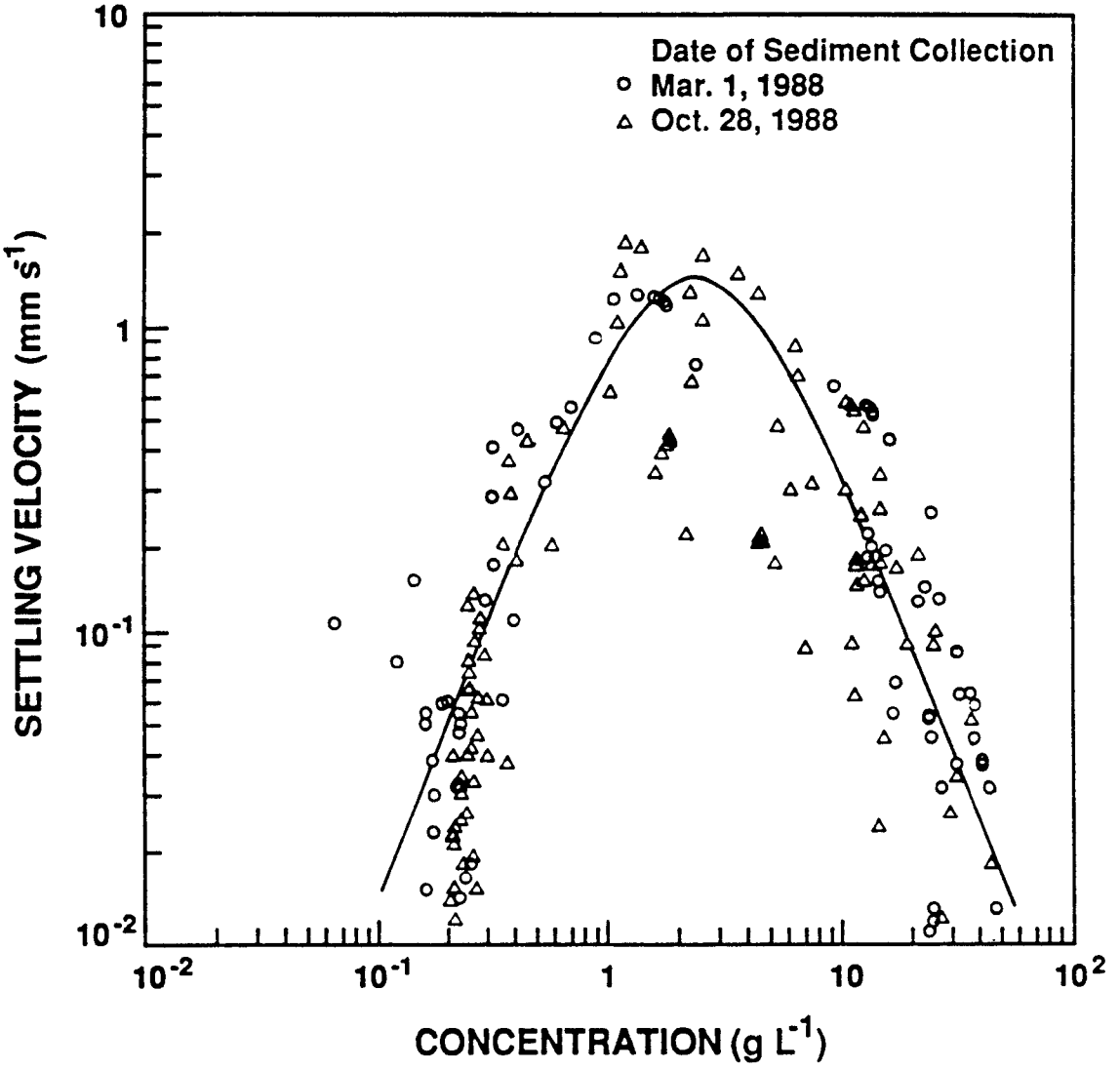

Figure 4.16: Seasonal Comparison (March, 1988 versus October, 1988) of Settling Velocity Variation with Concentration at Site 1

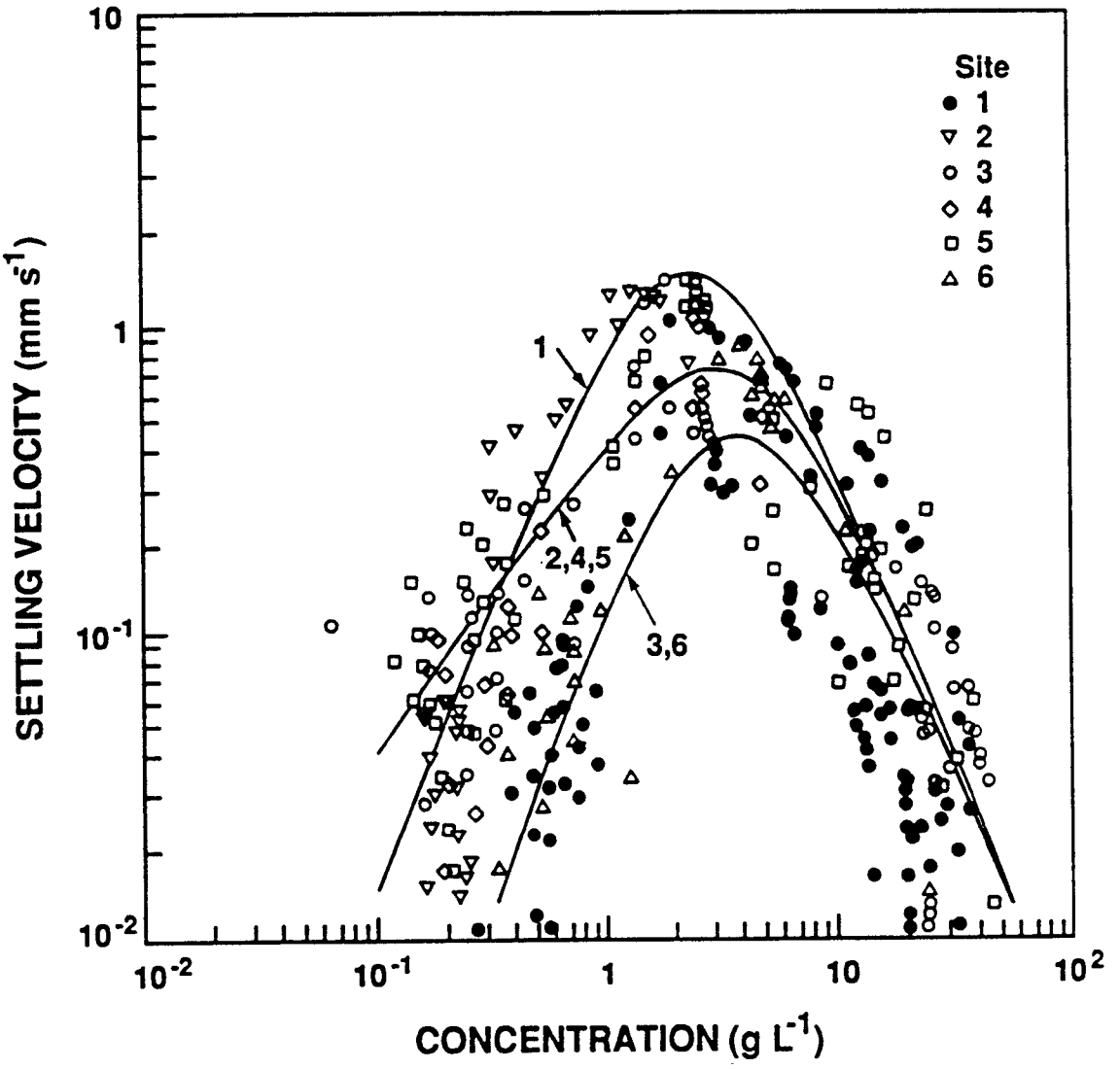

Figure 4.17: Spatial Comparison of Settling Velocity Variations with Concentration for Sites 1, 2, 3, 4, 5 and 6

As described in the previous section (Fig. 4.1), site 1 is located at the northern end of the muddy zone in Lake Okeechobee and sites 3 and 6 are at the eastern end and western end, respectively. Sites 2, 4 and 5 cover the central and southern parts of the muddy zone. From the data of Fig. 4.17, therefore, it can be concluded that sediment settling occurs fastest in the northernmost zone, more slowly in the eastern and western zones, and at a moderate rate in the central and southern mud zones.

In reference to both the fine particle size distributions in Fig. 4.2 and the grain size data in Table 4.1 in previous section, it appears to be difficult to correlate the dispersed particle size with the settling velocity of the aggregated sediment. The lack of correlation between the aggregate settling velocity and the corresponding dispersed particle size is somewhat unexpected. However, it in fact makes clear a basic difference between behaviors of cohesive and cohesionless sediments, which is that unlike the case of cohesionless sediment, in cohesive sediments the settling velocity can not always be uniquely defined by particle (dispersed) size. Note that even in the relatively low salt concentration environment of Lake Okeechobee, we are dealing with aggregated sediment whose properties seem greatly influenced by the presence of nearly 40 % organic matter. Unfortunately, specific factors related to the organic constituents which affect aggregation are generally not well known.

It is noticeable that over a fairly large portion of the muddy zone, represented by sites 2, 4, and 5, the settling velocities are similar. This in turn suggests a good degree of spatial mixing of the muddy sediment due to wind generated circulation and associated wave action. This could also explain why site 1 is different, since in the narrow neck region of the lake some sheltering from the effects of wind and insufficient communication with the rest of the muddy zone thereof is likely. With regard to the low settling velocities at sites 3 and 6, hydrodynamic influence on the bottom sediment distribution is believed to be the major factor.

4.5 Erosion Tests

4.5.1 Introduction

In order to investigate the erosional properties of sediments from various sites in Lake Okeechobee, erosion tests were conducted at the Coastal Engineering Laboratory, using the rotating annular flume originally designed by Mehta (1973).

The erosional behavior varies both with the magnitude of the bed shear stress and the structure of the bed. Beds are commonly classified into two categories: deposited beds and placed beds. A deposited bed, which is usually composed of freshly deposited mud undergoing consolidation, generally exhibits non-uniform property variation with depth. Typically, the density and the shear strength increase with depth in the top few centimeters. The bed properties of the placed bed are comparatively uniform over the depth so that the shear strength and the density are independent of depth.

In the case of the deposited bed, the time rate of concentration variation, $\partial C/\partial t$, decreases with time and the suspension concentration approaches a final constant value. In the placed bed case, the suspension concentration increases at a constant rate with time when a given shear stress exceeds the shear strength. Thus, the rate of erosion of these beds is constant for a given shear stress. For the present experiments, placed beds were used so that the erosion rate could be directly estimated for a given shear stress and bed density.

4.5.2 Annular Flume

The basic components of the annular flume consist of a system of a rotating annular ring and an annular channel. The annular channel, which is made of 0.95 *cm* thick fiberglass, has a width of 20 *cm*, depth of 46 *cm* and a median radius of 76 *cm*. The annular ring is made of 0.6 *cm* thick plexiglass, having the same mean radius as the channel but narrower by 0.6 *cm* than the width of the channel. The ring can be suspended at any required height within the channel by means of four vertical supports which are connected to the central vertical shaft by horizontal supports.

A control unit with an indicator panel is provided for both the ring and the channel to enable their operation at the desired speeds. These control units had to be calibrated, since they do not give the speeds of the ring and the channel directly in *rpm*. Therefore, *rpm* measurements of the ring and the channel were carried out for given different settings on the meters using a stopwatch. Calibration curves obtained in this way are given in Figure 4.18. Other equipment for bed shear stress measurements was previously calibrated by Mehta (1973). The required bed shear stress could be obtained by adjusting the rotation speeds of the ring and the channel. The ring and the channel were rotated in opposite directions to minimize the effect of secondary currents and to provide a uniform flow in the channel.

In order to collect samples of suspended sediment, tap tubes are provided at three different elevations on the outer wall of the channel, at elevations of 8 *cm*, 18.5 *cm* and 26.5 *cm* above the bottom of the channel. Flume configuration and additional details on the flume may be obtained from Mehta (1973).

4.5.3 Procedure

Placed beds were prepared by pouring a thick slurry of sediment into the annular flume. In reality, in the top few centimeters the bed is usually soft and has a relatively low density with high water content (> 100 %), since the bed is composed of freshly deposited mud undergoing consolidation. However, below the upper layer of the bed, it is typically more dense and more consolidated, with a lower water content. The sediment slurry, having a density corresponding to that of a soft bed, was obtained easily by setting aside the sediment in water in a quiescent condition, which gradually increased the density of the slurry through consolidation. However, it was difficult to obtain a sediment slurry density corresponding to that of a dense bed by this process alone. Therefore, in this case, the slurry was heated in an oven at a temperature less than $50°C$ for approximately two days, which lowered the water content. In order to make the experimental conditions similar to the field condition, lake water was used in all experiments.

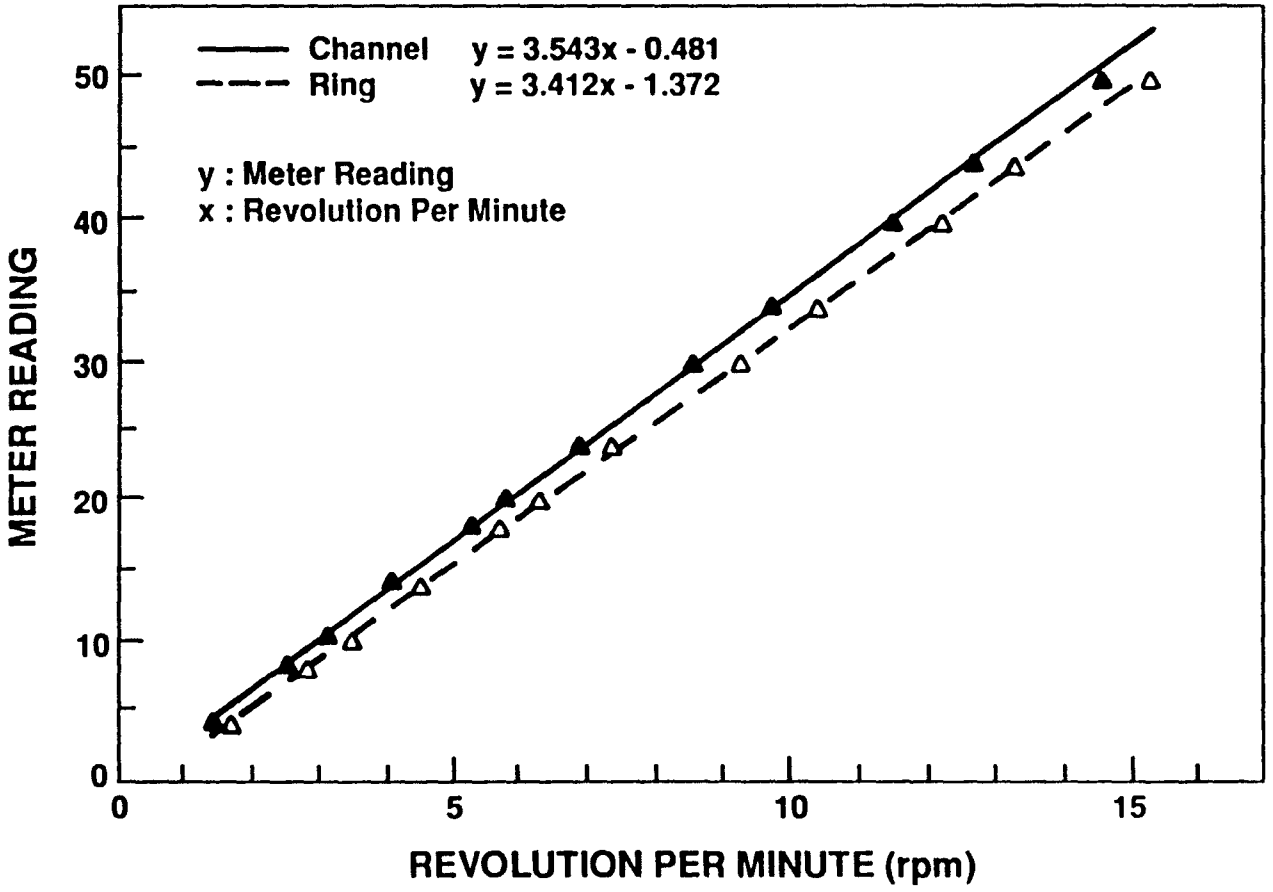

Figure 4.18: Speed Calibration Curves for Ring and Channel of the Annular Flume

The following procedure was used for each test:

1. A thick slurry of mud was well mixed by a mixer for an hour to obtain uniform density over the depth. In order to measure the bulk density of the slurry, a small amount of sediment was taken from the well-mixed slurry and its weight and volume were measured. The bulk density was obtained by dividing the weight of sediment by the volume. The slurry was placed over the flume bottom to uniform depth. All mud stains on the inside walls of the channel during the placement of bed were removed.

2. Lake water was then carefully added to the flume to give the desired water column height, using a very small pump made by Cole-Parmer Instrument Company (Model No. 7568). The ring was lowered to be in complete contact with the water surface. It is very important to set the ring properly, since a shear stress is transmitted to the sediment bed during the rotation of the ring, therefore the stress magnitude depends on the area of contact between the water surface and the ring.

3. The flume was kept in quiescence for one to three days to allow the sediment suspended in the process of adding the lake water into the flume to settle down.

4. For the present study, six to seven different shear stresses were applied in a step-wise manner with a increment of 0.1 $N\ m^{-2}$, in accordance with the procedure described in detail by Parchure (1984). The starting shear stress was 0.05 $N\ m^{-2}$ or 0.1 $N\ m^{-2}$, and time duration for each shear stress was 90 minutes. The sampling times used over each 90 min duration of application of shear stress were 2, 5, 10, 15, 20, 30, 40, 50, 60, 75 and 90 minutes with an initial sample taken at the start of the duration.

5. At each sampling time, suspension samples were taken simultaneously at two different elevations to give an average suspension concentration over the entire water column. The selected two elevations were 8 *cm* and 18.5 *cm* above the bottom of the channel. Samples were collected in 50 *ml* glass bottles which were capped, labeled, and set

Table 4.4: Erosion Test Conditions

Test No.	Date of Sediment Collection	ρ_B ($g\ cm^{-3}$)	Water Depth (cm)	Bed Thickness (cm)	Duration of Deposition (hr)
1	Mar. 1, 1988	1.10	27	3.0	24
2	Mar. 1, 1988	1.12	23	3.0	24
3	Mar. 1, 1988	1.09	23	3.0	24
4	Mar. 1, 1988	1.19	23	1.5	24
5	Oct. 28, 1988	1.07	23	5.0	72
6	Oct. 28, 1988	1.09	23	3.5	24

aside. Care was taken to flush the sampling tubes before each withdrawl. Lake water was periodically added to the flume to maintain a 23 cm water depth.

6. Gravimetric analysis was used to determine the suspension concentration of each sample. Gravimetric analysis procedure has been described in section 4.4.1. This analysis provided time-variation of suspension concentration over each 90 min duration at a given applied bed shear stress. The concentration-time profiles were then used to estimate the erosion rate at each given bed shear stress, and the critical shear stress for erosion, corresponding to the selected bed density, was obtained from the relationship between the erosion rate and the bed shear stress (Mehta, 1988b).

4.5.4 Test Condition Summary

Test conditions are summarized in Table 4.4. For tests 1 through 4, the sediment used was a mixture of sediments collected from sites 1, 2, 4, and 5 in Lake Okeechobee in March 1988. The approximate proportion (percent by weight) of sediment from these four sites in the mixture was 30, 25, 25, and 20, respectively. These samples could be combined since they showed similar properties through the characterization tests and settling velocity tests. Since the sediment from site 3, however, exhibited somewhat different properties, tests 5 and 6 were conducted using the sediment collected at site 3 in October 1988. It is surmized that the erosional properties of the sediment are not affected by the seasonal difference, based on the results of the examination of seasonal variation in the settling properties.

In test 4, a dense bed with a bulk density of 1.19 $g\ cm^{-3}$ was prepared. In all other tests less dense beds were used. The water column height was 23 cm in all tests except test 1, and the placed bed thickness varied from 1.5 cm to 5 cm according to the amount of sediment available for each test.

Even though a very sensitive small pump was used to add lake water into the flume, the surface of the sediment bed was disrupted and sediment particles were resuspended. Therefore, a long duration (24 hr) of deposition was required to allow the suspended sediment to settle down. In test 5, the duration of deposition was 72 hours because the sediment bed was disrupted more than in the other tests, due to low bulk density.

4.5.5 Results and Discussion

Concentration-time profile. Illustrative suspension concentration versus time profiles are shown in Figure 4.19 through 4.22. Other profiles are contained in Appendix C. As noted, in the case of the placed bed (which has uniform properties over the depth), the depth-averaged suspension concentration during erosion increased linearly with time for a constant shear stress in excess of the shear strength. This typical trend is clearly observed at high shear stresses.

Figure 4.20 shows a significant dependence of suspension concentration on the bed density in comparison with other figures. As observed, suspension concentrations for each shear stress were always less than 0.1 $g\ L^{-1}$. The bed bulk density for this test was 1.19 $g\ cm^{-3}$, which was relatively higher than the others, as seen from Table 4.4.

Fig. 4.21 illustrates that the concentration suddenly dropped at the beginning of the second applied stress duration step from the end. The concentration drop is attributed to a change in the vertical concentration profile, possibly as a consquence of a change in the inter-particle collision frequency at the beginning of the step (Parchure, 1984).

In most profiles the suspension concentration shows a different trend at low shear stresses, where the concentration shows a nearly constant value and sometimes even a decreasing trend with time. For example, such a trend is easily observed in the first three

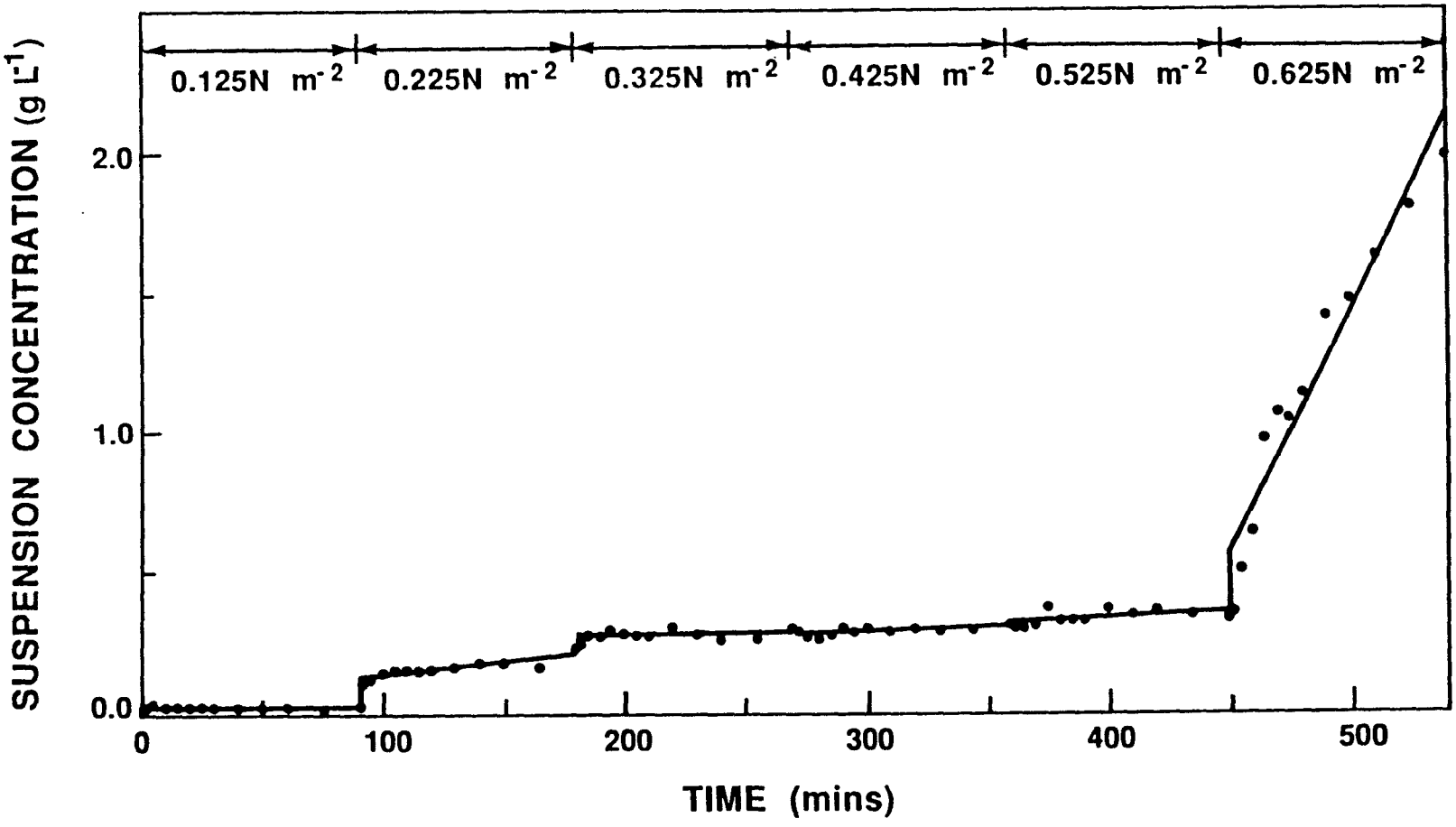

Figure 4.19: Time-Concentration Relationship in Test 3

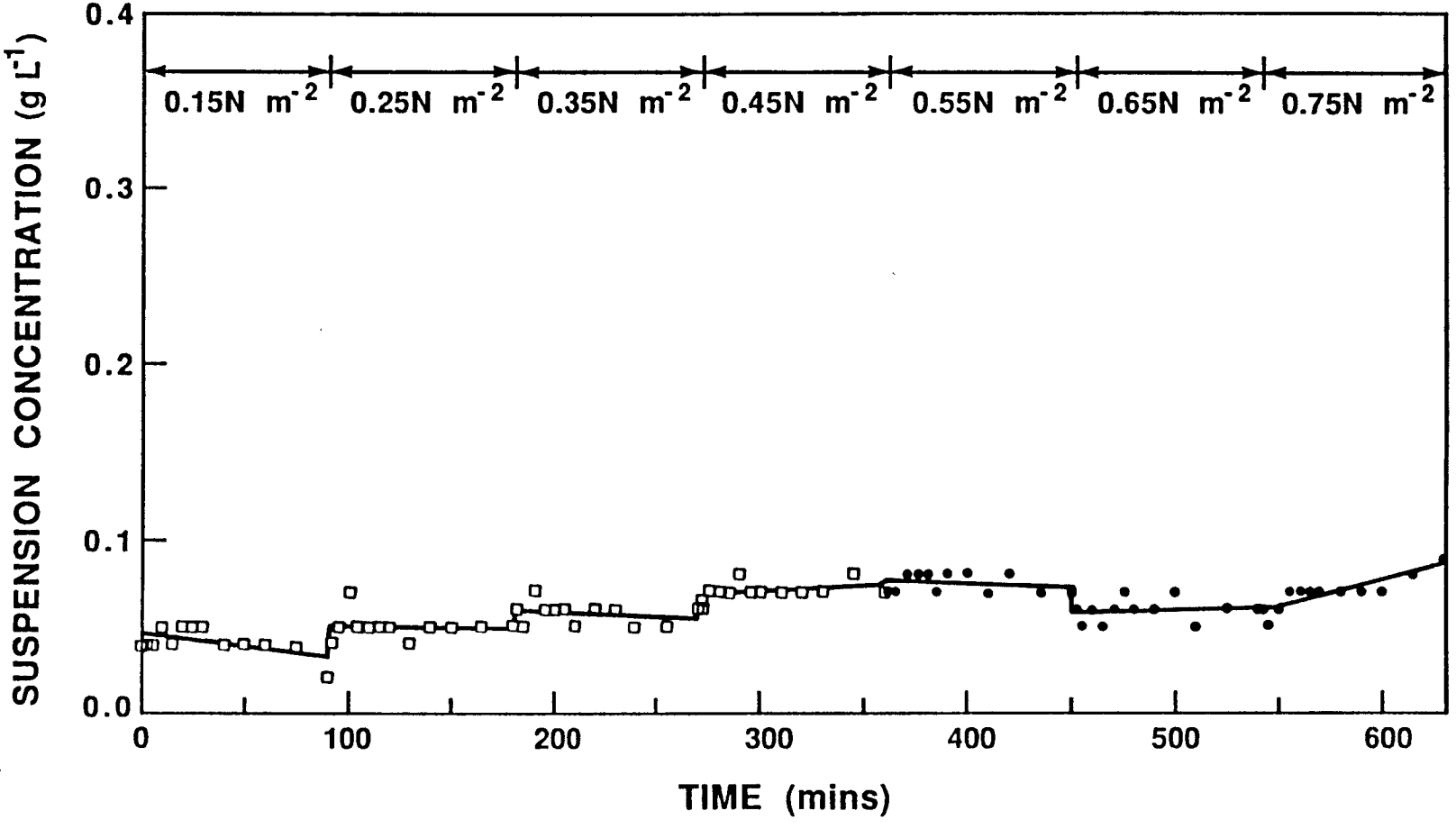

Figure 4.20: Time-Concentration Relationship in Test 4

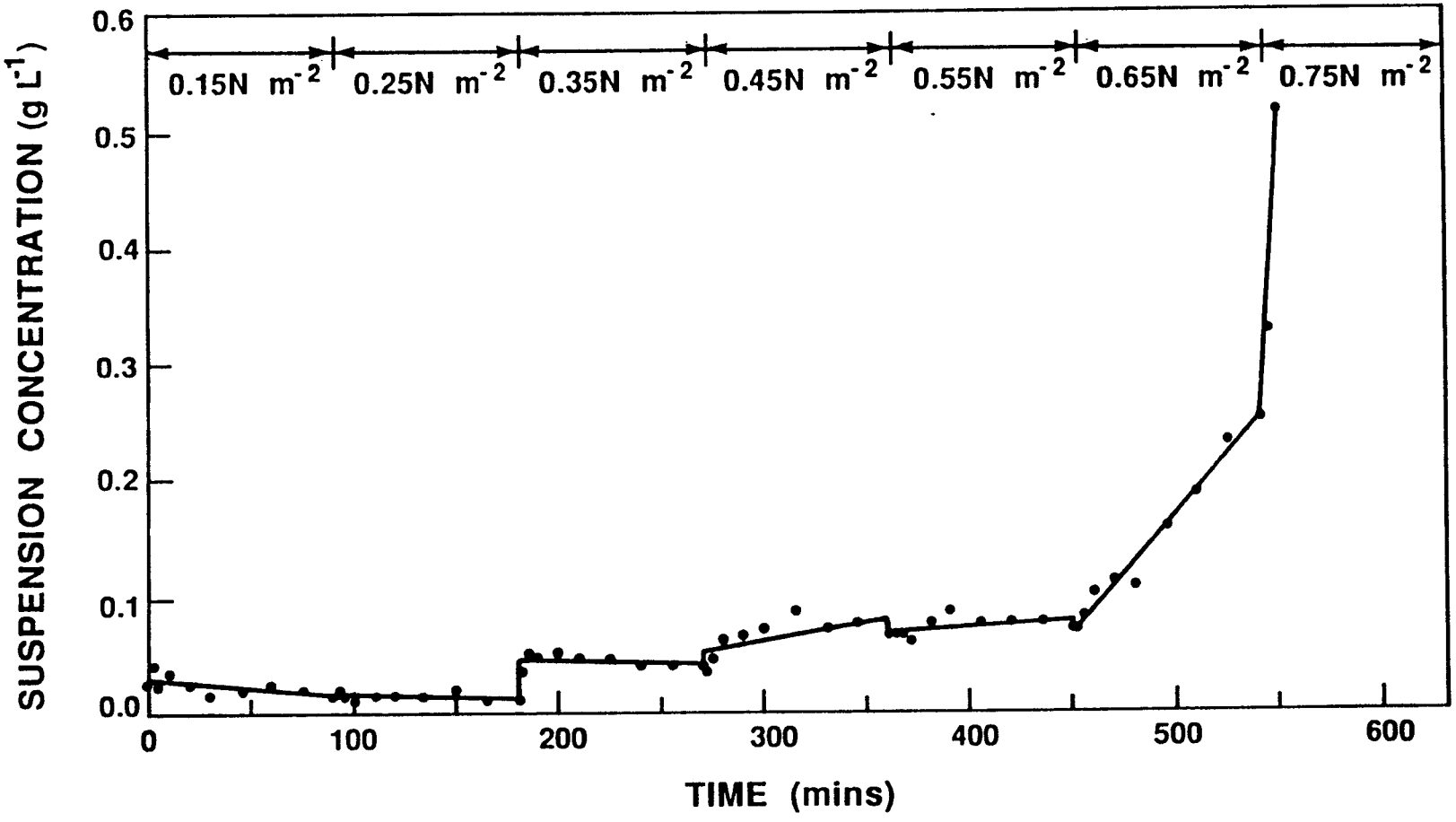

Figure 4.21: Time-Concentration Relationship in Test 6

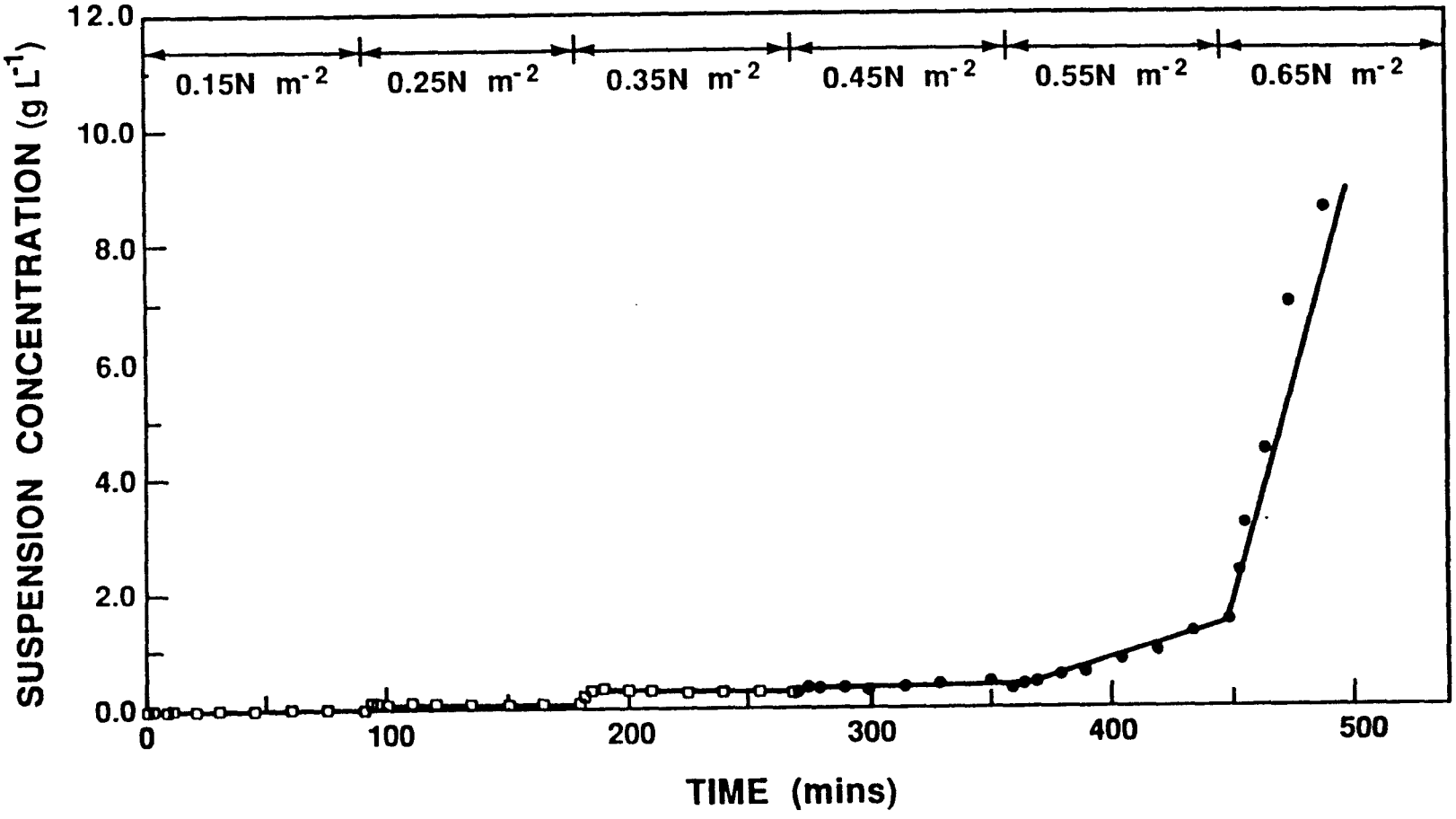

Figure 4.22: Time-Concentration Relationship in Test 5

duration steps in Figure 4.21. Without considering possible experimental error in the measurement of concentration, this trend can be explained by the effects of altered bed structure and occurrence of fluffy, highly organic sediment at the top bed. As noted, adding water into the flume in the manner described in section 4.5.3 caused the bed to become disturbed, following which the resuspended sediment settled down within 24 hrs. Due to this experimental difficulty, the top layer of the placed bed was essentially changed into a deposited bed. Therefore, during the erosion of this layer, the time-rate of change of suspension concentration initially decreased and finally became zero at each shear stress. Villaret and Paulic (1986) also observed such a trend and reported the placed bed in the annular flume exhibited an initial trend of steady state approach at low shear stresses.

In addition to the deposited bed behavior at the top bed layer, the effect of a very thin fluffy sediment layer at the top can explain the decreasing trend of concentration. It should be noted that the magnitude of concentration was typically very small at low shear stresses. This means that most sediment suspended at low shear stresses was possibly accounted for by the fluffy layer. The fluffy sediment may respond very sensitively to the initial shear stress application so that most of it would be suspended rapidly. Since the top layer of the bed exhibited the behavior of a deposited bed, bed erosion stopped at some level where the shear stress was equal to or less than the shear strength, and only resuspension of the deposited (as opposed to placed) sediment occurred. Therefore, the decreasing trend of concentration means that the amount of sediment resuspension was less than the amount deposited.

Another important observation in these tests was mass erosion, which usually occurred under high bed shear stress conditions and resulted in a structural breakdown of the bed at low bed densities.

An illustrative concentration profile for mass erosion is shown in Figure 4.22. This figure shows that at the highest shear stress (0.7 $N\ m^{-2}$) the suspension concentration rapidly increased with time, which is characteristic of mass erosion. Mass erosion seems

to be governed by bed shear stress as well as the time-rate of change of bed shear stress (Cervantes, 1987). This type of erosion was observed in every test except in tests 1 and 3.

Erosion rate and shear strength. Erosion rate (or erosion flux) for each shear stress was obtained by converting the time variation of the suspension concentration over the depth of flow to the corresponding time variation of the eroded sediment mass per unit bed surface area. The expression for this conversion is

$$\epsilon = \frac{\partial m}{\partial t} = h\frac{\partial C}{\partial t} \tag{4.14}$$

where ϵ is the erosion rate, m is the eroded sediment mass per unit bed surface area, and h is the depth of flow.

Using Fig. 4.21, for example, to calculate the erosion rate (ϵ) for surface erosion, the concentration difference (ΔC) during 1.5 hours (Δt) is calculated to be 0.027 $g\ cm^{-3}$ at $\tau_b = 0.45\ N\ m^{-2}$ over the water depth (h) of 23 cm. The substitution of ΔC, Δt and h into Equation 4.14 thus yields an erosion rate of 0.414 $mg\ cm^{-2}\ hr^{-1}$ at $\tau_b = 0.45\ N\ m^{-2}$.

Excepting negative values of ϵ due to the decreasing concentration variation for a given shear stress, erosion rate at each shear stress was calculated in the above manner and then plotted against the applied bed shear stress. The corresponding profiles of erosion rate related to bed shear stress are shown in Figs. 4.23 through 4.26. As observed from these figures, two straight fitted lines of slopes M_1 and M_2 (for example, see Fig. 4.23) were obtained. The line of slope M_1 represents the "fluff" erosion of bed surface at low shear stresses and the other line represents bed surface erosion at relatively high shear stresses. The actual mass of sediment eroded due to surface fluff (possibly of predominantly organic origin) is, however, not high, and for purposes here has been neglected from further consideration.

As has been described in section 3.2.1, the relationship between the erosion rate, $\epsilon = F_e$, and the bed shear stress is given as:

$$F_e = \epsilon_M(\frac{\tau_b}{\tau_{ce}} - 1) \tag{4.15}$$

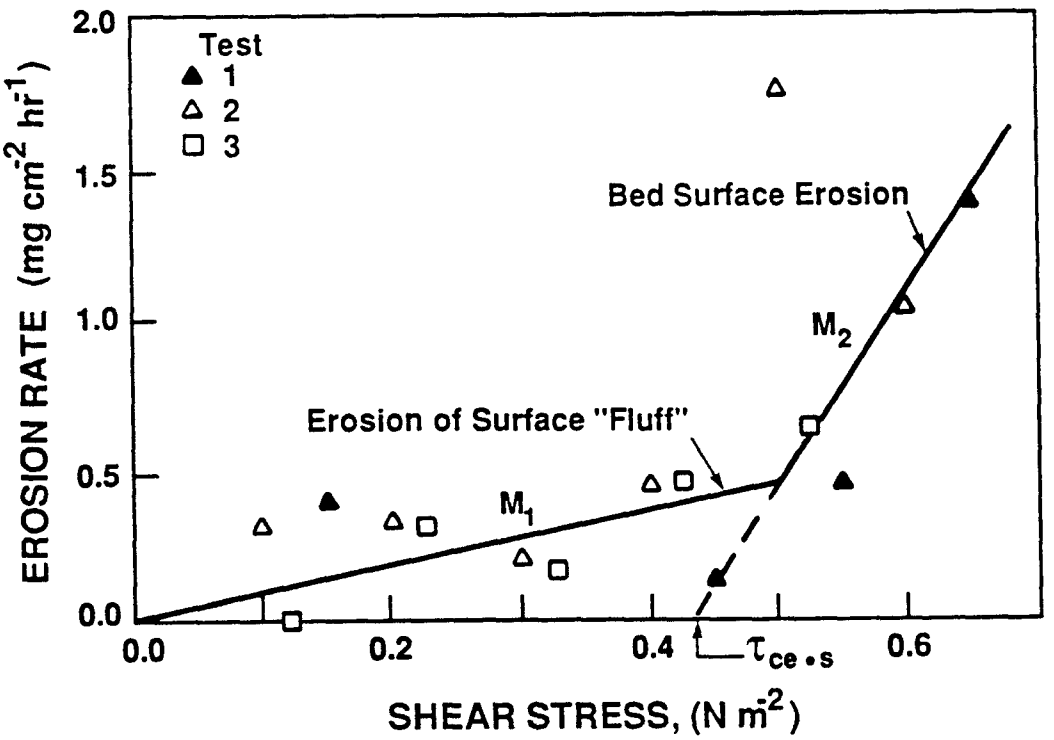

Figure 4.23: Composite Erosion Rate Variation with Bed Shear Stress for Tests 1, 2 and 3 at a Mean Density of 1.1 $g\ cm^{-3}$

where ϵ_M is an erosion rate coefficient, τ_{ce} is a erosion critical shear strength, and τ_b is a bed shear stress.

For surface erosion, the erosion critical shear strength, $\tau_{ce.s}$, can be determined by extrapolating the M_2 line back to the abscissa (Parchure and Mehta, 1985). The erosion rate coefficient, $\epsilon_{M.s}$, is obtained by multiplying $\tau_{ce.s}$ with M_2. Values of $\tau_{ce.s}$ and $\epsilon_{M.s}$ obtained through this method for each test are given in Table 4.5.

As shown in Fig. 4.23, erosion rates resulting from tests of 1, 2 and 3 were plotted to obtain the two parameters of $\tau_{ce.s}$ and $\epsilon_{M.s}$. The estimated values of $\tau_{ce.s}$ and $\epsilon_{M.s}$ are respectively 0.43 $N\ m^{-2}$ and 2.8208 $mg\ cm^{-2}\ hr^{-1}$ for a bulk density of 1.1 $g\ cm^{-3}$ averaged from bulk densities of all three tests. In this profile, since the bulk density for each test was not very different, the erosion rate data resulting from all tests could be combined together.

For mass erosion $\tau_{ce.m}$ may be considered to be equal to the applied shear stress at which mass erosion was observed. However, no reasonable method to estimate the erosion

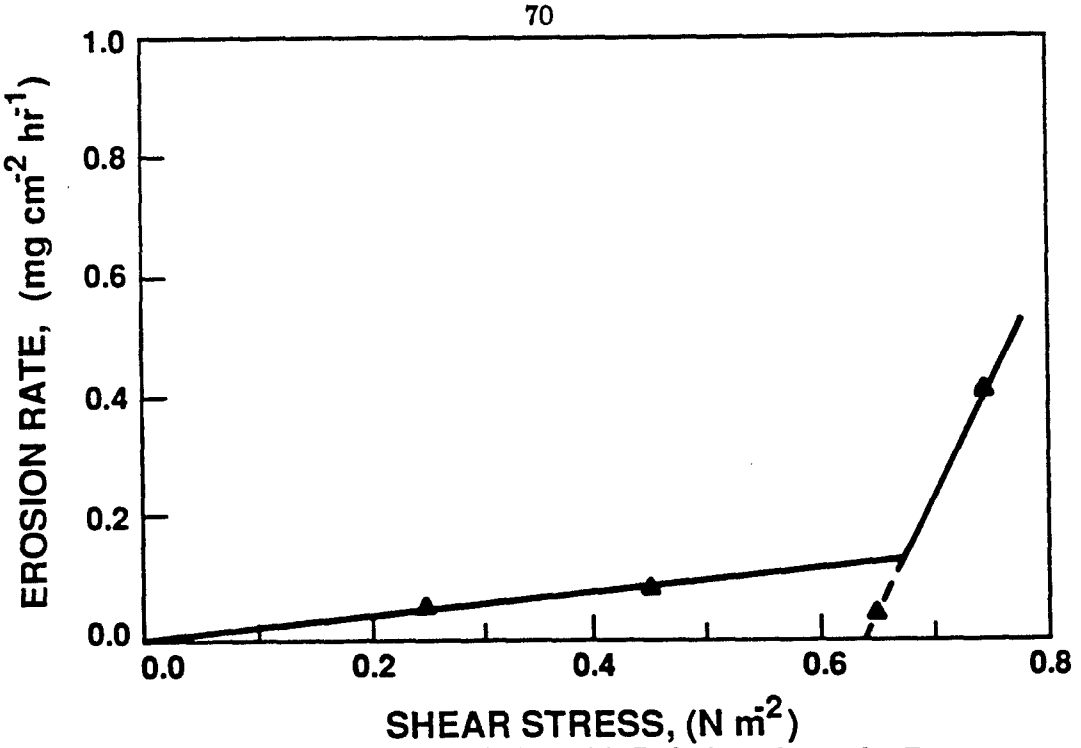

Figure 4.24: Erosion Rate Variation with Bed Shear Stress for Test 4

rate coefficient, $\epsilon_{M.m}$, has been suggested until now. Moreover, data obtained from this study were also not sufficient to determine $\epsilon_{M.m}$ in an acceptable manner. Therefore $\epsilon_{M.m}$ was assumed to be constant over a whole bed bulk density range and to be equal to $\epsilon_{M.s}$ at $\rho_B = 1.065\ g\ cm^{-3}$. As described in section 4.3.2, $1.065\ g\ cm^{-3}$ is the bulk density below which the bed was considered to be fluidized. The values of $\tau_{ce.m}$ for mass erosion for each tests are also given in Table 4.5.

In order to estimate the influence of bulk density (ρ_B) on the bed on two parameters, τ_{ce} and ϵ_M, these parameters were plotted against ρ_B and are presented in Fig. 4.27 and 4.28. As shown in Figure 4.27, which is a plot of bed shear strength against ρ_B, yields the following relationships for the two types of erosions

$$\tau_{ce.s} = a_s(\rho_B - \rho_l)^{b_s} + c_s \quad ; \quad \text{surface erosion} \tag{4.16}$$

$$\tau_{ce.m} = a_m\rho_B + b_m \quad ; \quad \text{mass erosion} \tag{4.17}$$

where $a_s = 0.883$, $b_s = 0.2$, $c_s = 0.05$, $a_m = 9.808$, $b_m = -9.934$, and ρ_l is the bulk density of uppermost bed level which is specified as $1.065\ g\ cm^{-3}$. Equation 4.16 seems to be

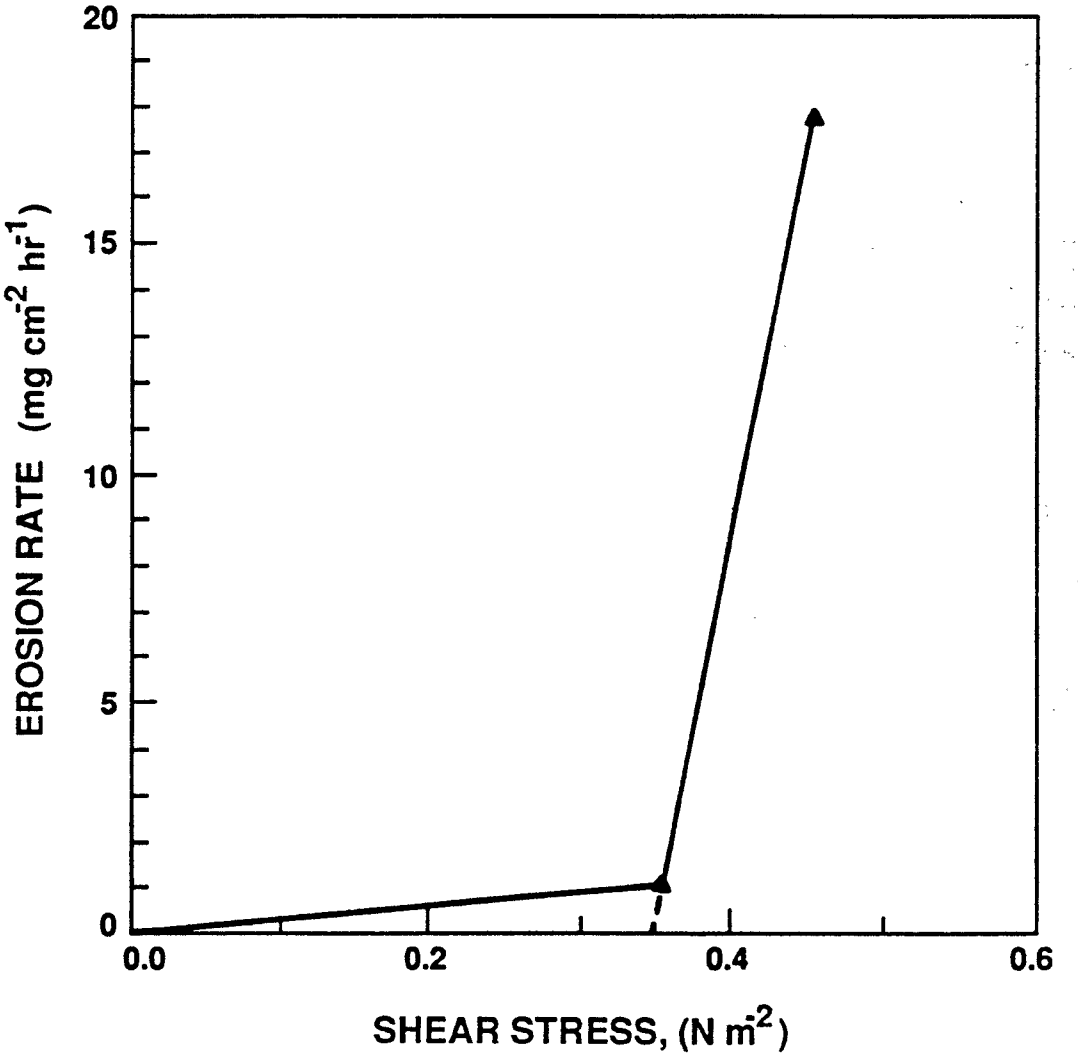

Figure 4.25: Erosion Rate Variation with Bed Shear Stress for Test 5

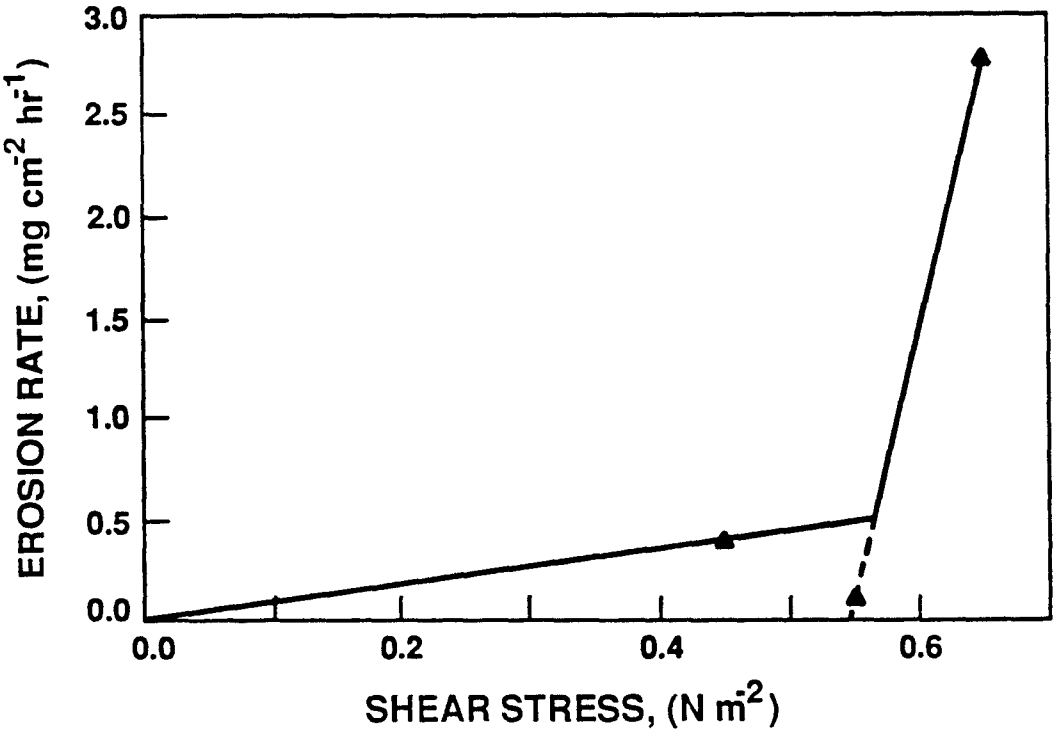

Figure 4.26: Erosion Rate Variation with Bed Shear Stress for Test 6

Table 4.5: Values of ρ_B, ϵ_M, and τ_{ce}

Test No.	ρ_B ($g\ cm^{-3}$)	$\epsilon_{M.s}$ ($mg\ cm^{-2}\ hr^{-1}$)	$\tau_{ce.s}$ ($N\ m^{-2}$)	$\tau_{ce.m}$ ($N\ m^{-2}$)
1	1.10			a
2	1.12	2.82*	0.43*	0.75
3	1.09			0.73
4	1.19	2.37	0.64	a
5	1.07	57.61	0.34	0.55
6	1.09	14.61	0.55	0.75

Note: * indicates that these values were obtained by combining the erosion rate data resulting from tests 1, 2 and 3.
Note: *a* indicates that no mass erosion was observed.

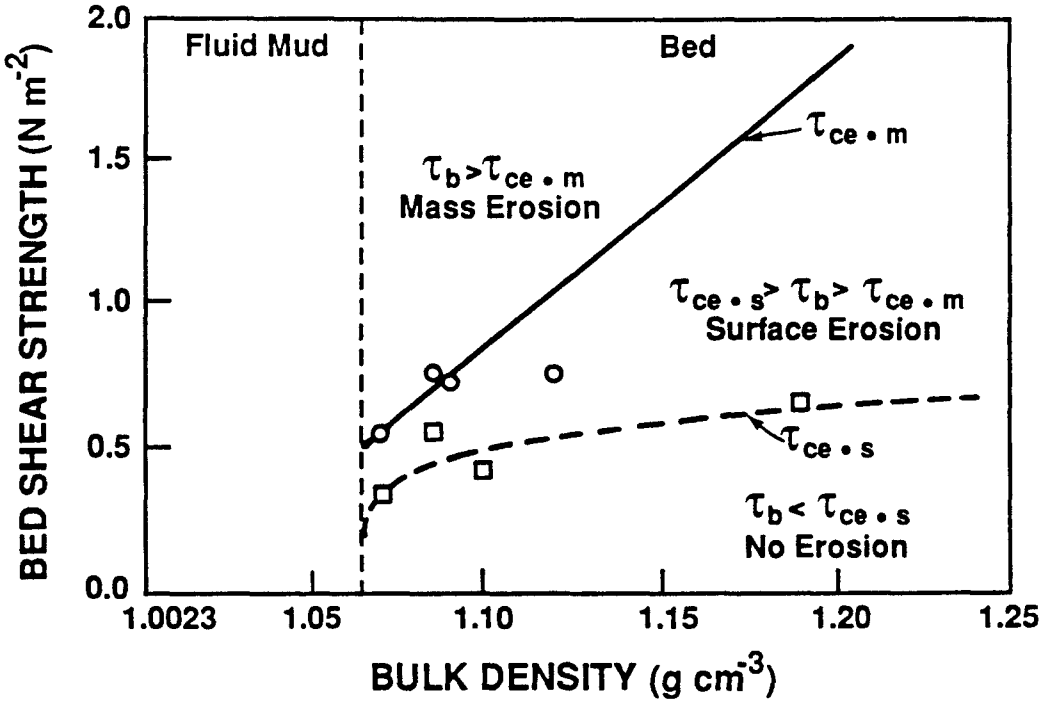

Figure 4.27: Critical Shear Stress, τ_{ce}, Variation with Bed Bulk Density, ρ_B

consistent with the expression, $\tau_{ce} = a\rho_B^b$, given by Owen (1970), while Equation 4.17 is in agreement with previous expression of the form, $\tau = a\rho_B + b$, given for surface erosion (Mehta et al., 1982; Villaret and Paulic, 1986).

In Fig. 4.28 the relationship between ϵ_M and ρ_B is expressed as

$$\ln \epsilon_{M.s} = s_1 \exp \frac{s_2}{\rho_B - \rho_3} \quad ; \quad \text{surface erosion} \tag{4.18}$$

$$\epsilon_{M.m} = m_1 \quad ; \quad \text{mass erosion} \tag{4.19}$$

where $s_1 = 0.23$, $s_2 = 0.198$, $m_1 = 224$, and ρ_3 is the bulk density at the upper level of the fluid mud zone selected to be 1.0023 $g\ cm^{-3}$. The assumed value of $\epsilon_{M.m} = m_1$ for mass erosion given in Equation 4.19 is likely to be reasonable since the calculated $\epsilon_{M.m}$ using data presented in Fig. 4.22, gives 239 $mg\ cm^{-2}\ hr^{-1}$, which is very close to m_1.

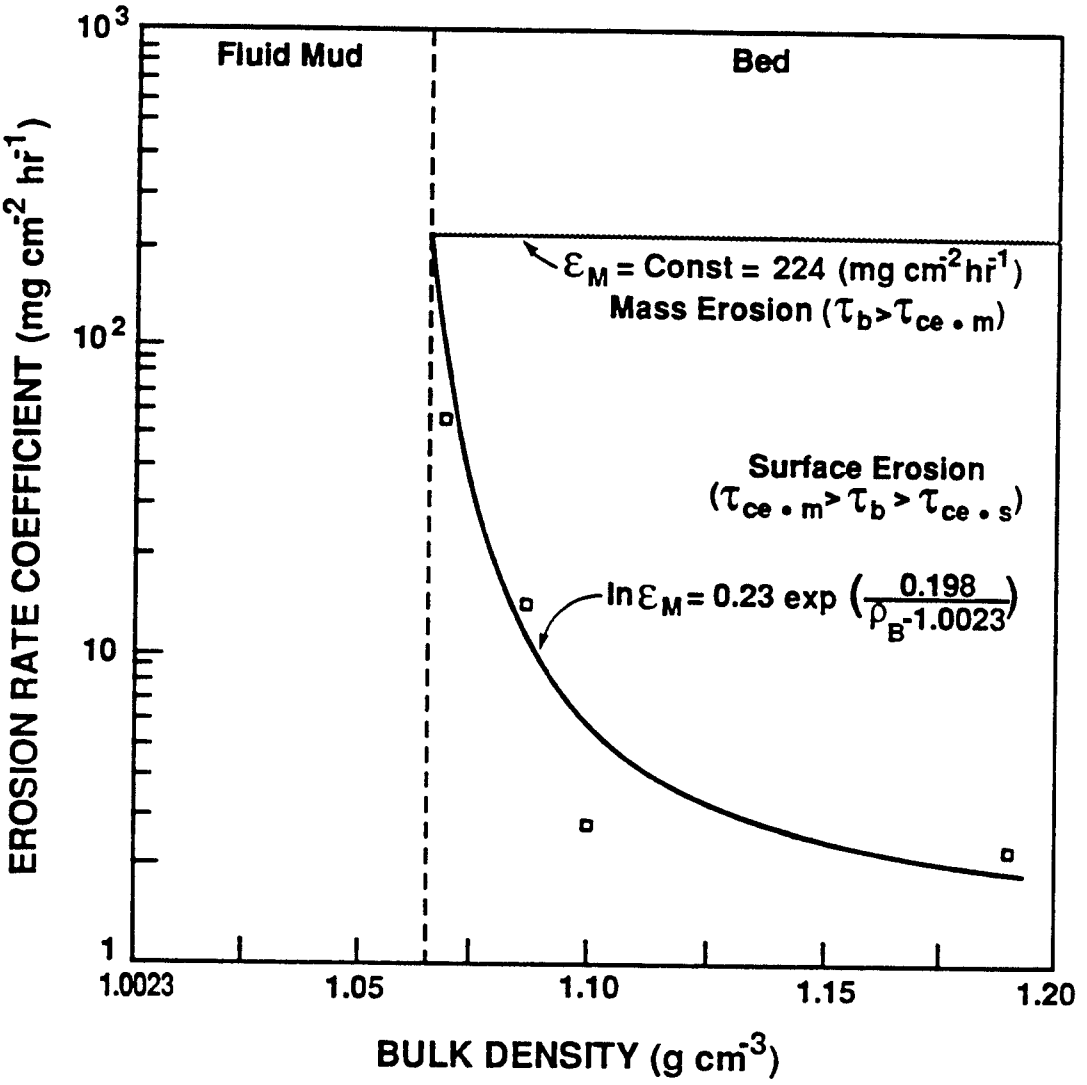

Figure 4.28: Erosion Rate Coefficient, ε_M, Variation with Bed Bulk Density, ρ_B

CHAPTER 5
APPLICATION TO LAKE OKEECHOBEE

5.1 Introduction

This chapter presents the application of the vertical sediment transport model to Lake Okeechobee using the theoretical aspects presented in chapter 3 and experimental data obtained in chapter 4. It must be emphasized that this is a realistic but simplified application using selected theoretical and experimental relationships to examine the evolution of vertical suspension concentrations of fine sediment in wave-dominated environments, in general. The vertical transport model was originally developed by Ross (1988). Since, however, his model did not include the calculation of eroded or deposited bed depth and the corresponding effects due to different degrees of wave action, the model was modified for these purposes. Details on modifications are described in following sections, including the modeling procedure and description of data used for simulation.

5.2 Numerical Model

5.2.1 Modeling Procedure

The vertical transport model solves equation 3.10 through a finite difference scheme, using boundary conditions 3.11 and 3.12. The model consists of an input data routine, an initialization routine, a main computation routine, a diffusion flux calculation routine, a settling flux calculation routine, a hydrodynamic calculation routine, a bed flux calculation routine and an output routine.

For each time step, the hydrodynamic routine calculates the changed the water depth of water column due to deposition or erosion, the maximum wave orbital velocities at the elevations corresponding to each grid point and the maximum wave-induced bed shear stress.

In the linear wave theory, the maximum orbital velocity at a given depth is obtained from Equation 3.30 as presented in section 3.4.1, and the maximum bed shear stress is computed using the relation

$$\tau_b = \frac{1}{2} f_w \rho u_b^2 \tag{5.1}$$

where f_w is the wave friction factor, ρ is the fluid density and u_b is the maximum orbital velocity just outside the bottom wave boundary layer. In this simple form for the bed shear stress the only unknown is f_w. Jonsson(1966) showed that the friction factor is dependent on the relative roughness of the boundary, and provided a diagram which gives the wave friction variation with Reynolds number and relative roughness (Dyer, 1986).

From this diagram it is possible to calculate τ_b, if an appropriate value for the equivalent bed roughness, k_s, can be chosen. The calculation of τ_b from u_b, and the selection of τ_b obtained in this way as the erosion forcing parameter, is valid only under quasi-steady conditions in which the rates of turbulence production and dissipation in the wave boundary layer can be assumed to be in equilibrium. This assumption is therefore inherent in the present study.

Initially, the water column height h is divided into n vertical layers, and each layer is represented by grid point i which is located at the center of the layer. For example, at the top layer $i = 1$ and at the layer just next to the bottom $i = n$. A definition sketch for grid schematization is given in Fig. 5.1. Vertical spacing, Δz, of each layer is equal except the vertical space, Δz_n, of the nth layer. The nth layer is represented initially by a fluid mud layer as noted further later, and eroded or deposited bed depth (z_b) at each time step is added to Δz_n.

Within the water column, at elevations corresponding to grid points, i, below the water surface, the neutral mass diffusivities are calculated through Equation 3.35. Mass diffusivities are then obtained through Equation 3.38. The diffusion fluxes are computed through a forward difference scheme:

$$F_d(i) \simeq K_z(i) \frac{C(i+1) - C(i)}{\Delta z} \tag{5.2}$$

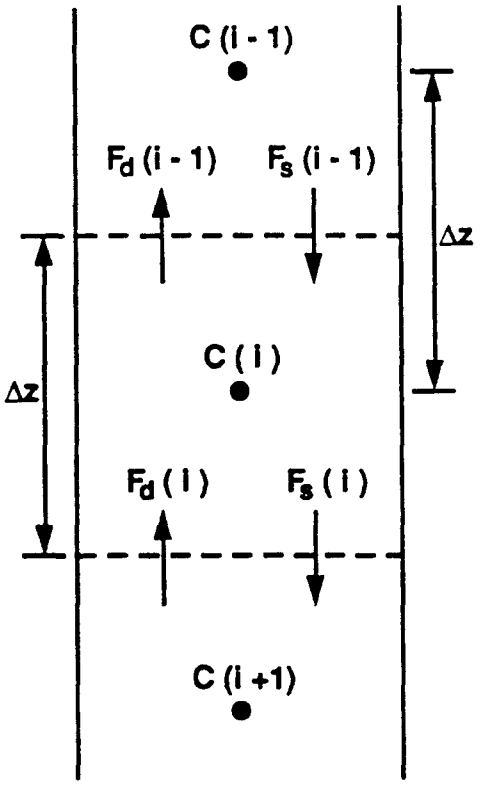

Figure 5.1: Definition Sketch for Grid Schematization

and the diffusion flux gradient is computed through backward differencing

$$\frac{dF_d(i)}{dz} \simeq \frac{F_d(i) - F_d(i-1)}{\Delta z} \tag{5.3}$$

The settling fluxes are computed at each grid point, i, by

$$F_s(i) = W_s(i)C(i) \tag{5.4}$$

where $W_s(i)$ is computed as a function of concentration using Equation 4.6, or a constant value is used to compute $W_s(i)$ if the concentration falls within the free settling range. In the range of concentrations for which the settling flux increases with C (flocculation settling), the settling flux gradient is computed using backward differencing:

$$\frac{dF_s(i)}{dz} \simeq \frac{F_s(i) - F_s(i-1)}{\Delta z} \tag{5.5}$$

while in the hindered flux range a forward differencing is used:

$$\frac{dF_s(i)}{dz} \simeq \frac{F_s(i+1) - F_s(i)}{\Delta z} \tag{5.6}$$

The concentration at every grid point within the water column is then computed as

$$C^{t+\Delta t}(i) = C^t(i) + \Delta t\left(\frac{dF_s(i)}{dz} + \frac{dF_d(i)}{dz}\right) \tag{5.7}$$

where Δt represents the time increment.

Bed fluxes are computed corresponding to one of four cases as defined by the value of the bed shear stress amplitude, τ_b:

1. For $\tau_b < \tau_{cd}$ the depositional flux F_p is obtained from Equation 3.16 with $H = 1$.

2. For $\tau_{ce.s} < \tau_b < \tau_{ce.m}$ erosion is specified by surface erosion and an erosion flux is obtained as follows

$$F_e = \varepsilon_{M.s}\left(\frac{\tau_b}{\tau_{ce.s}} - 1\right) \tag{5.8}$$

where both $\tau_{ce.s}$ and $\varepsilon_{M.s}$ are computed as functions of the sediment bulk density ρ_B of bed as given in Equations 4.16 and 4.18, respectively.

3. For $\tau_b > \tau_{ce.m}$ mass erosion occurs and the corresponding erosional flux is defined as

$$F_e = \varepsilon_{M.m}\left(\frac{\tau_b}{\tau_{ce.m}} - 1\right) \tag{5.9}$$

where $\tau_{ce.m}$ and $\varepsilon_{M.m}$ are also dependent on ρ_B according to Equations 4.17 and 4.19, respectively.

It should be noted that a bed bulk density profile with depth (for example, see Equation 5.13) is essentially required for calculating the erosion flux and eroded depth of the bed, since τ_{ce} and ε_M for both surface erosion and mass erosion vary with ρ_B of bed. For each time step, the amount of sediment mass eroded or deposited per unit bed area (F_e or F_p) is used to calculate the eroded or deposited bed depth (z_b) in accordance with the given profile of bed bulk density with depth. For each time step, Δt, the eroded or deposited bed depth is obtained from following expression

$$z_b^{t+\Delta t} = z_b^t + \Delta t\frac{F_b}{C_b} \tag{5.10}$$

where F_b is the bed flux represented by F_e or F_p and C_b is the concentration of the eroded or deposited bed during Δt corresponding to the bed bulk density profile. With this depth, the bulk density is recalculated and the height of water column (h) and Δz_n are redefined.

The new value of the concentration, $C(n)$, at the grid point just above the bed which represents the fluid mud layer is computed as

$$C^{t+\Delta t}(n) = C^t(n) + \Delta t[\frac{F_b}{\Delta z_n} + \frac{dF_s(n)}{\Delta z_n} + \frac{dF_d(n)}{\Delta z_n}] \tag{5.11}$$

where n indicates the grid point specifying the layer just above the bed.

5.2.2 Data used for Modeling

In order to simulate the vertical concentration profiles and the corresponding eroded depths, the vertical transport model requires the following data:

1. Hydrodynamic data
   - Wave data represented by the wave period (T) and the wave height (H)
   - Initial water column height (h)
2. Sediment parameters
   - Sediment granular density (ρ_s)
   - Parameters of a, b, m and n used to compute the settling velocity dependence on concentration
   - Maximum settling velocity (W_{so}) and the concentration (C_1) defining the limit of the free settling range
3. Diffusion parameters
   - Empirical parameter for neutral mass diffusivity (α_w)
   - Empirical parameters for stabilized diffusivity (α and β)

Table 5.1: Hydrodynamic Conditions

Run No.	h (m)	T (sec)	H (m)	L (m)
1	4.6	4.0	0.9	21.7
2	2.8	3.5	0.8	15.5
3	4.6	3.5	0.7	17.7
4	2.8	3.5	0.6	15.5

4. Bed characteristics

   - Bed density parameters needed to calculate bulk density variation with bed depth (p_1, p_2, p_3 and p_4 in Equation 5.13)
   - Friction factor (f_w) used to compute the maximum bed shear stress
   - Critical shear stress for deposition (τ_{cd})
   - Parameters (a_s, b_s, c_s, a_m and b_m in Equation 4.16 and 4.17) necessary to calculate the critical shear stresses ($\tau_{ce.s}$ and $\tau_{ce.m}$) for both surface and mass erosion at a certain ρ_B
   - Parameters (s_1, s_2, m_1 and ρ_3 in Equation 4.17 and 4.19) used to compute the erosion rate coefficients ($\epsilon_{M.s}$, and $\epsilon_{M.m}$) for both surface and mass erosion at a given ρ_B

5. Initial concentration profile

   - Initial values of sediment concentration at each grid point

For the hydrodynamic data, two different wave conditions at two different water depths were selected to run the model. Wave data and the depth used for each run are given Table 5.1. Wave conditions for runs 1 and 2 may be considered to represent those caused by a strong wind in Lake Okeechobee, while wave conditions for runs 3 and 4 correspond to those developed by a moderate wind (Ahn, 1989). Here, strong wind is represented by a wind which has approximately a wind velocity of 20 $m\ sec^{-1}$ 10 m above water surface,

and moderate wind is represented by a wind which has a wind velocity of 10 $m\ sec^{-1}$. Two different water depths were selected to be 2.8 m and 4.6 m, noting that the water depth within the muddy zone in Lake Okeechobee ranges approximately from 2 m to 5 m. The 4.6 m depth is that used by Gleason and Stone (1975) to calculate the erodible bed depth, while 2.8 m is representative of typical mean depth over the muddy zone. With the given wave period T, the wave length L in Table 5.1 was obtained from the relationship

$$L = \frac{gT^2}{2\pi} \tanh \frac{2\pi h}{L} \tag{5.12}$$

For the sediment granular density, ρ_s, which is one of the sediment parameters, 2.14 $g\ cm^{-3}$ obtained by averaging ρ_s of mud samples from five different sites as described in section 4.2.1 was used. For the settling parameters (a, b, m, n, and W_{so}), those obtained from the sample at site 1 were used as representative values (see Table 4.3). The concentration C_1 below which settling was considered to be free was selected to be 0.1 $g\ L^{-1}$.

Parameters α and β used in Equation 3.38 for stabilized diffusivity were both 0.5. In the fine-grained sediment transport study in Lake Erie, a shallow body of water with an average depth of 7 m, Lick (1982) reported that a representative mass diffusivity was approximately 25 $cm^2 sec^{-1}$. For present study α_w, which is a empirical constant for mass diffusivity in Equation 3.35 was calibrated to meet this condition. After trial and error, the selected value of α_w for Lake Okeechobee was 1.56×10^{-2}.

The eroded depth strongly depends on the given vertical profile of the bed bulk density (ρ_B). Therefore, it is important to know the real density profile in order to establish a proper sediment vertical transport model. For Lake Okeechobee, the vertical profile of ρ_B in the bottom layer was different depending upon the sites as shown through the bottom core sample analysis in section 4.3. However, these profiles could be divided into four typical profiles as presented in Figures 5.2 through 5.5.

In order to run the model, the vertical profile of ρ_B in Fig. 5.2 was representitively used. Through the least squares fit method, the expression for the bulk density variation

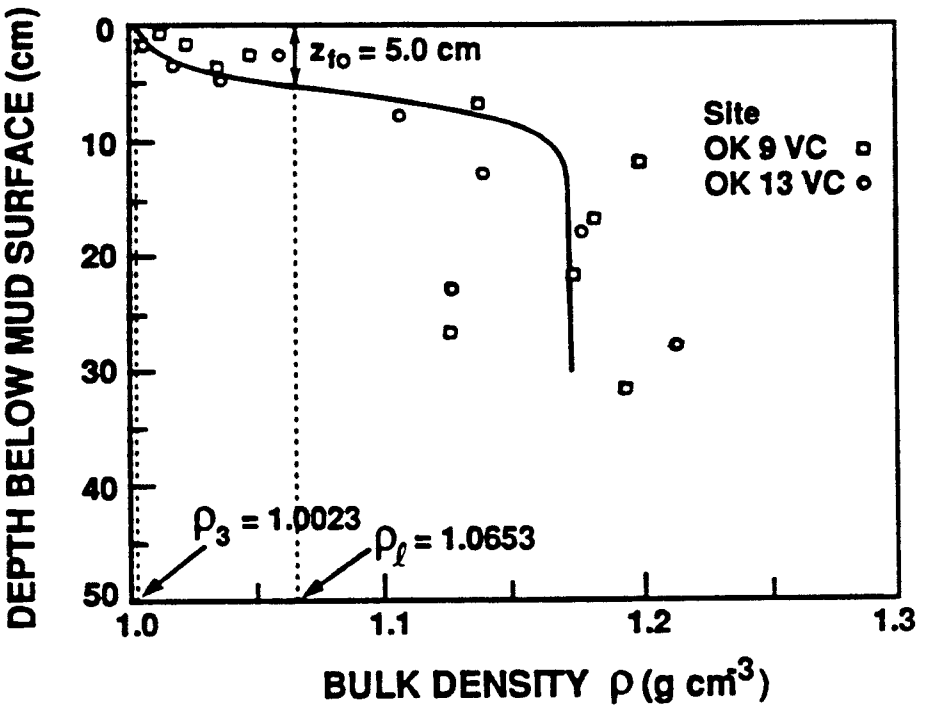

Figure 5.2: Typical Bulk Density Variation of the Bottom Mud Layer in Lake Okeechobee; Type 1

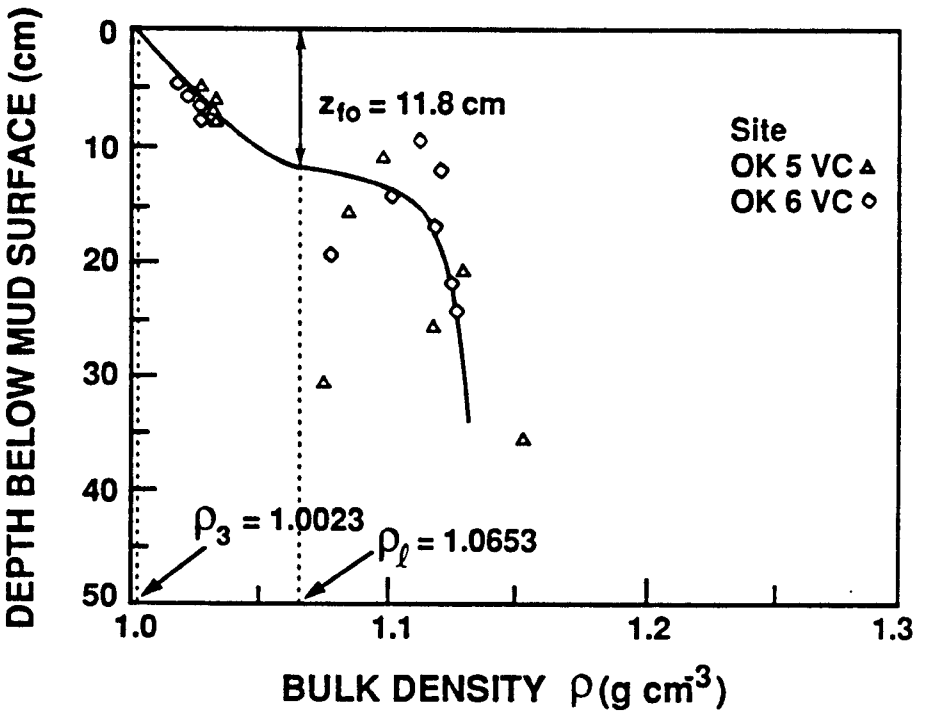

Figure 5.3: Typical Bulk Density Variation of the Bottom Mud Layer in Lake Okeechobee; Type 2

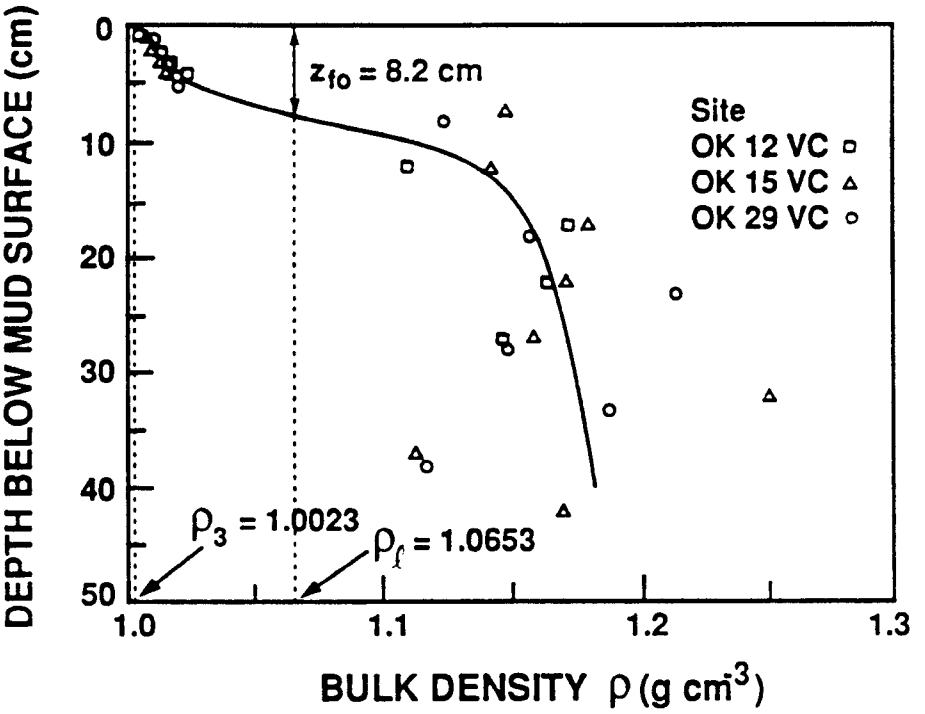

Figure 5.4: Typical Bulk Density Variation of the Bottom Mud Layer in Lake Okeechobee; Type 3

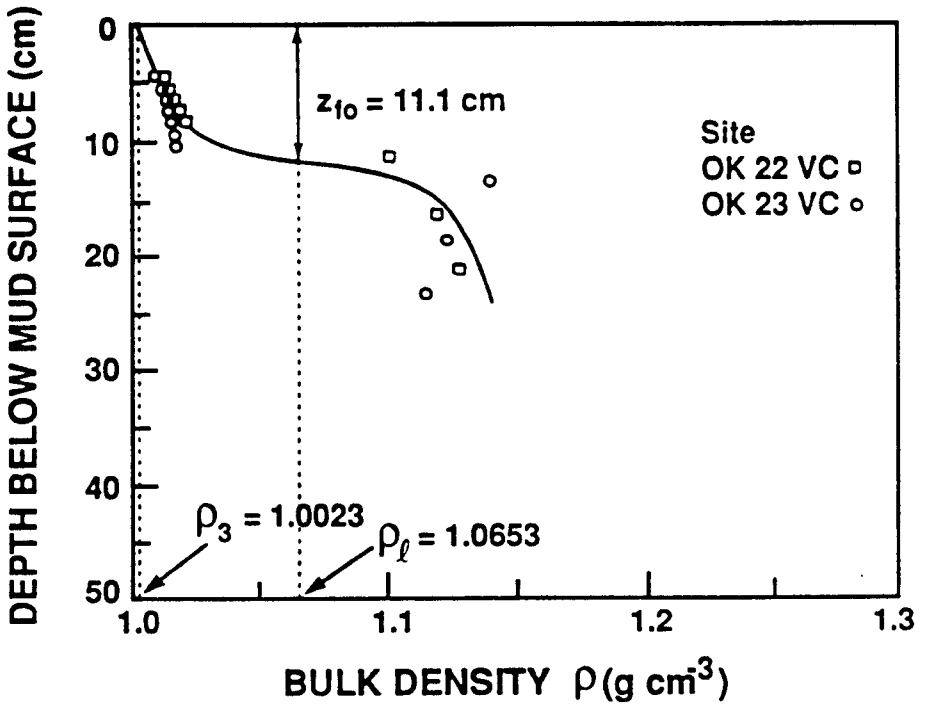

Figure 5.5: Typical Bulk Density Variation of the Bottom Mud Layer in Lake Okeechobee; Type 4

with bed depth was obtained as

$$\rho_B = p_1 \tanh[p_2(z + p_3)] + p_4 \tag{5.13}$$

where p_1, p_2, p_3 and p_4 are 0.087, 0.372, 5.8 and 1.087, respectively. ρ_3 and ρ_l shown in the figures represent the upper level and the lower level of the fluid mud layer, respectively and defined to be 1.0023 $g\ cm^{-3}$ and 1.065 $g\ cm^{-3}$. The determination of ρ_3 and ρ_l is described later in section 5.3.2. Given these values of ρ_3 and ρ_l, the thickness of the fluid mud layer, z_{fo}, was estimated to range from 5.0 cm (Type 1) to 11.8 cm (Type 2), which is in agreement with similar but qualitatively determined values reported by Gleason and Stone (1975).

As described in section 5.2.1, in order to determine the friction factor f_w from the diagram given by Jonsson (1966), the equivalent bed roughness k_s and the horizontal water motion (amplitude) at the bottom, A_b, must be estimated. In the study of bed friction characteristics at three locations on the Gulf Coast of Florida, Mehta (1978) used the following well known expressions for Manning's n and k_s

$$n = \frac{h^{1/6}}{g^{1/2}} \frac{u_*}{\overline{u}} \tag{5.14}$$

$$k_s = 3.15 \times 10^5 h (\frac{u_*}{\overline{u}})^6 \tag{5.15}$$

where u_* is the friction velocity, $\overline{u}$ is mean velocity over depth h of water and g is the gravity acceleration. Combining Equations 5.14 and 5.15, k_s can be expressed as follows (Manning-Strickler formula):

$$k_s = 3.15 \times 10^5 g^3 n^6 \tag{5.16}$$

Assuming $n = 0.011$ for Lake Okeechobee based on fine sediment bed resistance data reported by Dixit (1982), k_s obtained from Equation 5.16 was $5.27 \times 10^{-4}\ m$. With given k_s, f_w varies with A_b, which is given by

$$A_b = \frac{H}{2 \sinh \frac{2\pi h}{L}} \tag{5.17}$$

Table 5.2: Values of A_b, f_w and τ_b

run No.	A_b (m)	f_w	τ_b ($N\ m^{-2}$)
1	0.2576	0.011	0.92
2	0.2875	0.010	1.36
3	0.1437	0.014	0.48
4	0.2157	0.012	0.92

For each run, A_b was obtained using the hydrodynamic data given in Table 5.1 and the corresponding f_w was determined from Jonsson's diagram. By inserting the determined f_w into Equation 5.1, τ_b for each run was obtained. Note that ρ in Equation 5.1 is represented by $C(n)$, therefore τ_b varies with $C(n)$, since $C(n)$ changes with each time step. A_b, f_w and τ_b at initial time obtained for each run are given in Table 5.2.

Critical shear stress for deposition (τ_{cd}) was assumed to be 0.1 $N\ m^{-2}$ as described in section 3.2.2. The initial values of sediment concentration at each grid point were assumed to be zero, thus representing pre-wind or calm, clear water condition prior to resuspension,except the lowest grid point n. From the vertical profile of ρ_B in Fig. 5.2, Δz_n was assumed to be initially 5 cm and the initial concentration at the n th (lowest) grid point, to be 39 $g\ L^{-1}$ which was obtained by averaging ρ_B over the thickness of the fluid mud layer. Note that an additional simulation was also carried out, as described later, without the initial presence of fluid mud over the bed. In this case, $C(n)$ was, of course, zero initially.

5.3 Results and Discussion

5.3.1 Evolution of concentration profile

Model simulated concentration profiles for the four runs are shown in Figures 5.6 through 5.9. Concentration profiles for run 1, given in Fig. 5.6, pertain to the case which has been selected in accordance with the measurement of 102 $mg\ L^{-1}$ surface concentration at the water depth of 4.6 m during a storm by Gleason and Stone (1975), as noted previously in section 5.2.2. As noted, in Lake Okeechobee storm waves of 0.9 m height and 4 sec period are believed to occur under extreme conditions (strong wind); therefore,

these values were selected for the present purpose since Gleason and Stone did not report wave conditions during their concentration measurement. It was decided to initiate, also as noted, simulation beginning with a clear water column and fluid mud layer near the bottom and continue wave action until the concentration reached 102 $mg\ L^{-1}$, with the aim to determine the corresponding erodible depth of the bed layer and the corresponding thickness of the fluid mud layer. For this purpose, it was necessary to specify a representative density (concentration) of the fluid mud layer, which, as noted, was selected to be 39 $g\ L^{-1}$. This consideration is further described in section 5.3.2. As shown in Fig. 5.6, 102 $mg\ L^{-1}$ concentration occurred at about 11 hr after the beginning of wave action. At 11 hr, 1.3 cm of bed had eroded as opposed to 2.3 mm suggested by Gleason and Stone assuming uniform water column concentration.

Figure 5.7 shows the simulated concentration profiles resulting from run 2, in which the wave conditons considered were the same as in run 1 but a shallow water depth of 2.8 m was selected in order to compare with the results of run 1. As observed, the surface concentrations at 2 hr and 2.5 hr, which are relatively short times as compared with 11 hr in run 1, were 94 $mg\ L^{-1}$ and 130 $mg\ L^{-1}$, respectively, while the corresponding eroded depths were 1.7 cm and 1.8 cm, which were in agreement with run 1.

The simulated concentration profiles for the case of the moderate wave conditions at the above two different depths are shown in Fig. 5.8 and 5.9. In Fig. 5.8, which resulted from run 3, at 10 hr the surface concentration was at most 40 $mg\ L^{-1}$ with the corresponding eroded depth of 0.5 cm. Run 4 (Fig. 5.9) showed the surface concentration of 102 $mg\ L^{-1}$ at 6 hr and an eroded depth of 1.2 cm.

As expected, it is noted that the times required to reach a surface concentration of 102 $mg\ L^{-1}$ were different for each run depending on τ_b. However, the corresponding eroded bed depths were always on the order of $1-2$ cm. This indicates that in order to have the surface concentration of 102 $mg\ L^{-1}$, a bed material erosion of $1-2$ cm depth is necessary under any wave condition.

There is an evident qualitative agreement between the simulated results of Fig. 5.6 and profile evolution under prototype conditions (profiles 1, 2, 3) shown in Fig. 2.2 (Kemp and Wells, 1987). A noteworthy observation is that in both cases the concentration over 80 % of the water column down from the surface was quite low throughout, and that most of the sediment was elevated to a relatively small height above the bed. Further entrainment of the lutocline was undoubtedly constrained by the submerged weight of the high concentration layer below the lutocline, and the lack of a strong mechanism for diffusion.

Another run, for which results are shown in Fig. 5.9, was made to simulate the followup "post-storm" calm situation using the concentration profile at 11 hour given in Figure 5.6, assuming no wave action after this time. The profile at 35 hour resulted solely due to settling, indicating lower near-surface as well as near-bed concentrations than at 11 hour. At this stage, the redeposited bed depth was 2.7 *cm*. Eventually, of course, all of the material would settle provided the conditions remained calm. It is noteworthy that in reality the rate of reformation of the bed would most probably be slower than that implied from this simulation, because initially the redeposited material will have a lower density than during prior erosion of the comparatively more settled initial deposit. Freshly deposited materials dewater and their density increases with time relatively rapidly within hours (Parchure and Mehta, 1985). However, dewatering becomes slower in the presence of ongoing settling of the sediment from the upper water column (Sills and Elder, 1986).

5.3.2 Erodible depth

The erodible bed depth is dependent on the thickness and concentration of the overlying fluid mud zone. Consequently, it is essential to define this zone through physical reasoning. Here, an operational definition of the fluidized mud layer thickness, consistent with relatively easily and routinely obtained sedimentary data, is considered (see Fig. 5.11).

Under conditions defined by settling of suspension in the absence of upward diffusion, or very weak diffusion, the lutocline can be represented by concentration C_3 in Fig. 3.1.

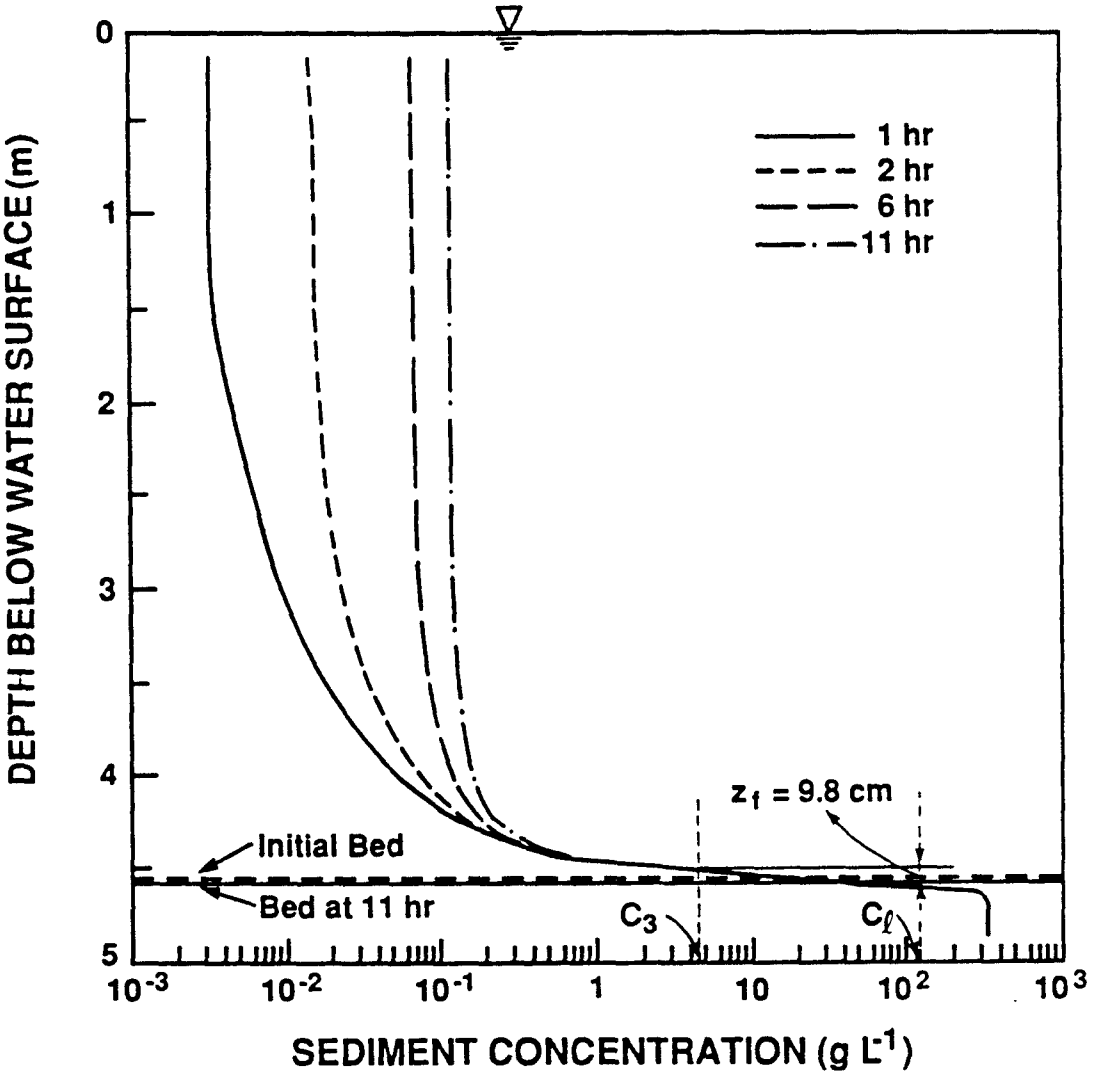

Figure 5.6: Simulated Evolution of Suspension Concentration Profile in Run 1

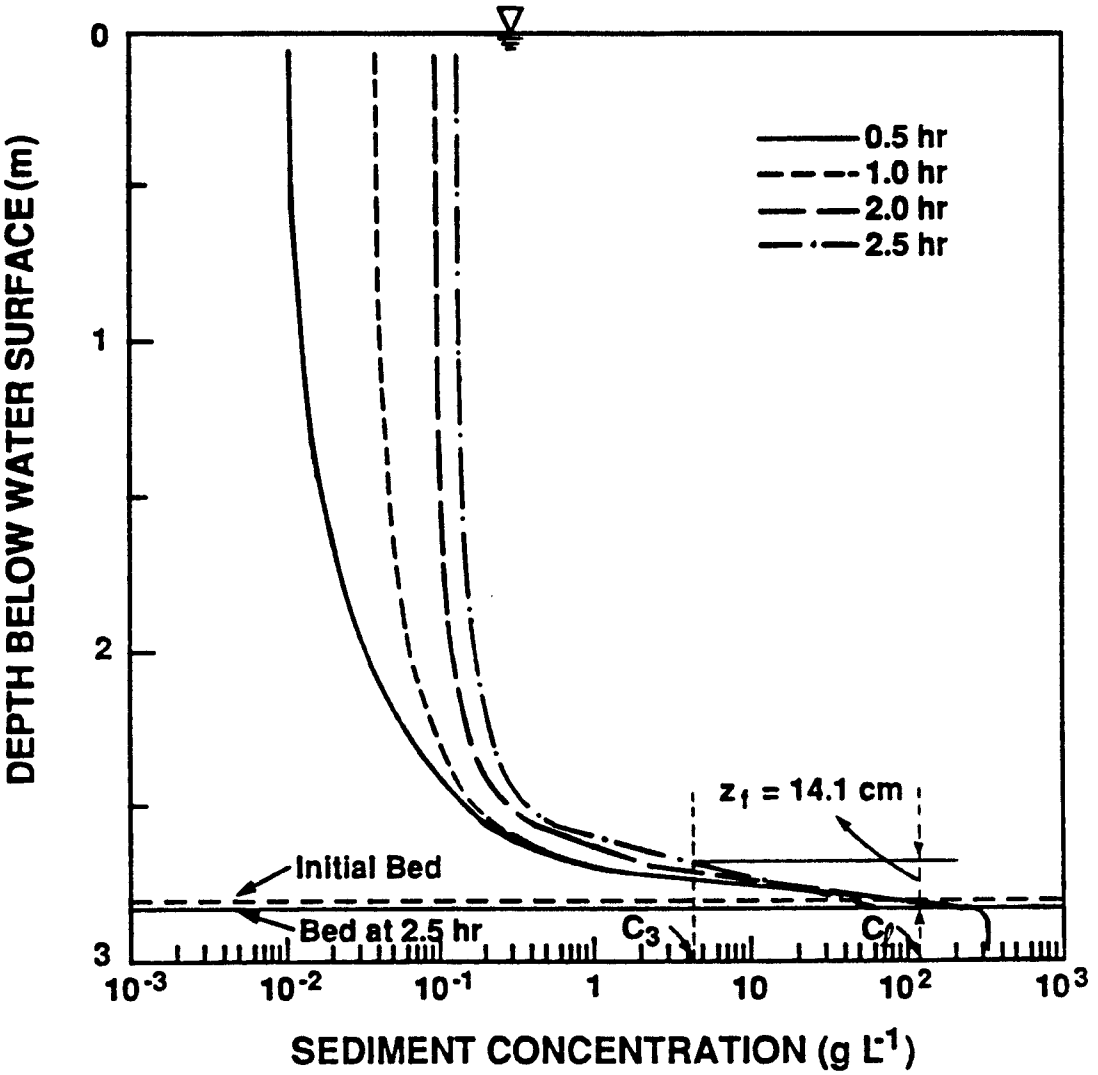

Figure 5.7: Simulated Evolution of Suspension Concentration Profile in Run 2

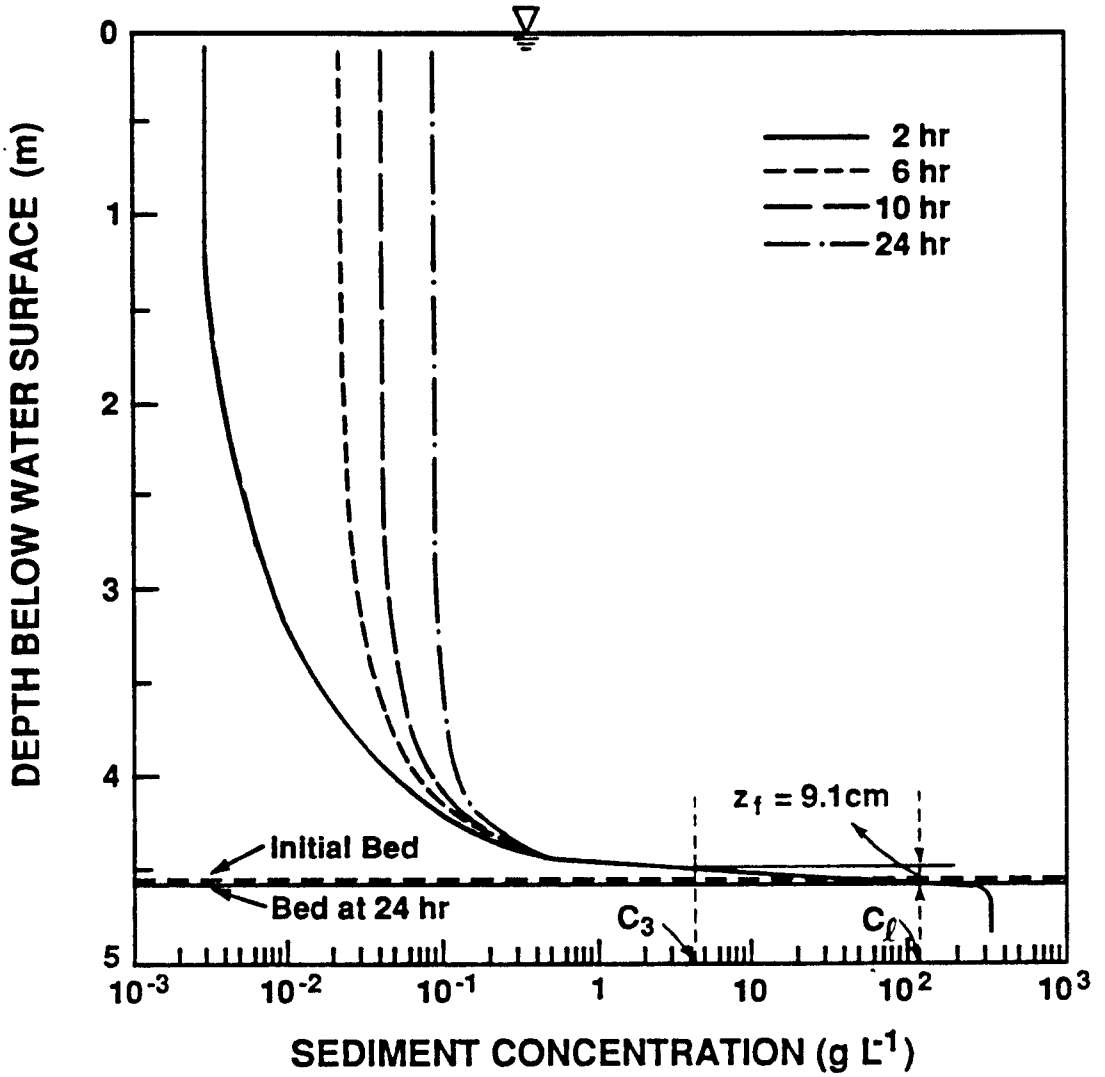

Figure 5.8: Simulated Evolution of Suspension Concentration Profile in Run 3

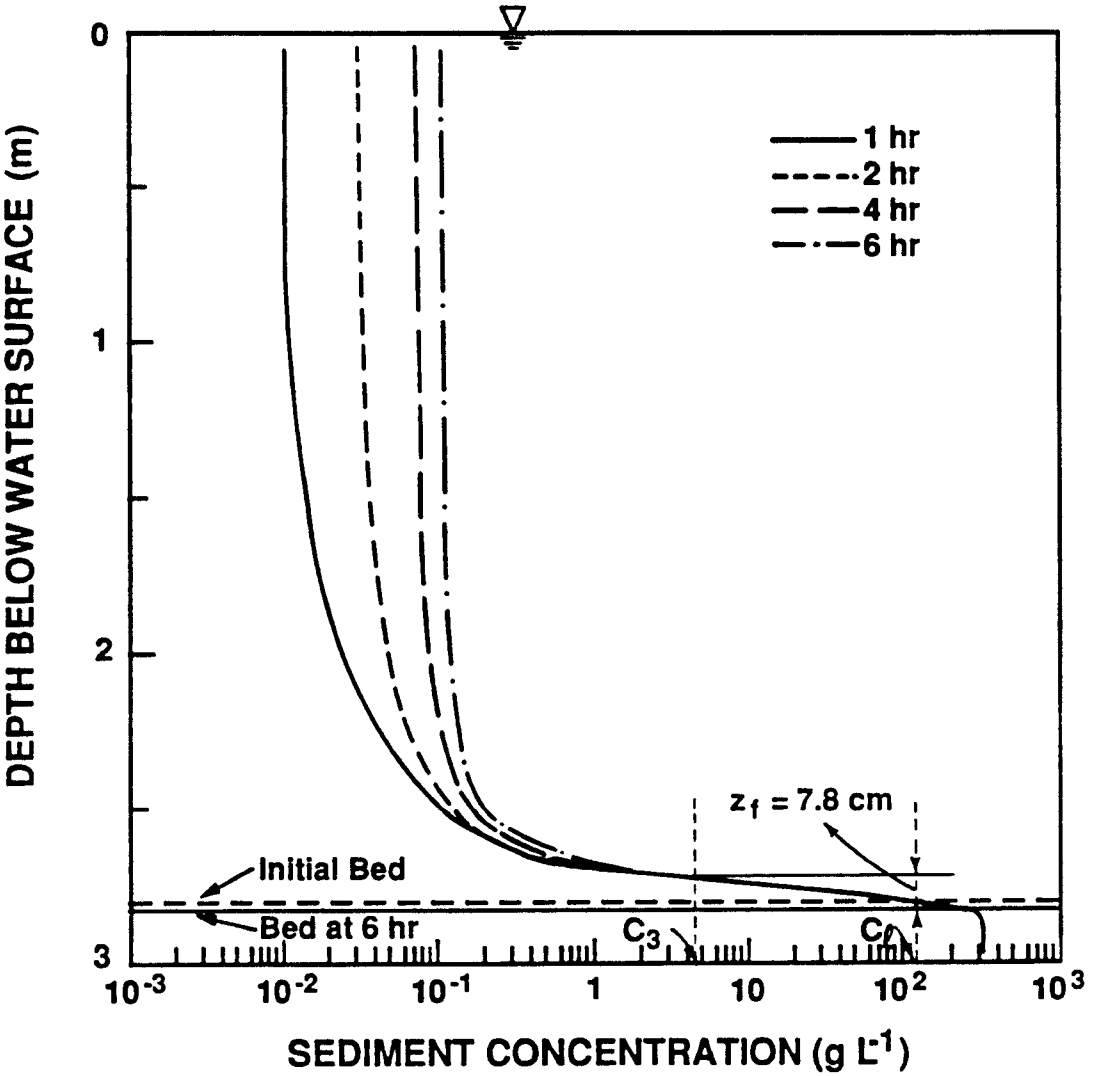

Figure 5.9: Simulated Evolution of Suspension Concentration Profile in Run 4

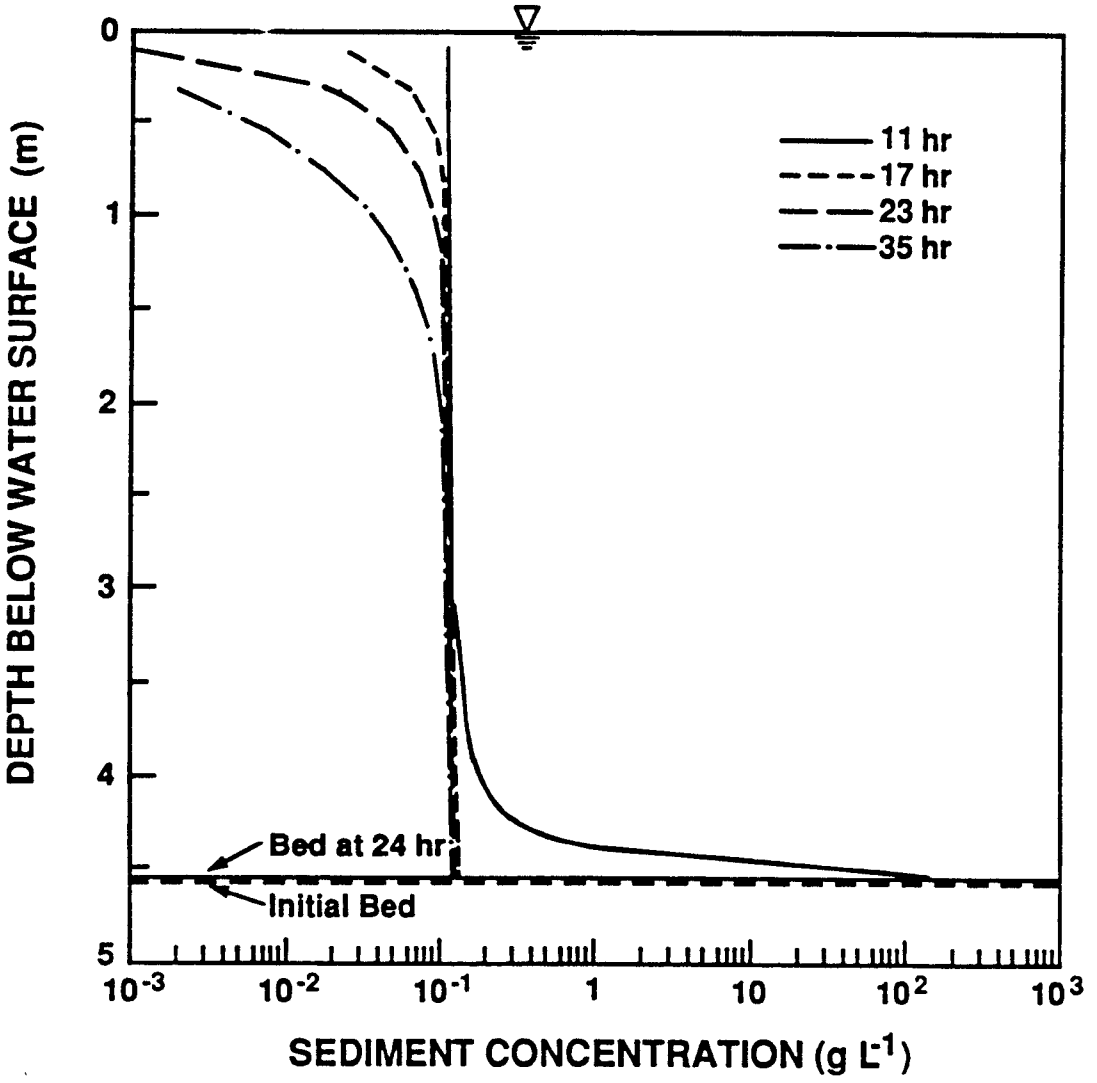

Figure 5.10: Simulated Settling of Suspended Sediment under No-Wave Condition: Extension of Run 1

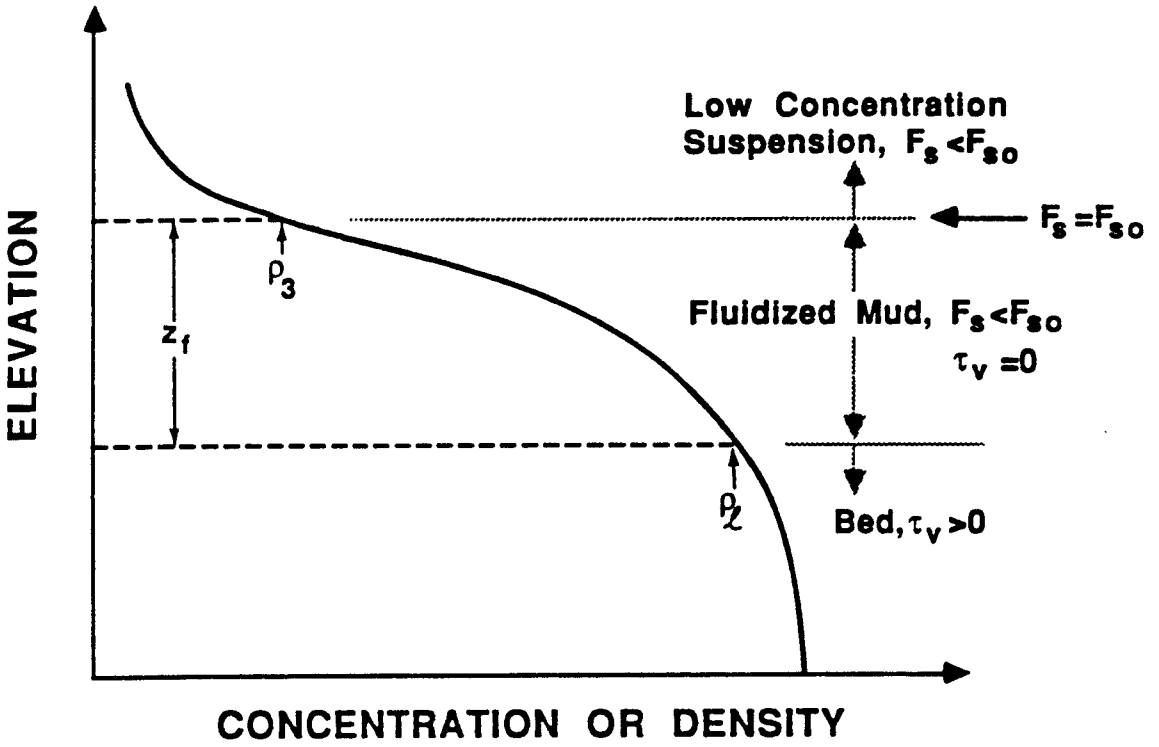

Figure 5.11: An Operational Definition of Fluid Mud Zone

The relevant argument for this statement is that at this elevation

$$\frac{\partial F_s}{\partial C} = 0 \tag{5.18}$$

By chain rule Equation 5.18 can be rewritten as

$$\frac{\partial F_s}{\partial C} = \frac{\partial F_s}{\partial z}\frac{\partial z}{\partial C} = \frac{\partial F_s / \partial z}{\partial C / \partial z} = 0 \tag{5.19}$$

Equation 5.19 implies that in order for $\frac{\partial F_s}{\partial C} = 0$, $\frac{\partial C}{\partial z}$ should approach to infinity, which precisely represents the lutocline. Therefore, ρ_3 converted from C_3 by Fig. 3.1 can be considered to represent the upper level of the fluid zone. Below this level settling is hindered and the flux, F_s, decreases with depth. From Fig. 4.13, $C_3 = 4.38\ g\ L^{-1}$, which yields $\rho_3 = 1.0023\ g\ cm^{-3}$, using $\rho_w = 1.0\ g\ cm^{-3}$ and $\rho_s = 2.14\ g\ cm^{-3}$.

The lower level of the fluid mud zone is conveniently defined here as the value of the bulk density, ρ_l, at and above which the substrate possesses a measurable shear strength, τ_v. τv is obtained from the standard vane shear test described in section 4.3; hence a value of $\rho_l = 1.065\ g\ cm^{-3}$ may be selected.

Given these values of ρ_3 and ρ_l, the density profile of Fig. 5.2 yields an approximately 5 *cm* thick fluidized mud layer. Other density profiles given in Fig. 5.3 through 5.5 showed a fluidized mud layer thickness up to 12 *cm*, which as noted is consistent with the fluid zone thickness range of Gleason and Stone (1975).

In order to comfirm the formation of the fluid mud layer and to examine the expanding thickness of fluid mud layer under wave action due to the rise of the lutocline, another simulation run was carried out starting with the same conditions with run 1 except the initial concentrations. In this case the concentration at the grid point n was also initially zero, thus assuming no fluid mud layer exists. The result is shown in Fig. 5.12. As observed, the surface concentration reached 102 $mg\ L^{-1}$ after 13 hr which is 2 hr later in comparison with run 1, and at this time the eroded depth was 1.3 *cm*. As compared with run 1, this shows that more time (2 hr) was required to reach 102 $mg\ L^{-1}$ at the surface, since initially zero fluid mud condition was used. However, it is noticeable that this run also gave a similar value of the eroded bed depth as in run 1.

In Fig. 5.12, the thickness (z_f) and the averaged concentration of fluid mud layer were calculated in an approximate manner, applying the same values of ρ_3 and ρ_l as before. As illustrated in the figure, a 7.8 *cm* thick fluid mud layer developed after 13 hr, and the average concentration of this layer, C_f, was 22 $g\ L^{-1}$. This simulated thickness of fluid mud layer is also consistent with those reported by Gleason and Stone (1975).

The other concentration profiles given in Figs. 5.6 through 5.9 were also examined for fluid mud layer expansion. Note that in each case the initial fluid mud thickness z_{fo} of 5 *cm*, with an average concentration C_{fo} of 39 $g\ L^{-1}$, were used as the initial condition. In Fig. 5.6, after 11 hr the average concentration (C_f) was 54 $g\ L^{-1}$ and z_f was 9.8 *cm*, showing a net increment of 4.8 *cm* in the thickness. Other figures also give similar values. As compared with z_f and the corresponding average concentration given in Fig. 5.12 (no initial fluid mud, i. e. $z_{fo} = 0$), it is noticeable that the average concentration of fluid mud layer in run 1 was relatively higher than that given in Fig. 5.12, while in both cases z_f were

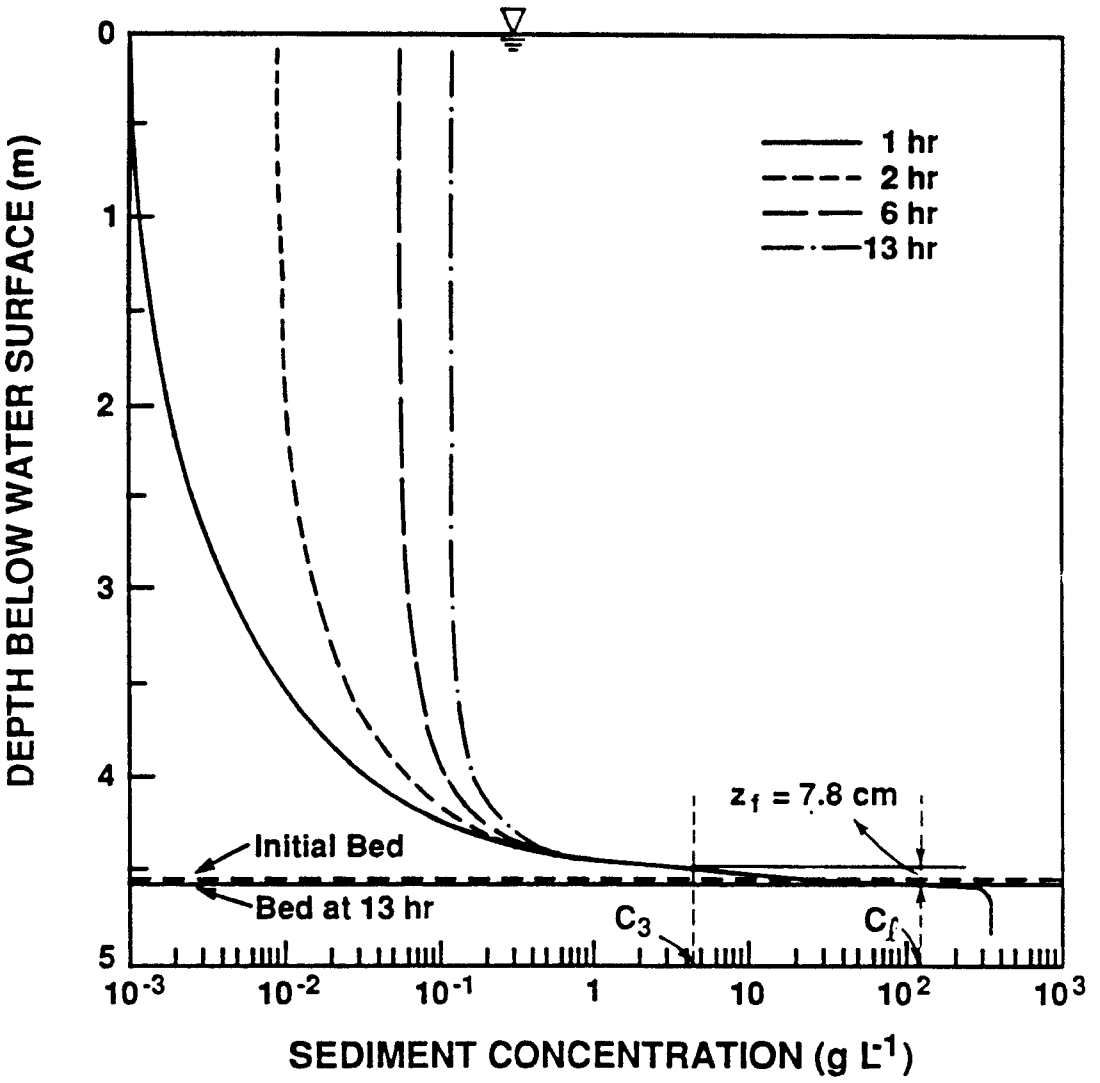

Figure 5.12: Simulated Evolution of Suspension Concentration Profile Starting with no Initial Concentration over the whole Water Column

of the same order (9.8 *cm* in the former case and 7.8 *cm* in the latter). This indicates that the fluid mud layer is formed rapidly with the rise of lutocline to a certain height, and that further entrainment of the lutocline is constrained due to buoyancy stabilization, while bed erosion continuously occurs, thus providing the eroded sediment mass to the fluid mud layer and resulting in an increment in the concentration of the fluid mud layer.

CHAPTER 6
CONCLUSIONS AND RECOMMENDATIONS

6.1 Conclusions

Prototype trends in the evolution of fine sediment concentration profiles and the corresponding eroded bed depth in a shallow lake have been examined assuming a purely wave determined flow environment. A vertical sediment mass transport model was used to simulate likely prototype trends resulting from wave action, given fine-grained bed material, and the corresponding eroded bed depth was calculated.

Information on characteristic parameters and relationships related to fine sediment erodibility were derived from field data on bottom sediments and laboratory experiments. The experiments consisted of characterization of the sediment, bed property tests, settling tests and erosion tests, with specific reference to bottom sediment from Lake Okeechobee, Florida.

Simulation of the vertical sediment concentration profiles under "storm" wave action exhibited an evident qualitative agreement with previous field observed trends in the evolution of the fine sediment concentration variation with depth. Characteristic features were the formation of a lutocline, and a fluid mud layer near the bed coupled with relatively low surficial concentrations. The concentration over approximately 80 % of the water column down from the surface was quite low throughout, and most of the sediment was elevated to a relatively small height above the bed. Furthermore, entrainment of the lutocline was undoubtedly constrained by the submerged weight of the high concentration, hyperpycnal layer below the lutocline, and by the lack of a strong mechnism for upward diffusion. As expected, simulation of the "post-storm" calm, assuming no wave action, resulted in a depression of the elevated lutocline and bed reformation.

It is emphasized that based on the these observations measurement of concentration at the surface alone, thus neglecting near-bed high concentration suspension dynamics, can lead to an order of magnitude underestimation of the erodible bed depth. Gleason and Stone (1975) measured the surface concentration of 102 $mg\ L^{-1}$ at a water depth of 4.6 m during a storm in Lake Okeechobee and suggested bed material erosion of 2.3 mm assuming uniform water column concentration. Considering the characteristic features of the vertical concentration profile, however, the simulated results suggest that the erodible bed thickness in Lake Okeechobee is likely to be on the order of 2 cm for a surface concentration of 102 $mg\ L^{-1}$ during storm events.

Through an operational definition of the fluidized mud layer thickness, bulk densities defining the upper and lower levels of the fluid mud layer were determined to be 1.0023 $g\ cm^{-3}$ and 1.065 $g\ cm^{-3}$, respectively. Applying these values to the bottom density profiles as identified from bottom cores, the thickness of the fluid mud layer was found to range from 5 cm to 12 cm, which is consistent with values reported by Gleason and Stone (1975).

The thickness of the fluid mud layer arising from wave action and associated rise of the lutocline were also examined through model simulations with and without the initial presence of fluid mud over the bed. The thickness of the resulting fluid mud layer in both cases was of the same order (9.8 cm in the former case and 7.8 cm in the latter), while the average concentration of this layer in the former case was somewhat higher than in the latter case (39 $g\ L^{-1}$ in the former case versus 22 $g\ L^{-1}$ in the latter). During resuspension this fluid mud layer rises rapidly with the rise of the lutocline to a certain height. However, further upward entrainment of the lutocline is constrained due to buoyancy stabilization, while bed erosion continues to occur as long as the applied wave bottom stress amplitude exceeds the bed shear strength, thus providing eroded sediment mass to the fluid mud layer and resulting in an increment in the concentration of this layer.

An effort has been made to establish the connection between the erodibile mud thickness due to resuspension during storm wave action, and the fluidized mud zone thickness as identified from bottom cores. The actual thickness of this "active" mud surficial layer at a site will of course depend on the intensity and frequency of wave action, water depth and the thickness and character of the bottom mud. In Lake Okeechobee, the thickness of this active mud layer (fluidized mud thickness plus erodible bed thickness) appears to be on the order of 10 cm below the stationary mud-water interface.

An evident conclusion is that accurate measurement of instantaneous vertical concentration profiles is vitally important in studies on bottom sediment-induced turbidity, and in establishing the erodible thickness of the bed by wave action. Such profiling, when carried out effectively, can also yield valuable information on the microstructure of fine sediment suspensions, as has been demonstrated elsewhere (Kirby, 1986). Furthermore, it is essential to track the evolution of the near-bed suspended sediment load, since this highly non-Newtonian "slurry" is usually responsible for sedimentation problems in many episodic environments.

With regard to field data collection and laboratory studies presented in this report, the following specific observations relative to Lake Okeechobee stand out:

1. Over the muddy zone, the sediment is mostly in the fine size range, and the fine-grained portion of the sediment seems to be spatially comparatively similar. The mean (dispersed) diameter ranges from 3 to 14 μm. The sorting coefficient of material (which reflects grading) is relatively large (ranging from 3 to 5). The measured average value of the sediment granular density is 2.14 $g\ cm^{-3}$. The percentage of organic matter appears to be fairly uniform, ranging from 36 to 41 %. This high organic fraction in the sediment is reflected in the rather low value of the sediment granular density. X-ray diffraction reveals that the predominant clay constituents are kaolinite, sepiolite, and montmorillonite.

2. Bottom mud bulk densities are in the typical range of 1.01 $g\ cm^{-3}$ and 1.2 $g\ cm^{-3}$. Vane shear strengths reach almost 6 $kN\ m^{-2}$, but most are less than 4 $kN\ m^{-2}$. The mud density and vane shear strength measurements show a correlation. However, it should be noted that density is not an unambiguous analog for strength, which also depends upon mud composition and other factors. Therefore, any relationship between density and strength must be accepted only for its practical value. From the observed approximate relationship between the density and the vane shear strength, the lowest density of the mud bed was defined to be 1.065 $g\ cm^{-3}$. Below this density the shear strength is zero, implying that the mud is a fluid.

3. An expression (Eq. 4.6) for the relationship between the settling velocity and the concentration was developed by modifying an empirical equation given by Wolanski et al. (1989), inasmuch as data obtained from the settling column tests showed somewhat different trends in comparison with those described in previous studies (Krone, 1962; Mehta, 1988), especially in the flocculation settling region. Settling velocity variation in general was found to be in the range of two orders of magnitude, from about 0.01 to 1 $mm\ sec^{-1}$ over corresponding concentration range of 0.1 to 50 $g\ L^{-1}$. It is concluded that seasonal effects (Fall - Spring) on the settling velocity of the sediment in the muddy zone may not be significant. Moreover, it may be concluded that sediment settling occurs fastest in the northernmost mud zone, more slowly in the eastern and western zones and at an intermediate rate in the central and southern zones.

4. During the erosion tests, a notable observation was mass sediment erosion, which usually occurred under high bed shear stress conditions and resulted in a structural breakdown of the bed at low bed densities (below 1.12 $g\ cm^{-3}$). An attempt was made to estimate the erosion rate constant and critical shear stress for simulating mass erosion.

6.2 Recommendations

The present study was primarily concerned with examining the erodibility of fine sediment and the evolution of vertical concentration profiles under wave action. During the modeling effort, simulation of the physical process of interfacial entrainment of fluid mud was omitted. For example, surface waves may enhance interfacial instabilities in conjunction with even weak, uni-directional currents (such as occur in lakes) resulting in high entrainment rates. Also, promise is shown in the area of turbulence modeling where a better definition of mass diffusivity can be made by calculating the ensemble mean for turbulent fluxes.

The effects of turbulent wave boundary layers were not adequately considered in this study. These boundary layers always occur in the prototype environments. For this purpose, appropriate analytical and experimental studies are available, and must be used in future work.

Although considerable amount of laboratory work and field data collection for bottom sediment were carried out, many parameters serving as input data for modeling had to be assumed or calibrated using the limited available information from other studies. Some assumed or calibrated parameters may have significant effects on the simulation of concentration profiles and corresponding eroded depth, depending on the surrounding environment including bottom topography, land boundaries and hydrodynamic factors. Consequently, sensitivity tests for each significant parameter are highly recommended.

Finally, verification of some of the observations regarding resuspension will require accurate near-bed suspension concentration profiling in future studies.

APPENDIX A
DESCRIPTION OF CORES FROM LAKE OKEECHOBEE

SITE: OK1 VC

Core sample description:

- 2.4 cm black sticky soft silty clay, no shell, no smell
- Sharp junction
- grey fine or medium quartz sand with fine shell fragments
- Sharp junction
- 5.5 cm mottled pale brown, dark brown or black sandy peat
- Sharp junction
- 38.5 cm whitish pebbly or broken "rotted" beach rock

No measurement of bulk density or shear strength.

SITE: OK2 VC

Core sample description:

- 32 cm black sticky mud, no smell
  - Very soft mud at top 10 cm, a few shells at the top
  - A thin small shell layer (about 0.5 cm) at 24 cm from the top
- 2 cm grey fine sand with fine shells
- Sharp junction
- 41 cm calcareous whitish clay with small lumps near the base, no shells

Bulk density and shear strength:

- See Table A. 1 and Figure 4.4.

SITE: OK3 VC

Core sample description:

Table A.1: Bulk Density and Vane Shear Strength Variations for Site OK2VC

Depth (cm)	Density ($g\ cm^{-3}$)	Shear strength ($N\ m^{-2}$)
0 - 5	1.106	386
5 - 10	1.084	531
10 - 15	1.099	627
15 - 20	1.102	1448
20 - 25	1.131	1448
25 - 30	1.112	1979

- 28 cm black sticky clay with no shell
- Sharp junction
- 6 cm calcareous sand with large gravel grade beach rock pebbles, no smell

No measurement of bulk density or shear strength.

SITE: OK4 VC

Core sample description:

- 19 cm black sticky soft silty clay, no shells, no smell
- Sharp junction
- 8 cm grey and white grey sand with fine shells and shell fragments
- Sharp junction
- 4 cm black peat
- Sharp junction
- 15 cm whitish calcareous "rotted", "crushed" rock with shells and shell fragments

Bulk density and shear strength:

- See Table A. 2 and Figure A. 1.

Table A.2: Bulk Density and Vane Shear Strength Variations for Site OK4VC

Depth (cm)	Density ($g\ cm^{-3}$)	Shear strength ($N\ m^{-2}$)
3 - 8	1.079	
8 - 13	1.116	
13 - 18	1.084	no measurement
18 - 23	1.119	

SITE: OK5 VC

Core sample description:

- 28 cm black sticky soft clay, no shell, no smell
- Sharp junction
- 2.5 cm grey and white grey sand with very fine shells
- Sharp junction
- 0.8 cm dark black peat, no shells

Bulk density and shear strength:

- See Table A. 3 and Figure A. 2.

SITE: OK6 VC

Core sample description:

- 21 cm soft black clay , no smell, one shell on the mud surface
- A very thin grey sandy layer at 4 cm from the top
- Sharp junction
- 4 cm grey/dark grey sand with fine shells and shell fragments
- Sharp junction

Table A.3: Bulk Density and Vane Shear Strength Variations for Site OK5VC

Depth (cm)	Density ($g\ cm^{-3}$)	Shear strength ($N\ m^{-2}$)
0 - 1	1.027	
1 - 2	1.033	
2 - 3	1.032	
3 - 4	1.033	
4 - 9	1.096	no measurement
9 - 14	1.083	
14 - 19	1.126	
19 - 24	1.114	
24 - 29	1.073	
29 - 34	1.149	

Table A.4: Bulk Density and Vane Shear Strength Variations for Site OK6VC

Depth (cm)	Density ($g\ cm^{-3}$)	Shear strength ($N\ m^{-2}$)
0.0 - 1.0	1.017	
1.0 - 2.0	1.021	
2.0 - 3.0	1.026	
3.0 - 4.0	1.026	
4.0 - 6.5	1.110	
6.5 - 9.0	1.118	2075
9.0 - 11.5	1.099	2075
11.5 - 14.0	1.116	2386
14.0 - 16.5	1.096	2386
16.5 - 19.0	1.123	5736
19.0 - 21.5	1.124	5736

- 12 cm white grey "rotted" and "crushed" beach rock with shell fragments

Bulk density and shear strength:

- See Table A. 4 and Figure A. 3.

SITE: OK7 VC

Core sample description:

- 1 cm very soft black silty clay , no smell, no shell
- 3 cm sandy black clay and whitish sand with small pebbly beach rock at the center

- Sharp junction
- 14 cm white grey calcareous pebbly beach rock with shell fragments

No measurement of bulk density or shear strength.

SITE: OK8 VC

Core sample description:

- 8 cm pale brown sand with fine shells
- Sharp junction
- 7 cm white brown sand with fine shells and shell fragments
- Sharp junction
- 15 cm grey "rotted", and "crushed" beach rock

No measurement of bulk density or shear strength.

SITE: OK9 VC

Core sample description:

- Total 35 cm black firm mud
- Sharp junction at the top
- 6 cm black soft mud, no shells, no smell
- Sharp junction
- 2 cm grey sand with fine shells and shell fragments
- Sharp junction
- 2 cm black soft mud, no shells, no smell
- Sharp junction

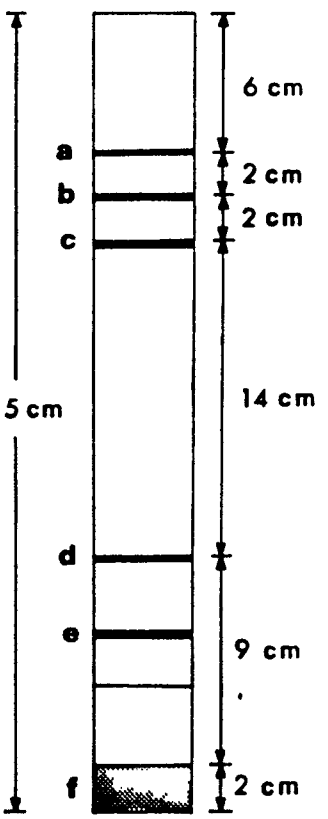

Table A.5: Bulk Density and Vane Shear Strength Variations for Site OK9VC

Depth (cm)	Density ($g\ cm^{-3}$)	Shear strength ($N\ m^{-2}$)
0 - 1	1.013	
1 - 2	1.023	
2 - 3	1.048	
3 - 4	1.035	
4 - 9	1.138	8494
9 - 14	1.200	7853
14 - 19	1.183	5681
19 - 24	1.175	5833
24 - 29	1.128	5833
29 - 34	1.195	5578

- 14 cm white and grey fine, small and large shells and shell fragments with a little sand
- a, b, c: thin layers of grey color with some very fine shells
- d, e: grey sandy layers with fine shells and shell fragments
- f: 2 cm grey sand with fine shells and shell fragments

Bulk density and shear strength:

- See Table A. 5 and Figure A. 4.

SITE: OK10 VC

Core sample description:

- 6 cm soft black mud, no shells, no smell
- Visible junction
- 18 cm dark grey soft mud, no shells, no smell
  - a: thin layer (0.4 cm) of fine shells with white grey mud
  - b: thin white grey mud layer
- Sharp junction

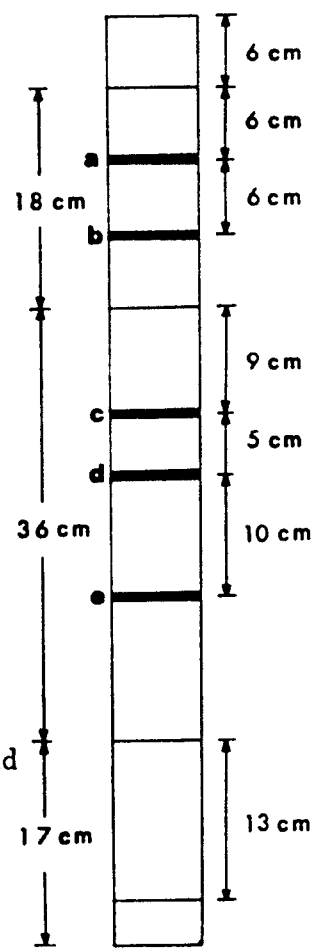

Table A.6: Bulk Density and Vane Shear Strength Variations for Site OK10VC

Depth (cm)	Density ($g\ cm^{-3}$)	Shear strength ($N\ m^{-2}$)
0 - 5	1.136	1641
5 - 10	1.146	1158
10 - 15	1.216	1303
15 - 20	1.235	2537
20 - 25	1.170	2434
25 - 30	1.116	2586
30 - 35	1.269	3034
35 - 40	1.287	3668
40 - 45	1.100	3620
45 - 50	1.171	3572
50 - 55	1.115	4537

- 36 cm black firm mud, a few small shells, no smell
  - c: thin white grey mud layer with fine shells
  - d: thin white grey mud layer
  - e: a dark grey thin mud layer, small shells (Augur)
- Sharp junction
- 17 cm hard whitish clay with shells and shell fragments at the top, shells and large shell fragment layer (4 cm) at the base

Bulk density and shear strength:

- See Table A. 6 and Figure 4.5.

SITE: OK11 VC

Core sample description:

- 60 cm black soft clay becoming finer grey clay towards the base (this core was damaged during the process of opening)

No measurement of bulk density or shear strength.

Table A.7: Bulk Density and Vane Shear Strength Variations for Site OK12VC

Depth (cm)	Density ($g\ cm^{-3}$)	Shear strength ($N\ m^{-2}$)
0 - 5	1.136	1641
5 - 10	1.146	1158
10 - 15	1.216	1303
15 - 20	1.235	2537
20 - 25	1.170	2434
25 - 30	1.116	2586
30 - 35	1.269	3034
35 - 40	1.287	3668
40 - 45	1.100	3620
45 - 50	1.171	3572
50 - 55	1.115	4537

SITE: OK12 VC

Core sample description:

- 27 cm black sticky clay, very fine shell fragments in the top 4 cm, no smell
- Sharp junction
- 3 cm white grey hard sandy clay with shell and shell fragments

Bulk density and shear strength:

- See Table A. 7 and Figure A. 5.

SITE: OK13 VC

Core sample description:

- 24 cm black sticky clay mud, no shell, no smell, top part silty
- 7 cm brown (earth color) clay with a few shell fragments

Bulk density and shear strength:

- See Table A. 8 and Figure A. 6.

Table A.8: Bulk Density and Vane Shear Strength Variations for Site OK13VC

Depth (cm)	Density ($g\ cm^{-3}$)	Shear strength ($N\ m^{-2}$)
0 - 1	0.999	
1 - 2	1.006	
2 - 3	1.060	
3 - 4	1.018	
4 - 5	1.036	
5 - 10	1.108	1158
10 - 15	1.141	1400
15 - 20	1.178	1786
20 - 25	1.128	1400
25 - 30	1.215	1400

SITE: OK14 VC

Core sample description:

- 5 cm black soft mud, no shell, no smell
- Sharp junction
- 1 cm white grey clay layer
- Sharp junction
- 10 cm grey mud with fine Auger shells
- Sharp junction
- 10 cm black soft mud, no shell
- Sharp junction
- 27 cm white-grey calcareous "rotted" beach rock with shell fragments

Bulk density and shear strength:

- See Table A. 9 and Figure A. 7.

Table A.9: Bulk Density and Vane Shear Strength Variations for Site OK14VC

Depth (cm)	Density (g/cm^3)	Shear strength (N/m^2)
0 - 5	1.149	386
5 - 10	1.172	1351
10 - 15	1.168	1937
15 - 20	1.139	1593
20 - 25	1.123	1544

SITE: OK15 VC

Core sample description:

- 23 cm black soft mud, no smell, no shell
- 19 cm black firm mud with a few visible deposition layers
- Sharp junction
- 3 cm dark grey sand with small shell fragments
- Sharp junction
- 10.5 cm mottled grey and white clay, fine and big shells and shell fragments at the base

Bulk density and shear strength:

- See Table A. 10 and Figure A. 8.

SITE: OK16 VC

Core sample description:

- 0.5 cm black fluid mud
- 29 cm "rotted" calcareous grey/white grey/dark grey beach rock with fine shells and small shell fragments
- Sharp junction

Table A.10: Bulk Density and Vane Shear Strength Variations for Site OK15VC

Depth (cm)	Density ($g\ cm^{-3}$)	Shear strength ($N\ m^{-2}$)
0 - 1	1.007	
1 - 2	1.010	
2 - 3	1.012	
3 - 4	1.015	
4 - 9	1.147	676
9 - 14	1.141	869
14 - 19	1.178	1207
19 - 24	1.169	1400
24 - 29	1.158	2089
29 - 34	1.248	3620
34 - 39	1.112	2386
39 - 44	1.168	2537

Table A.11: Bulk Density and Vane Shear Strength Variations for Site OK17VC

Depth (cm)	Density ($g\ cm^{-3}$)	Shear strength ($N\ m^{-2}$)
0.0 - 1.0	1.030	
1.0 - 2.0	1.040	
2.0 - 3.0	1.058	
3.0 - 8.0	1.776	11969
8.0 - 13.0	1.817	21863
13.0 - 18.5	1.732	24642

- 5 cm clean sand

No measurement of bulk density or shear strength.

SITE: OK17 VC

Core sample description:

- 15.5 cm mottled, grey/light grey/white grey sandy sticky clay

Bulk density and shear strength:

- See Table A. 11 and Figure A. 9.

SITE: OK18 VC

Core sample description:

- 4 cm black peat with a small part of sand
- 2 cm light brown peat
- 1.5 cm light brown peat
  - a and b: 0.5 cm black peat
- 48 cm mottled firm peat with visible plant roots, no shell, no smell
  - 40 cm mottled black and brown peat
  - 8 cm mottled dark grey/light brown peat and sand

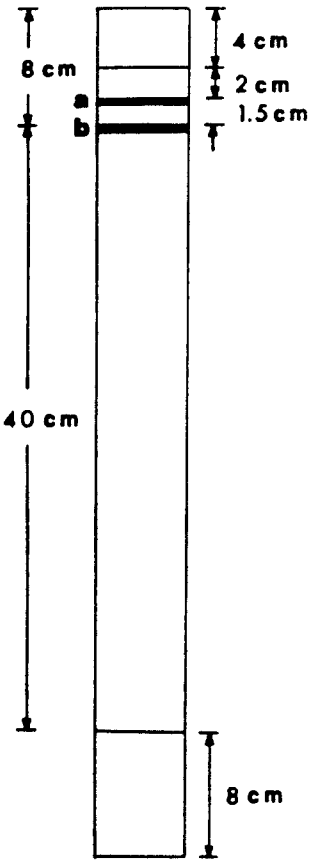

No measurement of bulk density or shear strength.

SITE: OK19 VC

Core sample description:

- 11 cm black and white rotted calcareous beach rock with big shell fragments

No measurement of bulk density and shear strength.

SITE: OK20 VC

Core sample description:

- 8 cm black firm sticky mud, no shell, no smell
- Sharp junction
- 13 cm fine sand with fine and small shells and small shell fragments
- Sharp junction
- 35 cm fine sand with no shells, varying color from dark grey at the top to light grey at the base, small pebbly clay at the base

Bulk density and shear strength:

Table A.12: Bulk Density and Vane Shear Strength Variations for Site OK20VC

Depth (cm)	Density ($g\ cm^{-3}$)	Shear strength ($N\ m^{-2}$)
0 - 8	1.195	1207

- See Table A. 12.

SITE: OK21 VC

Core sample description:

- Thin black silty shelly clay over rotted grey calcareous beach rock with few shells

No measurement of bulk density or shear strength.

SITE: OK22 VC

Core sample description:

- 17 cm black soft silty mud, no smell, no shell
- Sharp junction
- 20 cm medium shells and fragments with light brown sand
- Sharp junction
- 8.5 cm light grey "rotted" beach rock with shell fragments

Bulk density and shear strength:

- See Table A. 13 and Figure A. 10.

SITE: OK23 VC

Core sample description:

- 17 cm black sticky silty clay, no shell, no smell
- Sharp junction

Table A.13: Bulk Density and Vane Shear Strength Variations for Site OK22VC

Depth (cm)	Density ($g\ cm^{-3}$)	Shear strength ($N\ m^{-2}$)
0 - 1	1.013	
1 - 2	1.015	
2 - 3	1.017	
3 - 4	1.019	
4 - 5	1.021	
5 - 10	1.101	
10 - 15	1.119	531
15 - 20	1.127	579

Table A.14: Bulk Density and Vane Shear Strength Variations for Site OK23VC

Depth (cm)	Density ($g\ cm^{-3}$)	Shear strength ($N\ m^{-2}$)
0 - 1	1.010	
1 - 2	1.012	
2 - 3	1.014	
3 - 4	1.014	
4 - 5	1.015	
5 - 6	1.016	
6 - 7	1.017	
7 - 12	1.139	
12 - 17	1.123	869
17 - 22	1.115	676

- 18 cm white grey "rotted" beach rock, large or small shells at the top and shell fragments at the base

Bulk density and shear strength:

- See Table A. 14 and Figure A. 11.

SITE: OK24 VC

Core sample description:

- 26 cm whittish and white grey "rotted" and crushed beach rock with shells and shell fragments

No measurement of bulk density or shear strength.

SITE: OK25 VC

Core sample description:

- 12 cm small or medium shells and shell fragments with light grey sand

No measurement of bulk density or shear strength.

SITE: OK26 VC

Core sample description:

- 27 cm white grey stiff clay with a few shells at the top

No measurement of bulk density or shear strength.

SITE: OK27 VC

Core sample description:

- 12 cm white grey pebbly rotted beach rock with large shells and shell fragments at the base

No measurement of bulk density or shear strength.

SITE: OK28 VC

Core sample description:

- 14 cm dark grey firm mud, no shell, no smell
- 4 cm dark grey firm mud dotted with fine shells, no smell
- Sharp junction
- 2.5 cm fine shell layer with mud
- Sharp junction
- 4.5 cm black mud, no shell, no smell
- Sharp junction

Table A.15: Bulk Density and Vane Shear Strength Variations for Site OK28VC

Depth (cm)	Density ($g\ cm^{-3}$)	Shear strength ($N\ m^{-2}$)
0 - 1	1.020	
1 - 2	1.021	
2 - 3	1.027	
3 - 4	1.028	
4 - 5	1.025	
5 - 6	1.028	
6 - 7	1.027	
7 - 12	1.145	2289
12 - 17	1.165	3082
17 - 22	1.223	1255
22 - 27		2137

- 3.5 cm small shells and fragments with sand
- Sharp junction
- 5.5 cm whittish and white grey hard clay, no shell, no smell

Bed density and shear strength:

- See Table A. 15 and Figure A. 12.

SITE: OK29 VC

Core sample description:

- 11 cm black soft sticky mud, no smell, no shell
- Visible junction
- 3 cm grey soft mud, no shell, no smell
- Visible junction
- 22 cm dark grey firm mud, no shell, no smell, 2 cm shell fragments at the base
- Sharp junction

Table A.16: Bulk Density and Vane Shear Strength Variations for Site OK29VC

Depth (cm)	Density ($g\ cm^{-3}$)	Shear strength ($N\ m^{-2}$)
0 - 1	1.011	
1 - 2	1.014	
2 - 3	1.016	
3 - 4	1.019	
4 - 5	1.021	
5 - 10	1.124	1303
10 - 15	1.251	2537
15 - 20	1.156	2386
20 - 25	1.211	2434
25 - 30	1.147	3082
30 - 35	1.185	3447
35 - 40	1.116	2882

- 8 cm light grey pebbly "rotted" beach rock with lumps and no shell, 5 cm light blue and grey clay with no shell

Bulk density and shear strength:

- See Table A. 16 and Figure A. 13.

SITE: OK30 VC

Core sample description:

- 6 cm white grey sticky firm clay with no shell
- 3 cm mixture of gravel, sand, shells, and shell fragments

No measurement of bulk density or shear strength.

SITE: OK31 VC

Core sample description:

- 1 or 3 cm dark brown large sand, no shell
- fine shells and fine shell fragments with sand
- 2 cm grey medium sand, no shell

- 1 cm dark grey sand layer
- 5 cm light grey large sand with fine or medium shells and small shell fragments
- 5 cm brown medium sand, no shell
- 18 cm sand layer, no shell, varying color from black at the top to mottled black and light grey at the base, varying sand grain size from fine at the top to coarse at the base

No measurement of bulk density or shear strength.

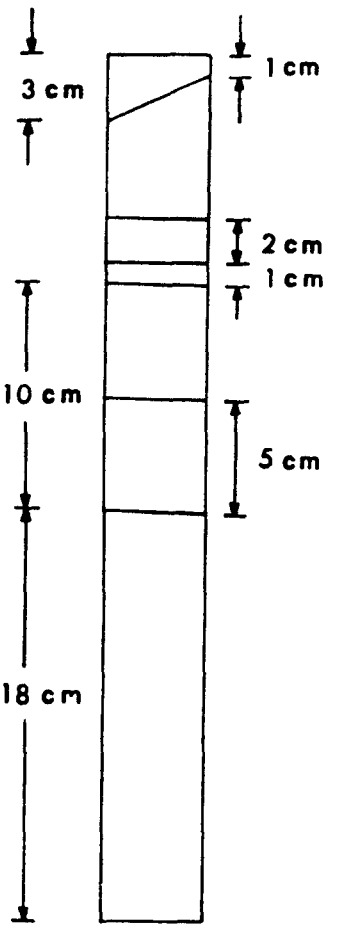

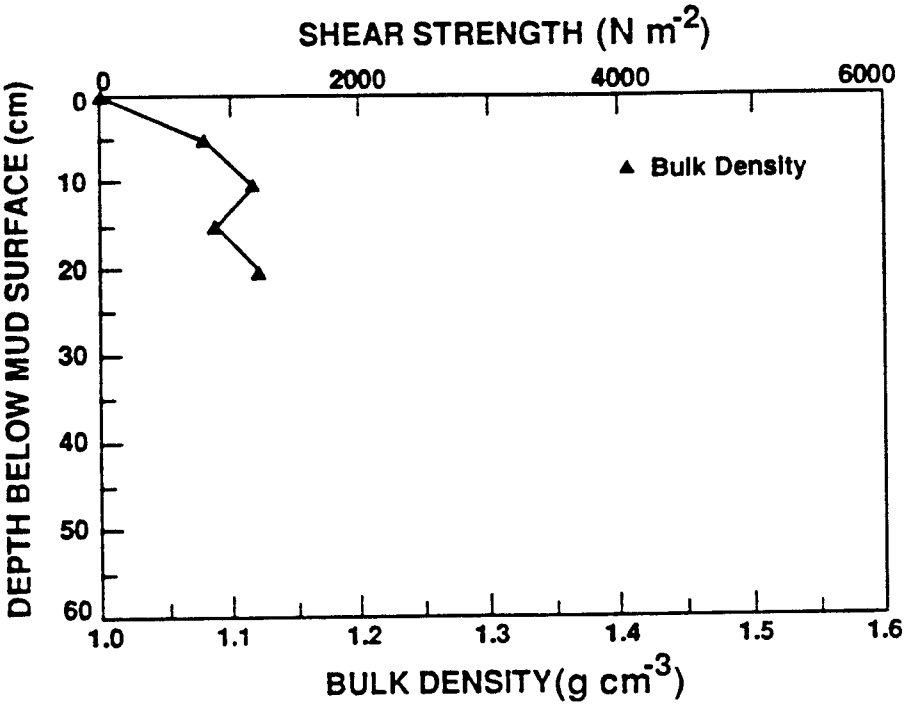

Figure A.1: Bulk Density and Vane Shear Strength Variations for Site OK4VC

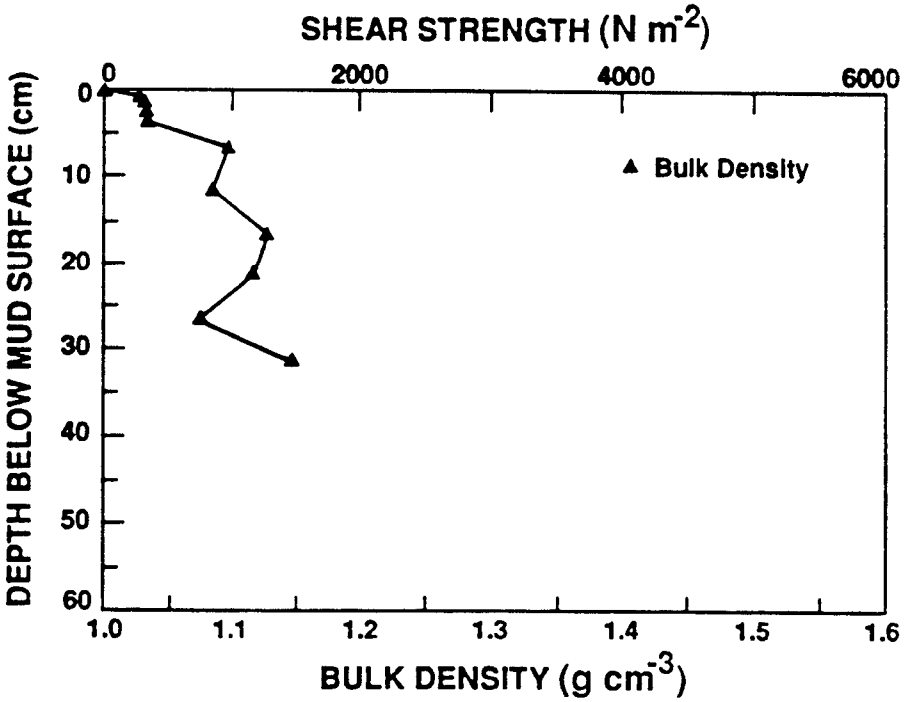

Figure A.2: Bulk Density and Vane Shear Strength Variations for Site OK5VC

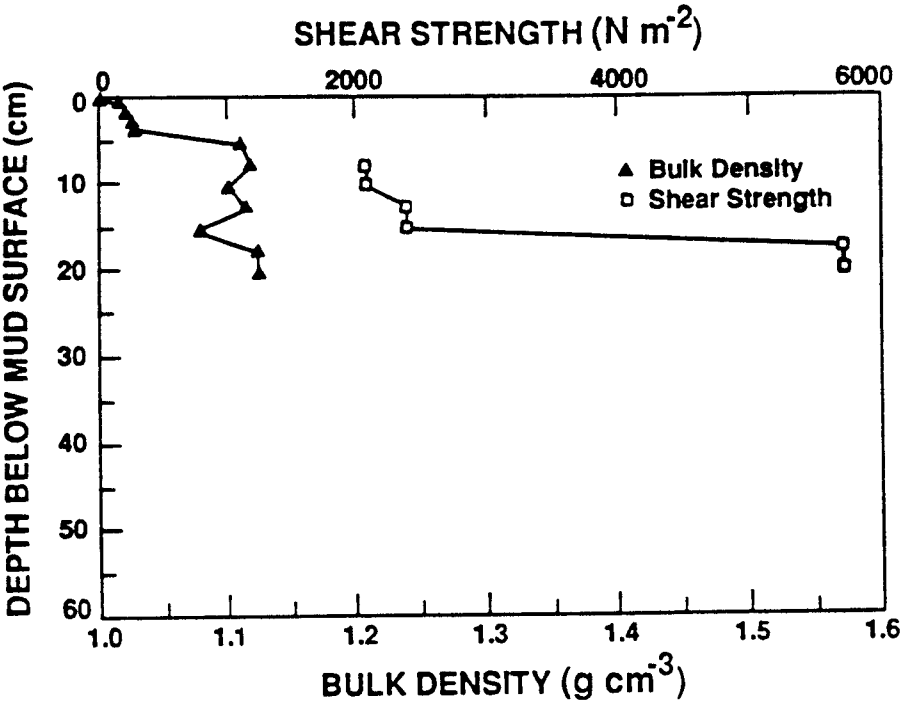

Figure A.3: Bulk Density and Vane Shear Strength Variations for Site OK6VC

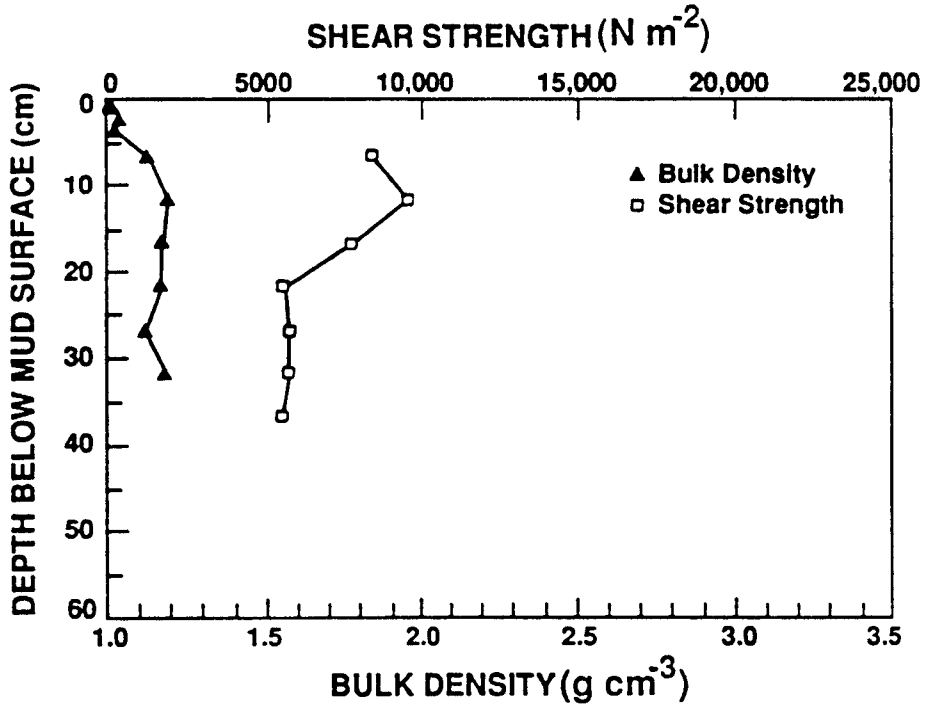

Figure A.4: Bulk Density and Vane Shear Strength Variations for Site OK9VC

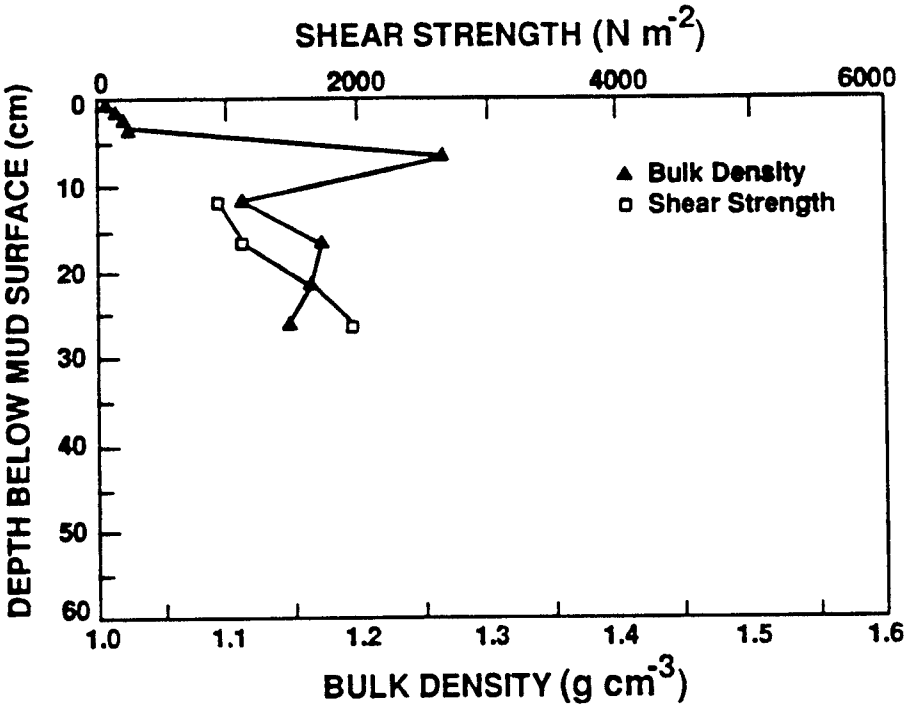

Figure A.5: Bulk Density and Vane Shear Strength Variations for Site OK12VC

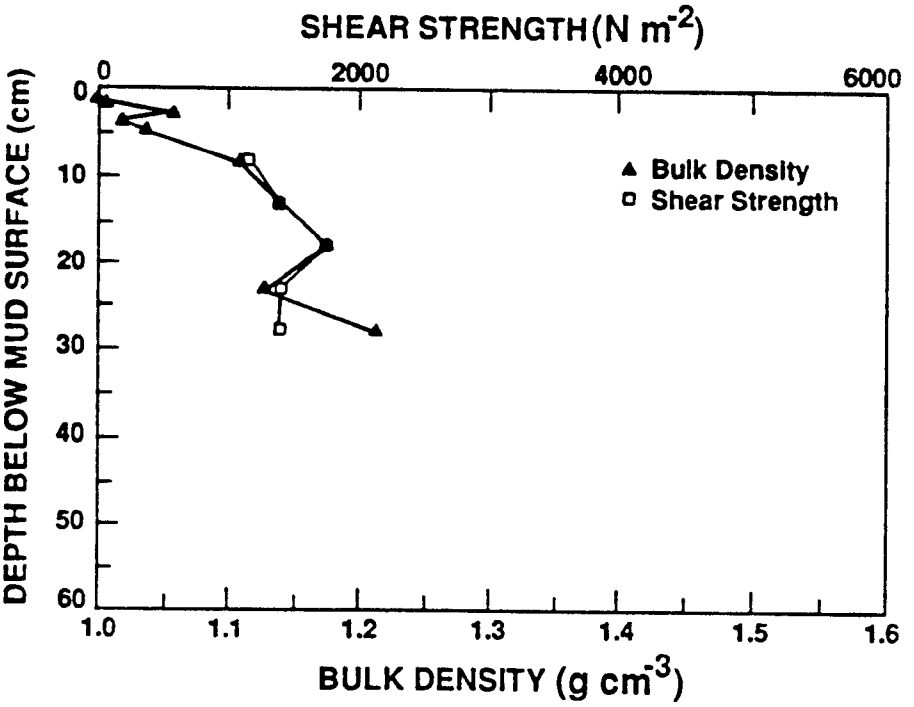

Figure A.6: Bulk Density and Vane Shear Strength Variations for Site OK13VC

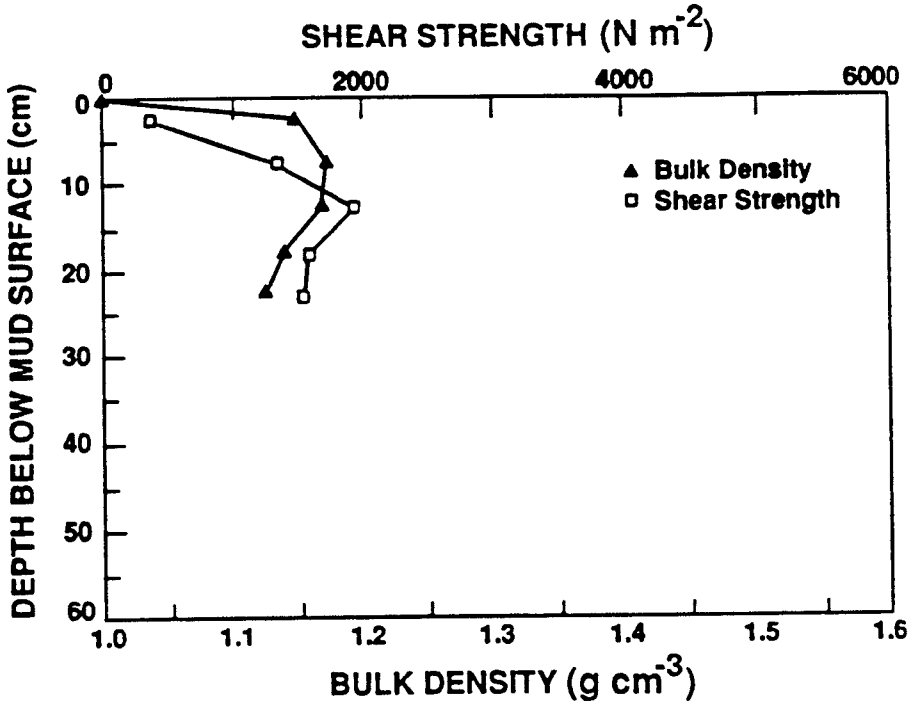

Figure A.7: Bulk Density and Vane Shear Strength Variations for Site OK14VC

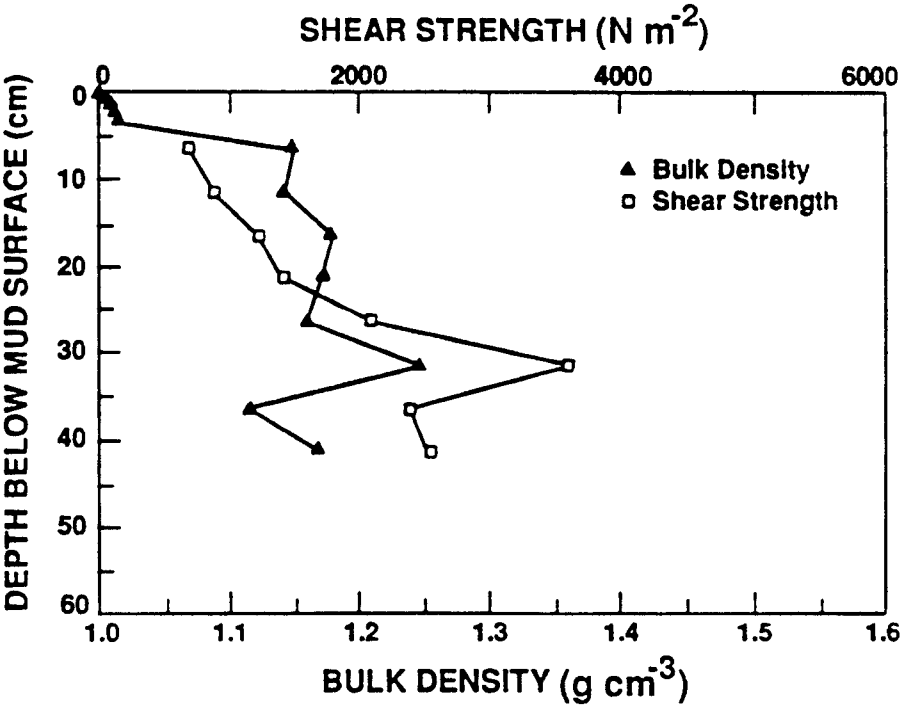

Figure A.8: Bulk Density and Vane Shear Strength Variations for Site OK15VC

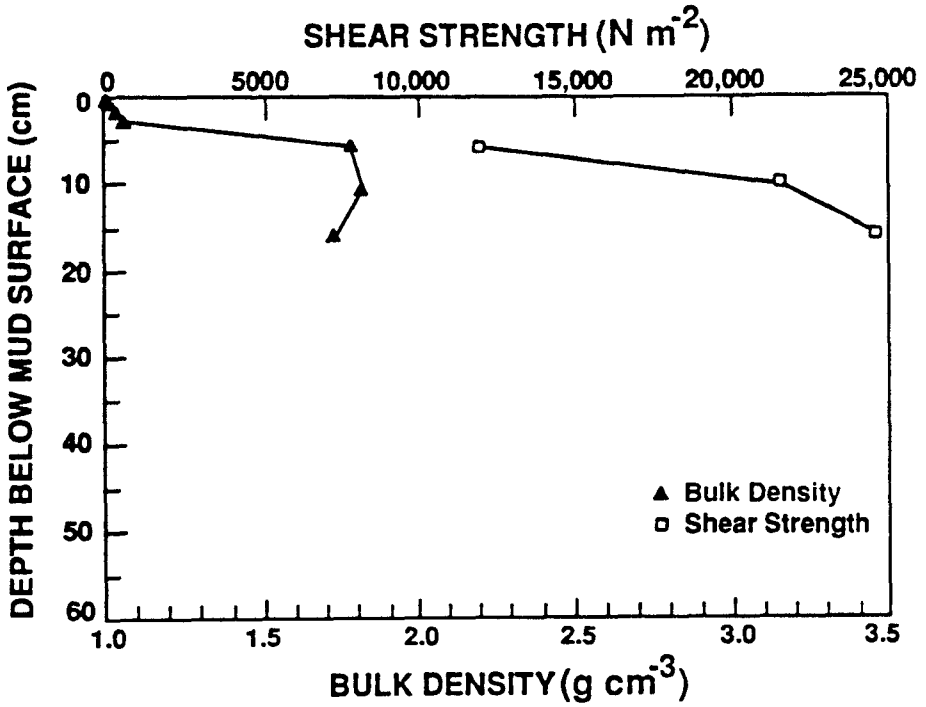

Figure A.9: Bulk Density and Vane Shear Strength Variations for Site OK17VC

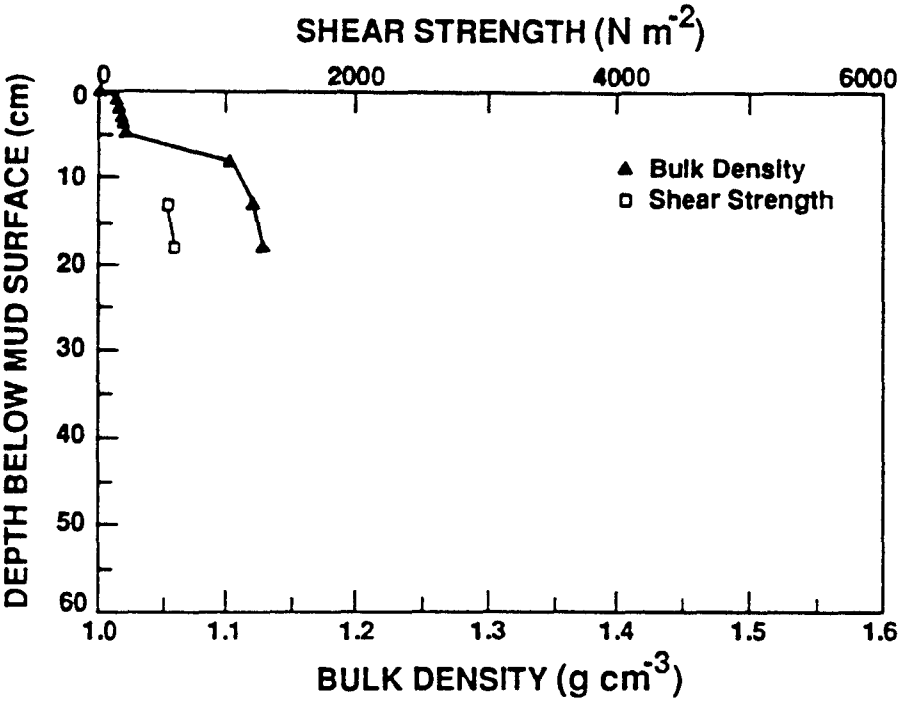

Figure A.10: Bulk Density and Vane Shear Strength Variations for Site OK22VC

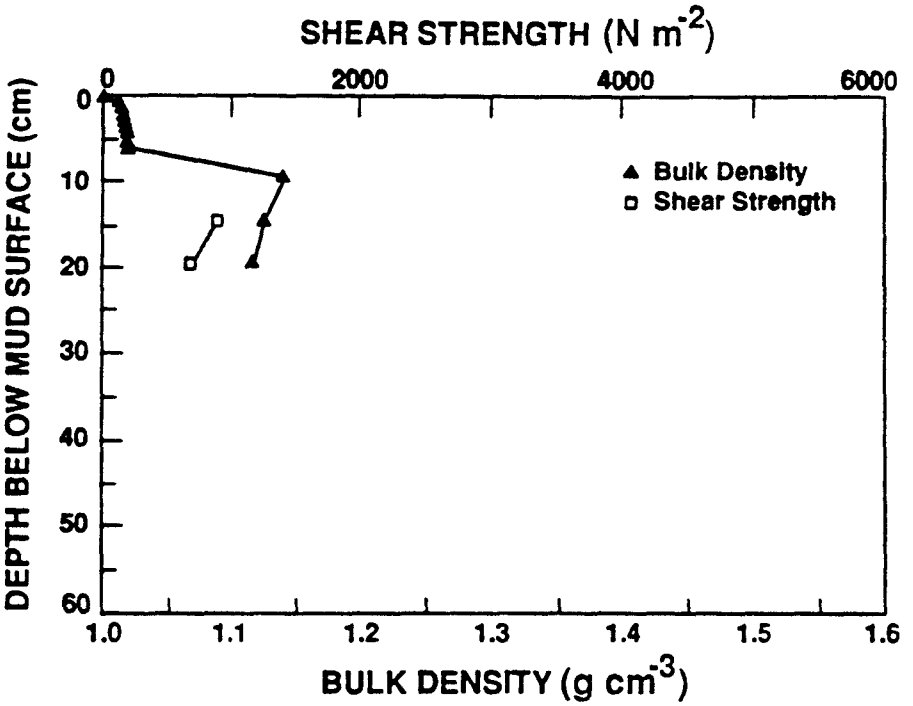

Figure A.11: Bulk Density and Vane Shear Strength Variations for Site OK23VC

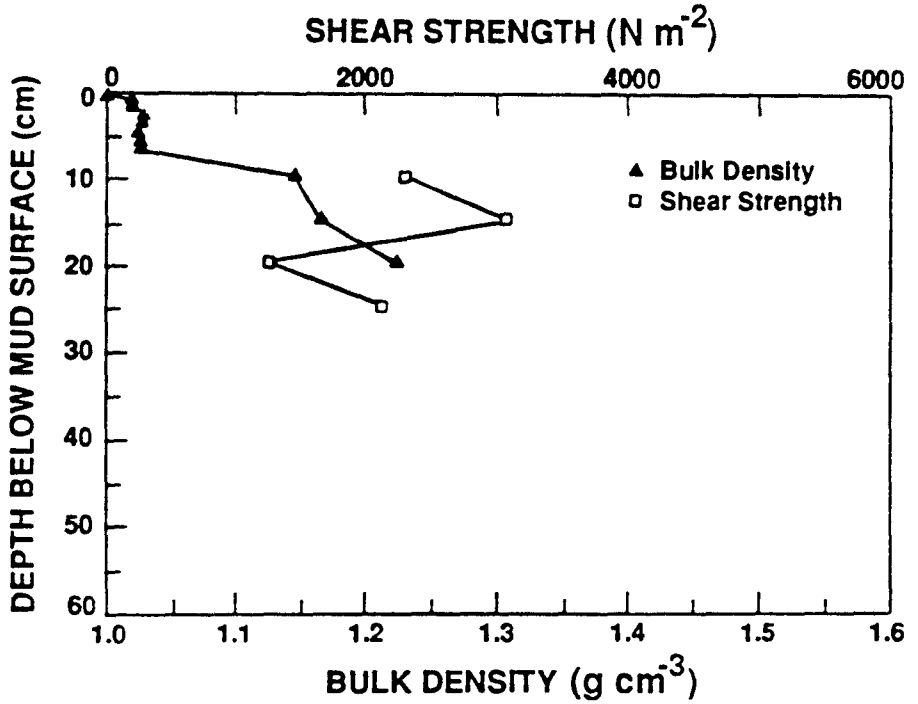

Figure A.12: Bulk Density and Vane Shear Strength Variations for Site OK28VC

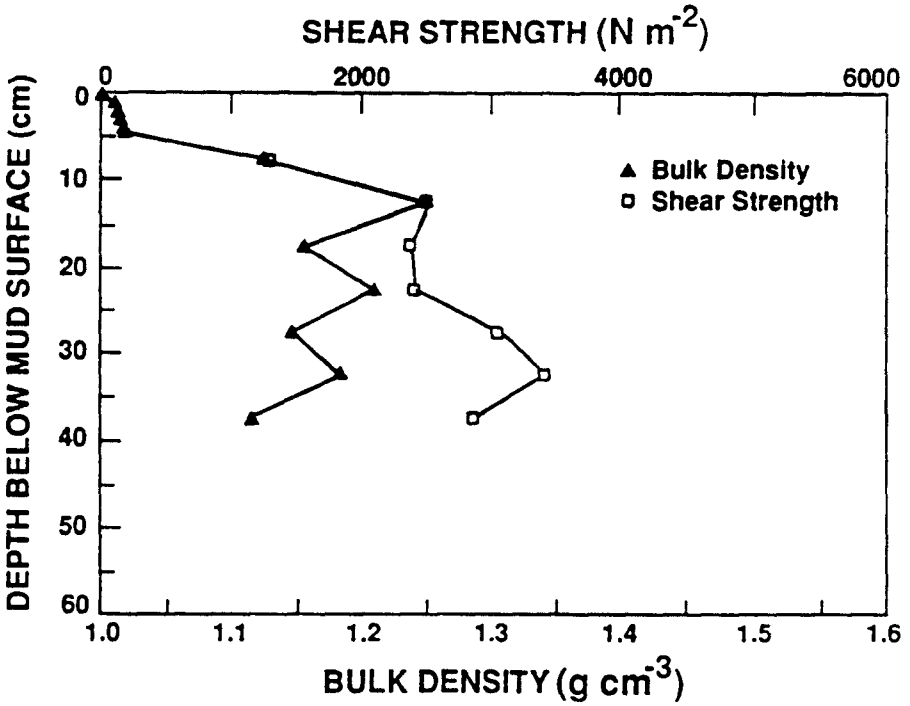

Figure A.13: Bulk Density and Vane Shear Strength Variations for Site OK29VC

APPENDIX B
CONCENTRATION PROFILES FROM SETTLING TESTS

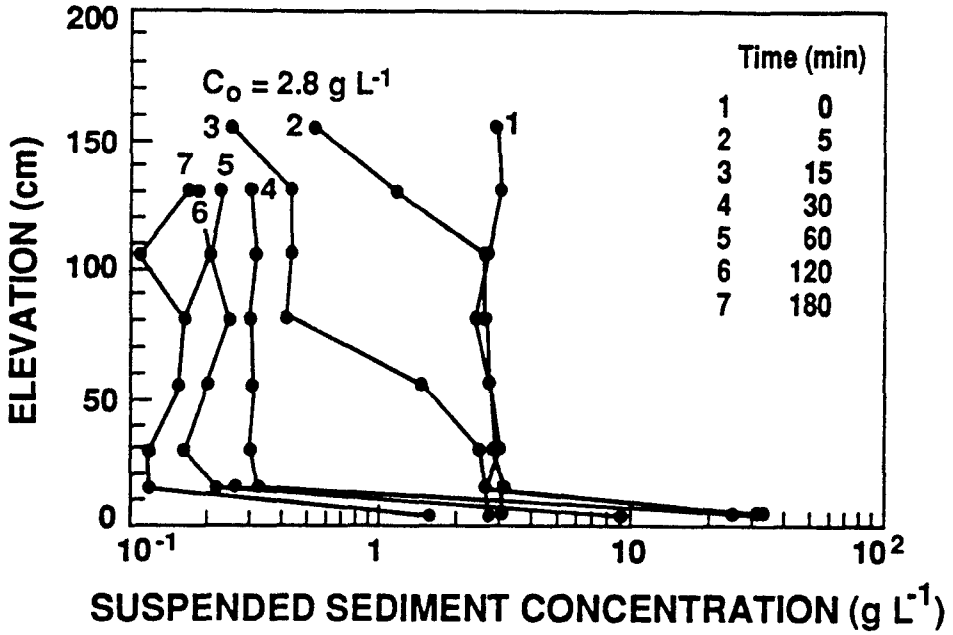

Figure B.1: Concentration Profiles from Settling Test 2; Initial Concentration of 2.8 $g\ L^{-1}$

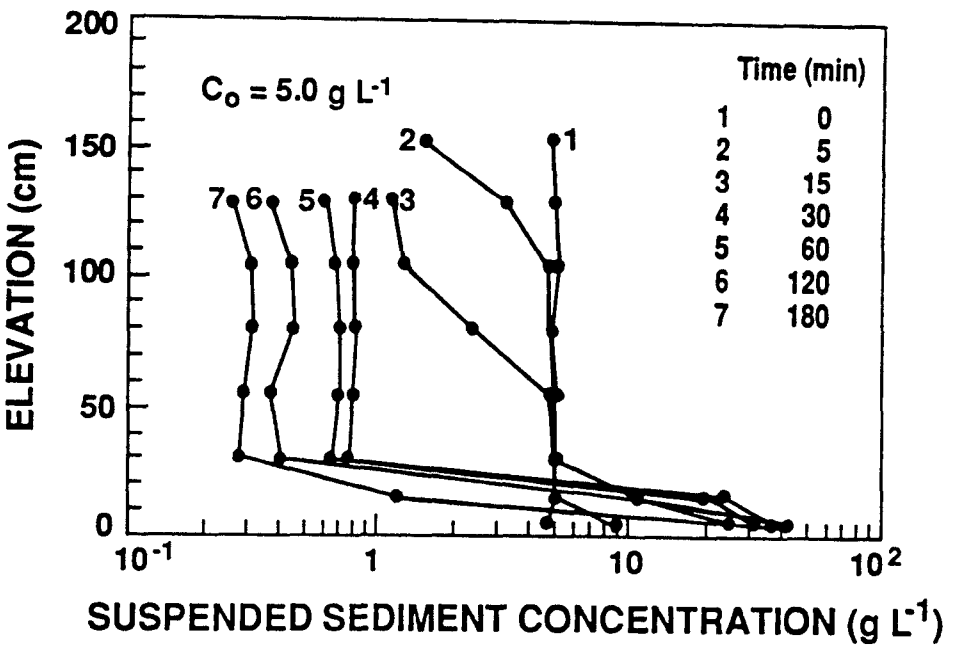

Figure B.2: Concentration Profiles from Settling Test 4; Initial Concentration of 5.0 $g\ L^{-1}$

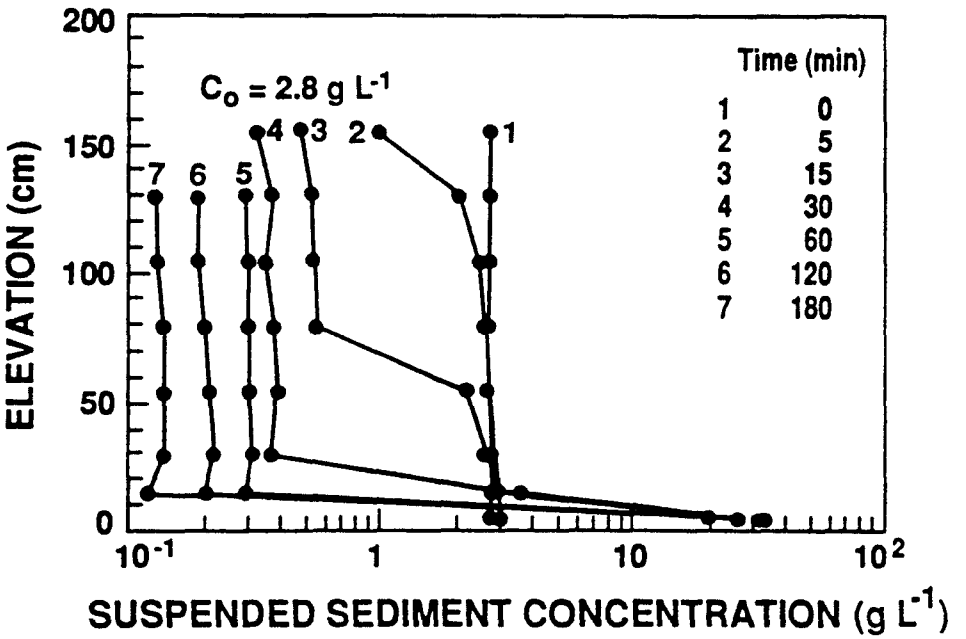

Figure B.3: Concentration Profiles from Settling Test 5; Initial Concentration of 2.8 $g\ L^{-1}$

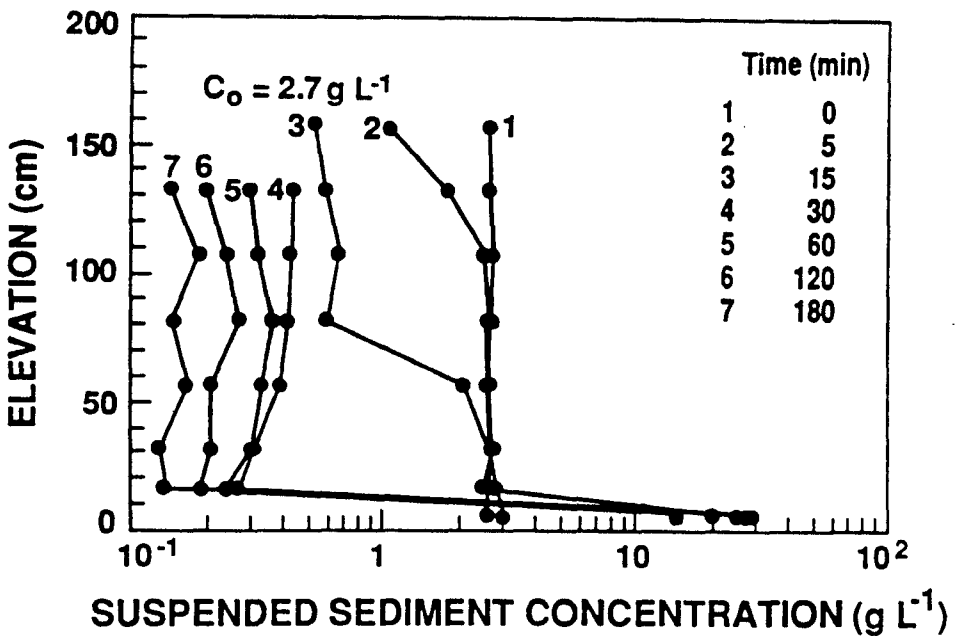

Figure B.4: Concentration Profiles from Settling Test 7; Initial Concentration of 2.7 $g\ L^{-1}$

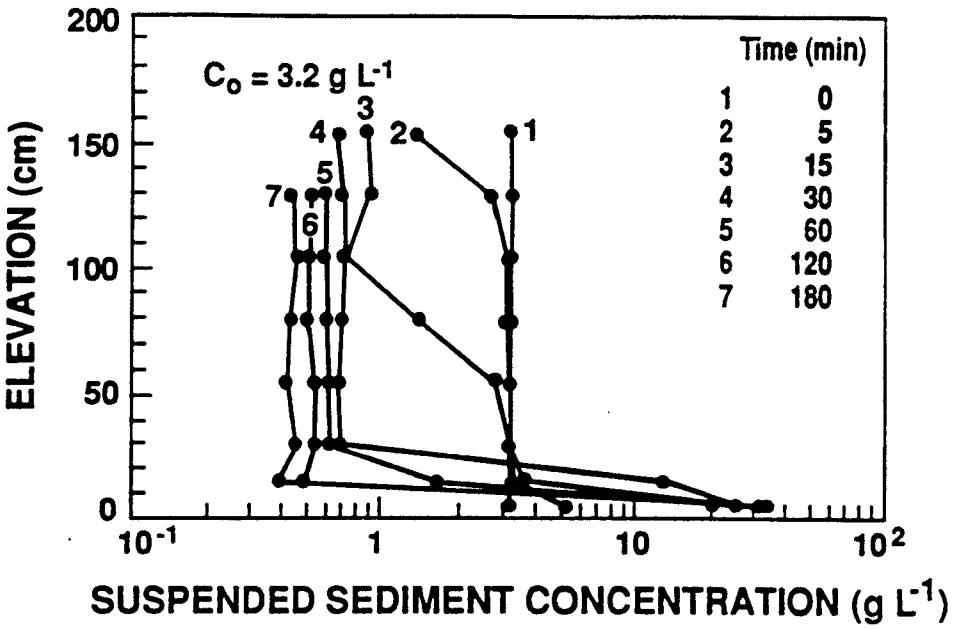

Figure B.5: Concentration Profiles from Settling Test 8; Initial Concentration of 3.2 $g\ L^{-1}$

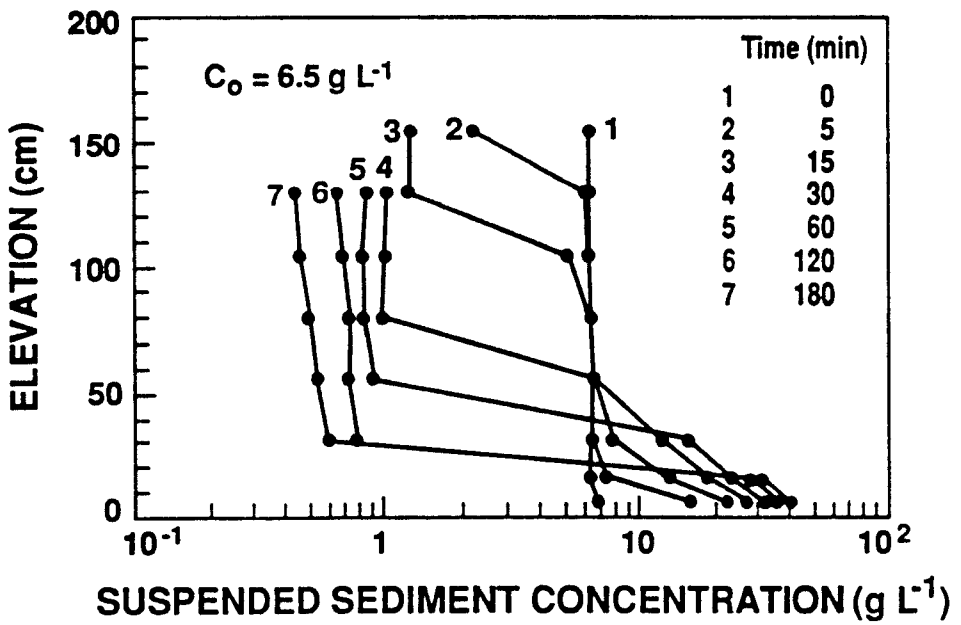

Figure B.6: Concentration Profiles from Settling Test 9; Initial Concentration of 6.5 $g\ L^{-1}$

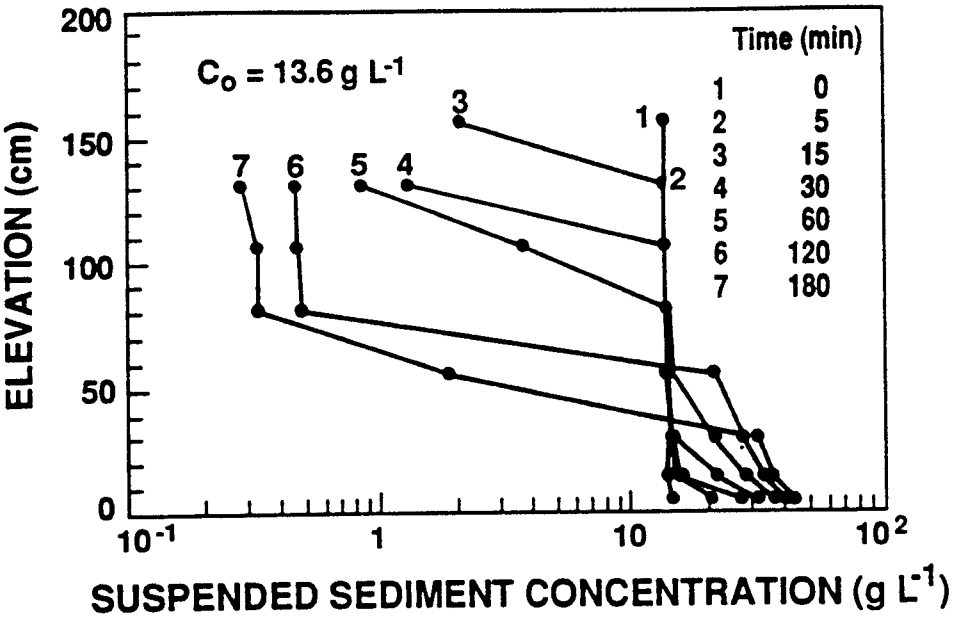

Figure B.7: Concentration Profiles from Settling Test 10; Initial Concentration of 13.6 $g\ L^{-1}$

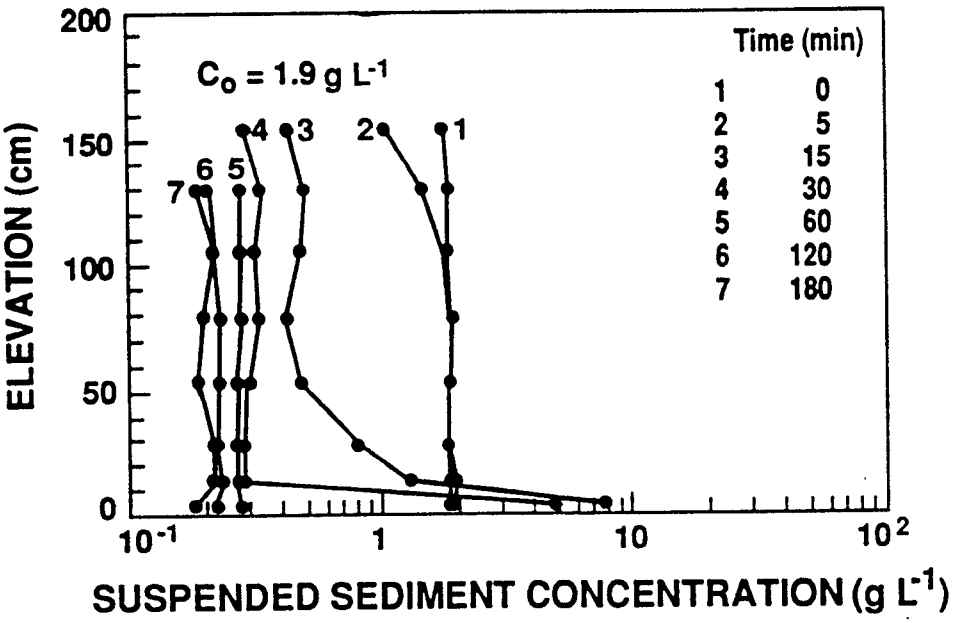

Figure B.8: Concentration Profiles from Settling Test 12; Initial Concentration of 1.9 $g\ L^{-1}$

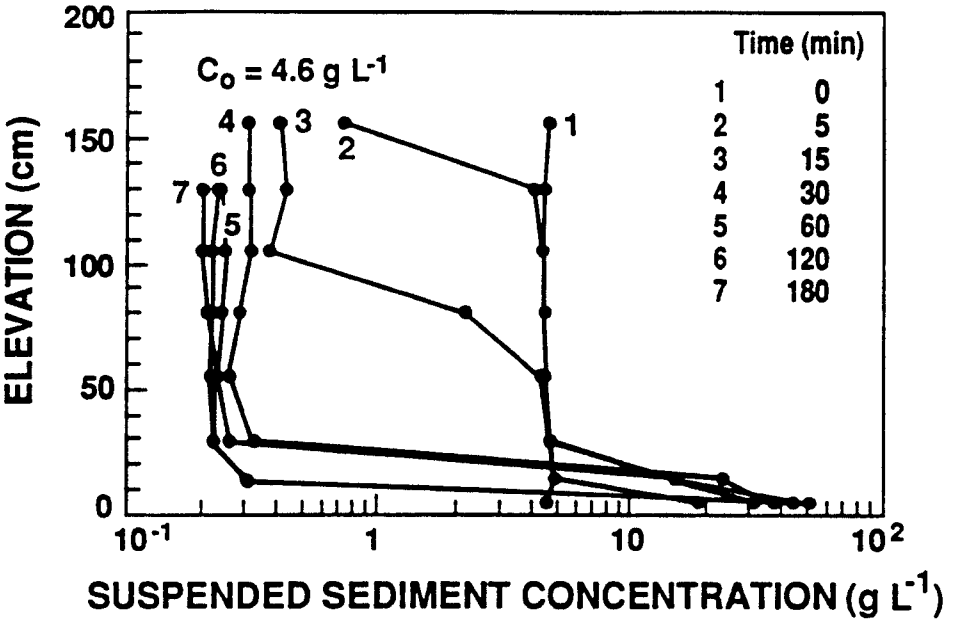

Figure B.9: Concentration Profiles from Settling Test 13; Initial Concentration of 4.6 $g\ L^{-1}$

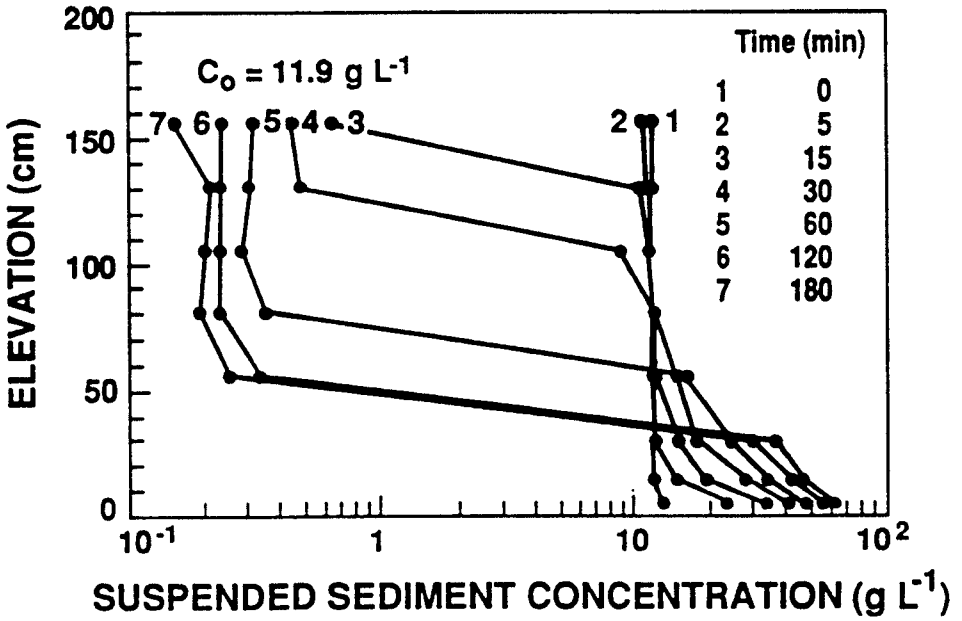

Figure B.10: Concentration Profiles from Settling Test 14; Initial Concentration of 11.9 $g\ L^{-1}$

APPENDIX C
TIME-CONCENTRATION RELATIONSHIP FROM EROSION TESTS

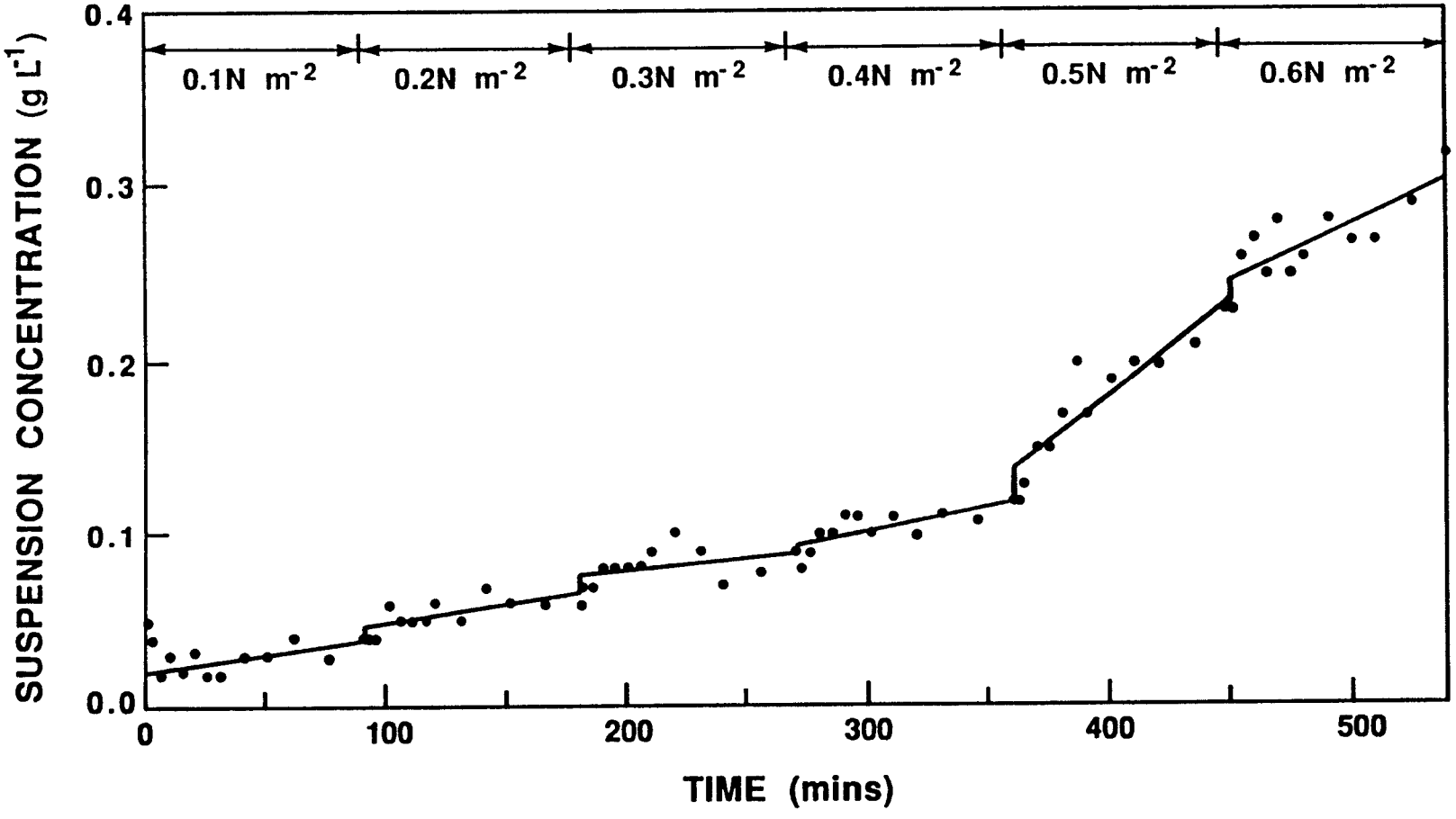

Figure C.1: Time-Concentration Relationship from Erosion Test 1

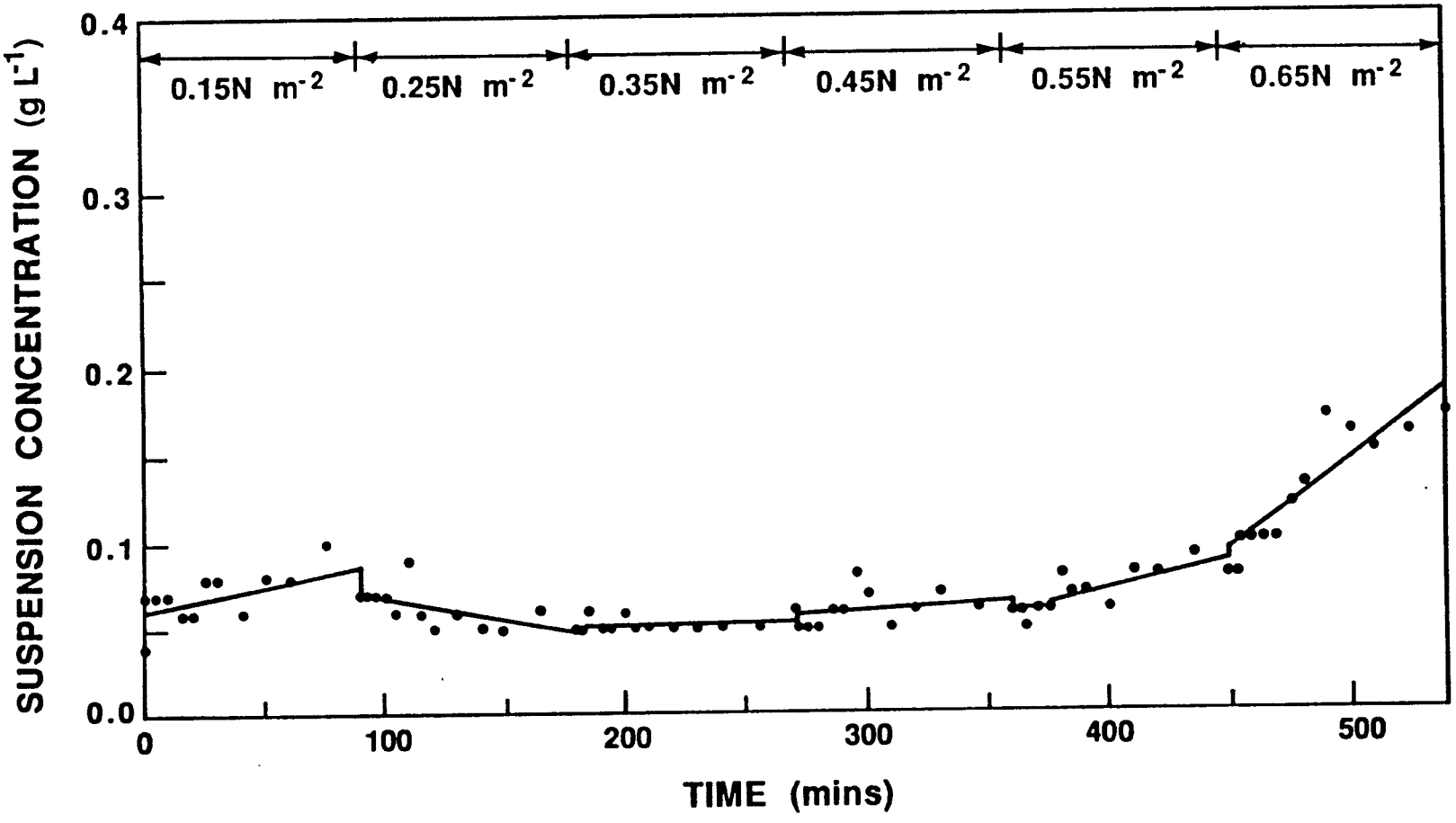

Figure C.2: Time-Concentration Relationship from Erosion Test 2

BIBLIOGRAPHY

Abraham, G. J., "Turbulence and Mixing in Stratified Tidal Flows," Physical Process in Estuaties, J. Dronkers and W. van Leussen, eds., Springer-Verlag, Berlin, 1988, pp. 149-180.

Ahn, K., Personal Communication, Department of Coastal and Oceanographic Engineering, University of Florida, Gainesville, Florida, 1989.

Alishahi, M. R., and Krone, R. B., "Suspension of Cohesive Sediment by Wind-Generated Waves," Technical Report HEL-2-9, Hydraulic Engineering Laboratory, University of California, Berkeley, California, August, 1964.

American Society for Testing and Materials, Annual Book of A. S. T. M. Standards, Vol. 04.08, American Society for Testing and Materials, Philadelphia, 1987.

Bhattacharya, P., "Sediment Suspension in Shoaling Waves," Ph. D. Dissertation, University of Iowa, Hydraulic Engineering, 1971.

Cervantes, E. E., "A Laboratory Study of Fine Sediment Resuspension by Waves," M. S. Thesis, University of Florida, Gainesville, Florida, 1987.

Dixit, J. G., "Resuspension Potential of Deposited Kaolinite Beds," M. S. Thesis, University of Florida, Gainesville, Florida, 1982.

Dyer, K. R., Coastal and Estuarine Sediment Dynamics, John Wiley and Sons, Chichester, U. K., 1986.

Fitch, E. B., "The Significance of Definition in Sedimentation," Sewage and Industrial Wastes, Vol. 29, No. 10, 1957, pp. 550-554.

French, R. H., Open Channel Hydraulics, McGraw-Hill, New York, NY, 1985.

Gleason, P. J., and Stone, P. A., "Prehistoric Trophic Level Status and Possible Cultural Influences on the Enrichment of Lake Okeechobee," Unpublished Report, South Florida Water Management District, West Palm Beach, Florida, 1975.

Heltzel, S. B., and Teeter, A. M., "Settling of Cohesive Sediments," Coastal Sediments '87, ASCE Specialty Conference on Advances in Understanding of Coastal Sediment Processes, Nicholas Kraus, ed., 1987, pp. 63-70.

Homma, M., and Horikawa, K., "Suspended Sediment due to Wave Action," Proceedings of the 8th Conference on Coastal Engineering, Mexico City, 1962.

Homma, M., Horikawa, K., and Kajima, R., "A Study of Suspended Sediment due to Wave Action," Coastal Engineering in Japan, Vol. 8, 1965.

Hwang, P. A., and Wang, H., "Wave Kinematics and Sediment Suspension at Wave Breaking Point," Technical Report No. 13, Department of Civil Engineering, University of Delaware, Newark, Delaware, 1982.

Jonsson, I. G., "Wave Boundary Layer and Friction Factors," Proceedings of the 10th Coastal Engineering Conference, ASCE, Vol. 1, 1966, pp. 127-148.

Kemp, G. P., and Wells, J. T., "Observations of Shallow-Water Waves over a Fluid Mud Bottom: Implications to Sediment Transport," Coastal Sediments '87, ASCE, New York, 1987, pp. 363-378.

Kennedy, J. F., and Locher, F. A., "Sediment Suspension by Waves," Waves on Beaches and Resulting Sediment Transport, R. E. Meyer ed., Academic Press, Inc., New York, 1972, pp. 249-296.

Kirby, R., "Suspended Fine Cohesive Sediment in the Severn Estuary and Inner Bristol Channel, U. K.," Report ETSU-STP-4042, Department of Atomic Energy, Harwell, United Kingdom, 1986.

Kirby, R., Hobbs, C. H., and Mehta, A. J., "Fine Sediment Regime of Lake Okeechobee, Florida and its Possible Significance in Phosphorus Cycling," Unpublished Report, Coastal and Oceanographic Engineering Dept., University of Florida, Gainesville, Florida, 1989.

Krone, R. B., "Flume Studies of the Transport of Sediment in Estuarial Shoaling Process," Final Report, Hydraulic Engineering Laboratory and Sanitary Engineering Research Laboratory, University of California, Berkeley, California, 1962.

Kynch, G. J., "A Theory of Sedimentation," Transactions of the Faraday Society, Vol. 48, 1952, pp. 166-176.

Lick, W., "Entrainment, Deposition and Transport of Fine-Grained Sediment in Lakes," Hydrobiologia, Vol. 91, 1982, pp. 31-40.

Lott, J. W., "Laboratory Study on the Behavior of Turbidity Current in a Closed-end Channel," M. S. Thesis, University of Florida, Gainesville, Florida, 1987.

Luettich, R. A., Jr., Harleman, D. R. F., and Somlyody, L., "Suspended Sediment Concentration in a Shallow Lake," Limmology and Oceanography, 1989.

Maa, P. -Y., "Erosion of Soft Muds by Waves," Ph. D. Dissertation, University of Florida, Gainesville, Florida, 1986.

Maa, P. -Y., and Mehta, A. J., "Mud Erosion by Waves: A Laboratory Study," Continental Shelf Research, Vol. 7, Nos. 11/12, 1987, pp. 1269-1284.

McCutcheon, S. C., "Vertical Mixing in models of Stratified Flow," Proc. Conference on Frontiers in Hydraulic Engineering, ASCE, 1983, pp. 15-20.

McLaughlin, R. J., Jr., "On the Mechanics of Sedimentation in Artificial Basins," Ph. D. Dissertation, California Institute of Technology, Pasadena, 1958.

Mehta, A. J., "Depositional Behavior of Cohesive Sediments," Ph. D. Dissertation, University of Florida, Gainesville, Florida, 1973.

Mehta, A. J., "Bed Friction Characteristics of Three Tidal Entrances," Coastal Engineering, Vol. 2, 1978, pp. 69-83.

Mehta, A. J., "Characterization of Cohesive Sediment Properties and Transport Processes in Estuaries," Estuarine Cohesive Sediment Dynamics, A. J. Mehta, ed., Springer-Verlag, Berlin, 1986.

Mehta, A. J., "Cohesive Sediments in Estuarine Environment," Invited Contribution to AGU Chapman Conference, Bahia Blanca, Argentina, 1988a.

Mehta, A. J., "Laboratory Studies on Cohesive Sediment Deposition and Erosion," Physical Processes in Estuaries, J. Dronkers and W. van Leussen, eds., Springer-Verlag, Berlin, 1988b, pp. 427-445.

Mehta, A. J., and Lott, J. W., "Sorting of Fine Sediment During Deposition," Coastal Sediments '87, ASCE Specialty Conference on Advances in Understanding of Coastal Sediment Processes, Nicholas Kraus, ed., 1987, pp. 348-362.

Mehta, A. J., Parchure, T. M., Dixit, J. G., and Ariathurai, R., "Resuspension Potential of Deposited Cohesive Sediment Beds," Estuarine Comparisons, V. S. Kennedy, ed., Academic Press, New York, 1982, pp. 591-609.

Munk, W. H., and Anderson, E. R., "Notes on the Theory of the Thermocline," Journal of Marline Research, Vol. 1, 1948, pp. 276-295.

Neilson, P., "Some Basic Concepts of Wave Sediment Transport," Paper No. 20, Institute of Hydrodynamics and Hydraulic Engineering, Technical University of Denmark, Lyngby, Denmark, 1979.

Oduyemi, K. O. K., "Turbulent Transport of Sediment in Estuaries, Ph. D. Dissertation, University of Birmingham, Birmingham, U. K., 1986.

Otsubo, K., and Muraoka, K., "Field Studies on Physical Properties of Sediment Resuspension in Lake Kasumigaura," The Japanese Journal of Limnology, Vol. 48, Special Issue, 1987, pp. 131-138.

Owen, M. W., "A Detailed Study of the Settling Velocities of an Estuary Mud," Report No. INT 78, Hydraulics Research Station, Wallingford, United Kingdom, 1970.

Parchure, T. M., "Erosional Behavior of Deposited Cohesive Sediments," Ph. D. Dissertation, University of Florida, Gainesville, Florida, 1984.

Parchure, T. M., and Mehta, A. J., "Erosion of Soft Cohesive Sediment Deposits," Journal of Hydraulic Engineering, ASCE, Vol. 3, No. 10, 1985, pp. 1308-1326.

Parker, W. R., "On the Observation of Cohesive Sediment Behavior for Engineering Purposes," Estuarine Cohesive Sediment Dynamics, A. J. Mehta ed., Springer-Verlag, Berlin, 1986, pp. 270-289.

Parker, W. R., and Kirby, R., "Time Dependent Properties of Cohesive Sediment Relevant to Sedimentation Management-European Experience," Estuarine Comparisons, V. S. Kennedy, ed., Academic Press, New York, 1982, pp. 573-590.

Richardson, J. F., and Zaki, W. N., "The Sedimentation of a Suspension of Uniform Spheres under Conditions of Viscous Flow," Chemical Engineering Science, Vol. 3, 1954, pp. 65-72.

Ross, M. A., "Vertical Structure of Estuarine Fine Sediment Suspensions," Ph. D. Dissertation, University of Florida, Gainesville, Florida, 1988.

Schlichting, H., Boundary-Layer Theory, 7th ed., McGraw-Hill Book Company, New York, 1979.

Sills, G. C., and Elder, D. McG., "The Transition from Suspension to Settling Bed," Estuarine Coehesive Sediment Dynamics, A. J. Mehta ed., Springer-Verlag, Berlin, 1986, pp. 192-205.

Task Committee on Erosion of Cohesive Materials, "Erosion of Cohesive Sediments," Journal of the Hydraulics Division, Pro. of the ASCE, Vol. 94, No. HY4, July, 1968, pp. 1017-1049.

Teeter, A. M., "Vertical Transport in Fine-Grained Suspension and Newly-Deposited Sediment," Estuarine Cohesive Sediment Dynamics, A. J. Mehta, ed., Springer-Verlag, Berlin, 1986.

Thimakorn, P., "Resuspension of Clays Under Waves," Seabed Mechanics, B. Denness, ed., Graham and Trotman Ltd., London, 1984, pp. 191-196.

van Olphen, H., An Introduction to Clay Colloid Chemistry, Interscience Publishers, New York, 1963.

Vanoni, V. A., "Sedimentation Engineering," Report of Engineering Practice, No. 54, American Society of Civil Engineers, New York, 1975.

Villaret, C., and Paulic, M., "Experiments on the Erosion of Deposited and Placed Cohesive Sediments in an Annular Flume and a Rocking Flume," UFL/COEL-86/007, Coastal and Oceanographic Engineering Dept., University of Florida, Gainesville, Florida, 1986.

Wolanski, E., Aseda, T., and Imberger, J., "Mixing Across a Lutocline," Limnology and Oceanography, Vol. 31, 1989, pp. 931-938.

Zelazny, L. W., and Calhoun, F. G., "Palygorskite, (Attapulgite), Sepiolite, Talc, Pyrophyllite, and Zeolites," Minerals in Soil Environments, J. B. Dixon and S. B. Weed, eds., Soil Science Society of America, Madison, 1977, pp. 435-470.